

Beyond Imidazolyidenes: Investigation of Mesoionic bis-Azolylidene Au(I) Complexes as Anticancer Drugs

Leon Ferdinand Richter

Vollständiger Abdruck der von der TUM School of Natural Sciences der Technischen Universität München zur Erlangung eines

Doktors der Naturwissenschaften (Dr. rer. nat.)

genehmigten Dissertation.

Vorsitz: Priv.-Doz. Dr. Alexander Pöthig

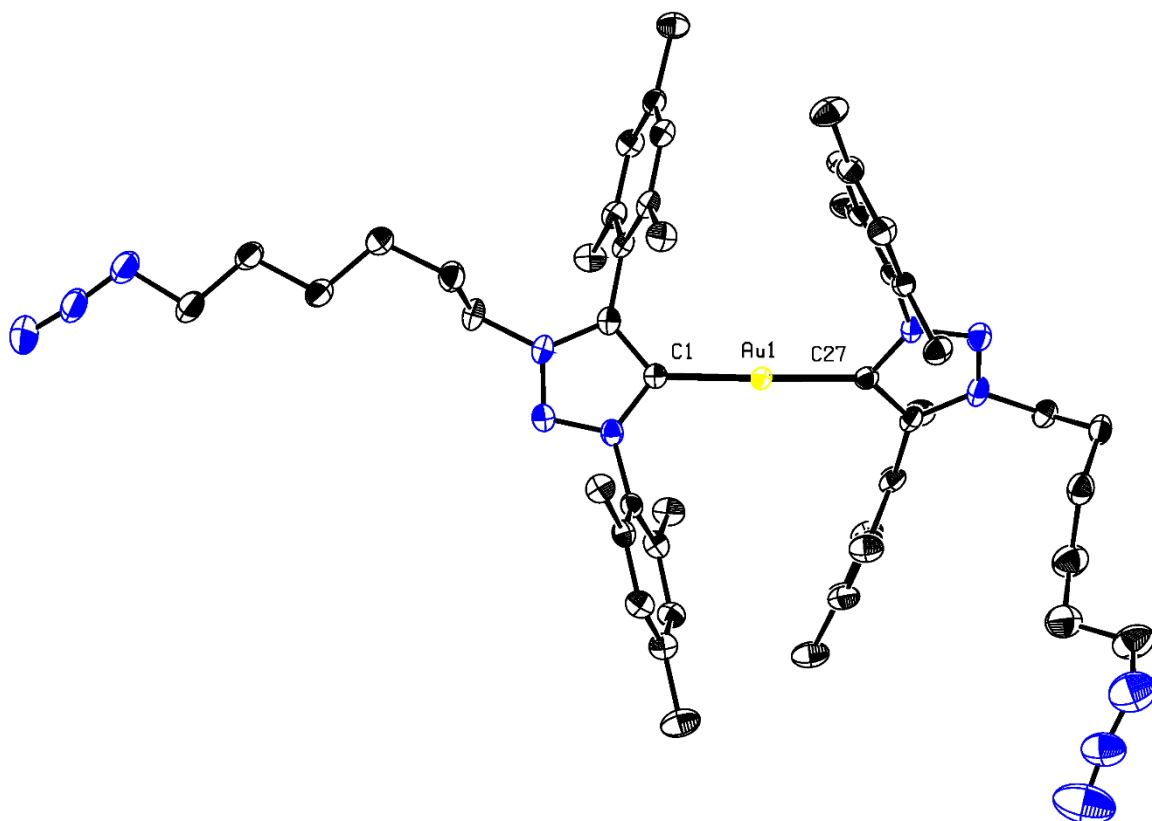
Prüfende der Dissertation:

1. Prof. Dr. Fritz E. Kühn
2. Prof. Dr. Klaus Köhler
3. Prof. Dr. João Domingos Galamba Correia

Die Dissertation wurde am 15.11.2024 bei der Technischen Universität München eingereicht und durch die TUM School of Natural Sciences am 07.01.2025 angenommen.

„Yesterday's the past, tomorrow's the future, but today is a GIFT. That's why it's called the present”

- Bill Keane



ORTEP-style representation of the azide-functionalized gold(I) NHC complex. Hydrogen atoms and anions are omitted for clarity. Thermal ellipsoids are shown at a 50% probability level.

Table of Contents

Acknowledgment & Danksagung	2
Abstract	4
Kurzzusammenfassung	5
List of Abbreviations	6
1. Introduction	9
1.1. Cancer and Forms of Cancer Treatment	9
1.2. Cell Division and Modes of Action of Chemotherapeutic Agents	11
1.3. Controlled Cell Death: Apoptosis	14
1.4. Metallodrugs in Cancer Therapy (Au and Pt)	16
1.5. Gold(I) Complexes bearing <i>N</i> -heterocyclic Carbenes (NHCs) in Medicinal Chemistry	19
1.6. Bioorthogonal Click-Chemistry and Other Bioconjugation Reactions	23
1.7. Targeted Therapy: Oncology	25
1.8. NHC-Au(I) Complexes for Targeted Cancer Therapy: Frameworks and Examples	27
2. Objective	29
3. Results: Publication Summaries	30
3.1. Exploiting click-chemistry: backbone post-functionalisation of homoleptic gold(I) 1,2,3-triazole-5-ylidene complexes	30
3.2. A new class of Gold(I) NHC Complexes with Proapoptotic and Resensitizing Properties towards Multidrug Resistant Leukemia Cells Over-expressing BCL-2	31
4. Unpublished Results	32
4.1. Synthesis and antiproliferative effects of a series of Au(I) 1,2,3-triazolylidene NHC/chloro and NHC/phosphine complexes	33
4.2. Investigation of backbone-functionalized heteroleptic bis-NHC complexes.	35

4.3. Synthesis and antiproliferative effects of a series of Au(I) tetrazolylidene NHC/chloro complexes	37
4.4. Structure-activity relationship of a variety of antiproliferative azolium salts.	39
4.5. Bioconjugation of a homoleptic azide functionalized Au(I) 1,2,3-triazolylidene complex with antibodies and miniproteins to enable targeted delivery for cancer therapy.....	41
5. Conclusion and Outlook.....	43
6. Reprint Permissions.....	45
7. Bibliographic Data of First Author Publications.....	46
7.1. Royal Society of Chemistry (RSC).....	46
7.2. American Chemical Society (ACS)	46
7.3. Elsevier.....	47
8. Complete List of Publications.....	48
8.1. Journal Articles (Peer-reviewed).....	48
8.2. Conference Contributions	49
8.3. Others.....	49
9. Figures, Schemes and Tables.....	50
10. Literature	51

Die vorliegende Arbeit wurde im Zeitraum von August 2021 bis November 2024 an der Professur für Molekulare Katalyse der Technischen Universität München angefertigt.

Mein ganz besonderer Dank gilt meinem Doktorvater

Herrn Prof. Dr. Fritz E. Kühn

für die Aufnahme in seinen Arbeitskreis und das mir entgegengebrachte Vertrauen in vielerlei Hinsicht. Vielen Dank für die spannenden Forschungsmöglichkeiten und die Betreuung und Unterstützung während der gesamten Arbeit, sowie für die großzügigen Freiräume auch in anderen Angelegenheiten wie das Arbeiten als Vertretungslehrer, den Ausbau des 3D-Drucks am Lehrstuhl und die persönliche Weiterbildung im Rahmen des Ausbilderscheins und des Zertifikats der Hochschullehre, welche mir die Zeit an der Professur nachhaltig als fortschrittliches Arbeitsumfeld nahegebracht haben.

Acknowledgment & Danksagung

First, I would like to thank **Prof. João D.G. Correia** for his support during my PhD project. Your feedback during our Zoom meetings was always very helpful. Also, you were very welcoming during the two times I visited Lisbon and made me feel like I was at home! This is also especially true for **Dr. Fernanda Marques, Dr. Bruno Oliveria, Ruben Silva**, and all other members of the research group who made my research stay at C2TN memorable.

Außerdem möchte ich **Prof. Aram Prokop** und seiner Arbeitsgruppe (speziell **Franzi, Jenny** und **Johanna**) für die fruchtbare Zusammenarbeit und den warmherzigen Empfang bei unserem Treffen in Schwerin bedanken.

Ebenfalls möchte ich meinem Mentor **Dr. habil Alexander Pöthig** danken. Du hast mich wie selbstverständlich in dein wöchentliches Seminar, diverse Gruppenaktivitäten und Projekte eingebunden, sowie immer ein offenes Ohr bei kristallographischen (und anderen) Fragestellungen gehabt.

Ein besonderer Dank gilt **Dr. Robert Reich** für die Unterstützung zu Beginn meiner Doktorarbeit (du hast unsere Gruppe ja leider verlassen müssen) und für die Möglichkeit mich im Rahmen des „studium MINT“ und während der Betreuung diverser Azubis persönlich weiterzuentwickeln. Du hattest immer ein offenes Ohr für mich. An dir werden sich meine zukünftigen Führungskräfte messen müssen.

Ulla Hifinger möchte ich für die riesige Unterstützung in allen bürokratischen Angelegenheiten danken. Ich hoffe ich konnte Sie mit Kuchen für meine komplizierten Anträge gebührend entschädigen. **Markus Drees** danke ich für die Unterstützung bei diversen Anträgen und Fragen zu dem Promotionsverfahren der TUM.

Großer Dank geht auch an meine Azubis: **Miriam, Hanna** und **Michelle**. Mit euch hat sich die Laborarbeit plötzlich fast wie von selbst erledigt und an das frühe Aufstehen hat man sich auch schnell gewöhnt. Danke an der Stelle auch an das gesamte AuTUM, insbesondere an **Monika Partsch** und **Ramona Schütt**.

Auch meinen Bachelorstudenten **Simon Stifel** und **Annsophie Haberhauer** sowie den Forschungspraktikanten **Simon Stifel, Anna Ressel** und **Arina Weber** möchte ich für die tatkräftige Unterstützung danken.

Meinen beiden Masteranden **Alberto Piccoli** und (zum dritten Mal) **Simon Stifel** danke ich ebenfalls für die unkomplizierte Zusammenarbeit. Du wirst jetzt hoffentlich auch bald in deine Promotion starten; viel Erfolg dabei!

Für die tatkräftige Unterstützung während der AC-Praktika und darüber hinaus danke ich außerdem **Thomas Miller** und **Tobias Kubo** sowie **Hanna Kern** aus der AC-Vorbereitung.

Meinen Kollegen möchte ich ebenfalls danken: **Alex, Alex, Carla, Greta, Johannes, Melanie, Michi, Nici, Stefan, Tim** und **Yogi** (aka Wolfgang). Ihr hattet immer Zeit für fachliche und nicht-fachliche Diskussionen und mit euch war die Zeit nie langweilig! Von **Johannes** trenne ich mich nach unseren gemeinsamen Übernachtungen in den USA 2024 nur sehr ungern. Auch wenn ich hier nicht individueller auf euch eingehe, bin ich unglaublich froh euch als Kollegen zu haben.

Für ihre Unterstützung auch nach ihrer Zeit an der TUM danke ich meinen „Vorgängern“ **Jonas** und **Chris**. Danke für die großartige Betreuung während meiner Masterarbeit.

Bei anspruchsvollen Verfeinerungen von Kristallen und undurchsichtigen NMR-Spektren warst du oft mein erster Ansprechpartner; Dafür möchte ich mich auch bei dir bedanken, **Thomas**.

Der größte Dank gebührt jedoch meiner (erweiterten) Familie für die Unterstützung während der letzten Jahre; Da wären meine Eltern, mein Bonuspapa **Roger** sowie meine Bonus-schwiegereltern **Dieter & Sylvia**. Auch meinen beiden Brüdern **Fabi** und **Benni** sei gedankt.

Meinen Freunden und Freundinnen möchte ich ebenfalls danken! Danke für all' die Ablenkungen während diversen Konzerten, Brettspielabenden und Mariokart-Turnieren.

Zu guter Letzt gibt es noch eine Person, die mich in den letzten fünf Jahren so sehr unterstützt hat wie kein anderer: **Toni**. Danke für alles, was du für mich getan hast; wenn ich das alles aufzählen würde, wäre die Arbeit doppelt so lang geworden. Mit dir an meiner Seite habe ich das Gefühl, dass ich alles schaffen kann!

Abstract

Cancer continues to be one of the most common causes of death worldwide, making the treatment of this disease a challenge for medicine to overcome. The metal complex cisplatin and its derivatives are used in chemotherapy alongside the frequently used organic molecules, although their use can lead to serious side effects or the development of resistance to cytostatic drugs. Therefore, there is a need to develop alternative approaches that have a lower side effect rate or can overcome emerging resistance. Gold(I) compounds represent a promising alternative, as they have a different mechanism of action: the inhibition of sulfur- or selenium-containing enzymes causes the cell to initiate controlled cell death (apoptosis). Therefore, the enzyme thioredoxin reductase (TrxR) - which is overexpressed in some cancer cells - has been identified as a potential target for numerous gold complexes.

This research focuses on the synthesis, characterization, and medical investigation of novel gold(I)-to-N-heterocyclic carbene complexes as potential anticancer agents. The focus of this work is particularly on mesoionic NHCs (1,2,3-triazolylidene and tetrazolylidene) instead of the widely used imidazolylidenes. The resulting complexes are characterized by exceptional physicochemical properties. On the one hand, the inclusion of two NHC ligands ensures their stability under physiological conditions; on the other hand, other studies indicate that the cationic complexes can accumulate to a high degree in the mitochondria of cancer cells, which could lead to a selective effect. The plan to equip the NHCs with functional groups for the coupling of biomolecules also increases their potential for targeted cancer therapy.

The first added value of this work lies in the modification of the backbone of the ligands of highly active 1,2,3-triazolylidene complexes. The introduction of a terminal azide functionality allows a simple and reliable post-synthetic modification of the complexes with biomolecules using "click chemistry". Several proof-of-concept experiments have shown that the high antiproliferative activity is maintained.

In the second part of the work, a class of ligands that has hardly been explored so far is used to prepare corresponding gold(I) bis-tetrazolylidene complexes. These complexes show impressive antiproliferative activity in the nanomolar range and appear to undergo a similar molecular mechanism of action as other gold(I) bis-NHC complexes: The induction of apoptosis via the mitochondrial pathway by interfering with the BCL-2 protein family.

Kurzzusammenfassung

Die Erkrankung an Krebs stellt nach wie vor eine der häufigsten Todesursachen weltweit dar, sodass die Behandlung dieser Erkrankung eine Herausforderung für die Medizin darstellt, die es zu bewältigen gilt. Der Metallkomplex Cisplatin und seine Derivate finden neben den häufig angewandten organischen Medikamenten Anwendung in der Chemotherapie. Dennoch kann deren Einsatz zu schwerwiegenden Nebenwirkungen oder einer Resistenzbildung gegenüber Zytostatika führen. Daher besteht die Notwendigkeit, alternative Ansätze zu entwickeln, die eine geringere Nebenwirkungsrate aufweisen oder in der Lage sind, auftretende Resistenzen zu überwinden. Gold(I)-verbindungen stellen eine vielversprechende Alternative dar, da sie einen anderen Wirkmechanismus aufweisen: die Hemmung von Schwefel- oder Selenhaltigen Enzymen bringt die Zelle dazu den kontrollierten Zelltod einzuleiten (Apoptose). Daher wurde das Enzym Thioredoxin Reduktase (TrxR) – welche in einigen Krebszellen überexprimiert ist – als potenzielles Ziel für zahlreiche Goldkomplexe identifiziert.

Diese Forschungsarbeit konzentriert sich auf die Synthese, Charakterisierung und medizinische Untersuchung von neuartigen Gold(I)-bis-*N*-heterozyklischen Carbenkomplexen als potenzielle Antikrebsmittel. Der Fokus dieser Arbeit liegt insbesondere auf mesoionischen NHCs (1,2,3-Triazolylidene und Tetrazolylidene) anstelle der weit verbreiteten Imidazolylidene. Die resultierenden Komplexe zeichnen sich durch außergewöhnliche physiochemische Eigenschaften aus. Zum einen gewährleistet die Einbeziehung von zwei NHC-Liganden ihre Stabilität unter physiologischen Bedingungen, zum anderen deuten andere Studien darauf hin, dass sich die kationischen Komplexe in hohem Maße in den Mitochondrien von Krebszellen anreichern können, was zu einer selektiven Wirkung führen könnte. Der Plan, die NHCs mit funktionellen Gruppen für die Kopplung von Biomolekülen auszustatten, erhöht zudem ihr Potenzial für eine gezielte Krebstherapie.

Der erste Mehrwert dieser Arbeit liegt in der Modifikation des Rückgrats der Liganden von hochaktiven 1,2,3-triazolyriden Komplexen. Die Einführung einer terminalen Azid-funktionalität erlaubt eine einfache und verlässliche Post-synthetische Modifikation der Komplexe mit Biomolekülen mittels „Klick-Chemie“. Mehrere Proof-of-Concept Experimente haben gezeigt, dass die hohe antiproliferative Aktivität hierbei erhalten bleibt.

Im Zweiten Teil der Arbeit wird eine bisher kaum erforschte Klasse von Liganden verwendet um entsprechende Gold(I) bis-tetrazolyriden Komplexe herzustellen. Diese Verbindungen zeigen eine beeindruckende antiproliferative Aktivität im nanomolaren Bereich und scheinen einen ähnlichen molekularen Wirkmechanismus zu durchlaufen wie andere Gold(I) bis-NHC Komplexe: Die Induktion von Apoptose über den mitochondrialen Stoffwechselweg mittels Beeinflussung der BCL-2 Proteinfamilie.

List of Abbreviations

A2780	human ovarian cancer cells
AA	amino acid
Ac	acetyl-
ADC	antibody-drug conjugate
AF	auranofin
al	aliphatic
ALL	acute lymphoblastic leukemia
aNHC	abnormal/mesoionic <i>N</i> -heterocyclic carbene
AOC	antibody-oligonucleotide conjugate
ATP	adenosine tri phosphate
BCL-2	B-cell lymphoma 2
CTR1	high affinity copper uptake protein 1
CuAAC	copper-catalyzed azide-alkyne cycloaddition
DAR	drug-to-antibody ratio
DBCO	dibenzocyclooctyne
DFT	density functional theory
Dipp	2,6-diisopropylphenyl
DNA	deoxyribonucleic acid
ESI	electron spray ionisation
GPx	glutathione peroxidase
HDI	human development index
HPLC	high-performance liquid chromatography
HSA	human serum albumin

IC ₅₀	half maximal inhibitory concentration
IMM	inner mitochondrial membrane
<i>i</i> Pr	<i>iso</i> -propyl-
MC38	murine colon carcinoma
MCF7	human estrogen-sensitive breast cancer cells
Me	methyl-
Mes	2,4,6-trimethylphenyl-
MOMP	mitochondrial outer membrane permeabilization
MS	mass spectrometry
MTT	3-(4,5-dimethylthiazol-2-yl)-2,5-diphenyltetrazolium bromide
NHC	<i>N</i> -heterocyclic carbene
NMR	nuclear magnetic resonance spectroscopy
OCT	organic cationic transporter
PDC	peptide drug conjugate
PD-L1	programmed cell death 1 ligand 1
Ph	phenyl-
Prx	peroxiredoxin
PT	pore transition
RNA	ribonucleic acid
ROS	reactive oxygen species
RuAAC	ruthenium-catalyzed azide-alkyne cycloaddition
SMDC	small molecule-drug conjugate
SPAAC	strain-promoted azide-alkyne cycloaddition
<i>t</i> Bu	<i>tert</i> -butyl-

Tol	toloyl-
TP53	gene coding for p53
Trx	thioredoxin
TrxR	thioredoxin reductase
ValCit	valine-citrulline (enzymatically cleavable linker)
VERO	non-human healthy kidney cells

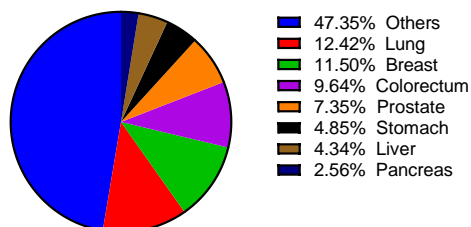
1. Introduction

1.1. Cancer and Forms of Cancer Treatment

Cancer is a serious medical condition characterized by uncontrolled cell growth that leads to the development of malignant tumors.^[1] It can occur in various tissues, such as the lungs, breasts, or prostate. Tumorigenesis, the formation of tumor cells from normal, healthy cells, is a complex process that involves several individual steps that are not yet fully understood.^[2] In 2022, there were an estimated 20 million new cases of cancer and 9.7 million deaths.^[3] Approximately one in five people will develop cancer during their lifetime, while the disease is fatal for about one in nine men and one in twelve women.^[4] According to the new estimates available on IARC's Global Cancer Observatory, roughly two-thirds of new cases and deaths globally in 2022 were caused by only ten types of cancer. The data covers 185 countries and 36 types of cancer and is also visualized in **Figure 1**.^[3]

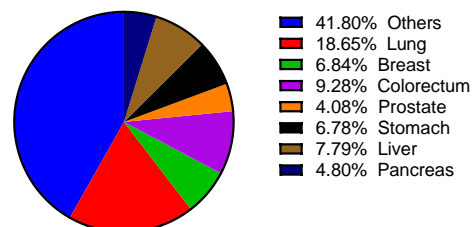
In 2022, lung cancer was the most commonly occurring cancer worldwide, accounting for 12.4% of all new cases, with 2.5 million new cases in total. Female breast cancer ranked second with 2.3 million cases (11.6%), followed by colorectal cancer with 1.9 million cases (9.6%), prostate cancer with 1.5 million cases (7.3%), and stomach cancer with 970,000 cases (4.9%). The re-emergence of lung cancer as the most common cancer since 2020 (whereas breast cancer was the dominating type of cancer) is likely due to persistent tobacco use in Asia.^[5] The deadliest type of cancer in 2022 was lung cancer, accounting for a total of 1.8 million deaths worldwide, or 18.7% of all cancer deaths. Colorectal cancer follows second with 900,000 deaths (9.3%), then liver cancer with 760,000 deaths (7.8%), breast cancer with 670,000 deaths (6.9%), and stomach cancer with 660,000 deaths (6.8%).

Cancer Incidence (World, 2022, Both sexes)



Total : 19 976 499

Cancer Mortality (World, 2022, Both sexes)



Total : 9 743 832

Figure 1: Number of worldwide cancer incidences and deaths in 2022^[3].

From this data, it becomes evident that the mortality and incidence rates do not necessarily correlate and are strongly dependent on the specific type and stage of cancer. For example, although breast cancer has the highest incidence rate among females, the mortality rate is

relatively low. This is also true for prostate cancer. On the other side, the mortality rate for lung, liver, stomach, and pancreas cancer is quite high, as indicated by Figure 1. In general, there are several reasons why we do not have a cure for cancer yet:^[6]

First of all, it should be clear by now that cancer is not just a single disease; the term cancer encompasses over 200 distinct diseases. Second, since cancer is the result of genetic mutations in our DNA, which are responsible for the proper functioning of our cells, two people with the same type of cancer may have unique sets of mutations. This can render an effective treatment for one person completely ineffective for another person. This behavior can also occur in the same patient after the cancer cells have mutated, making them resistant to the treatment. Furthermore, similar to antibiotics, cancer cells can develop resistance against chemotherapeutic medication, limiting the use of previously highly effective drugs.^[7-9]

Effective treatment of cancer typically involves surgery,^[10] radiotherapy,^[11] and/or systemic therapy, such as chemotherapy,^[12,13] hormonal treatments,^[14,15] or targeted biological therapies^[16,17]. As previously mentioned, the cancer's stage and type heavily influence the likelihood of a successful cure. Typically, the earlier the cancer is detected, the greater the chance of a successful cure. Surgery can often completely remove tumors when cancer is detected early, as is often the case for prostate and breast cancer. This is why these types of cancer have high survival rates in countries with a high human development index (HDI).^[4] If the cancerous cells have spread from their origin (primary site) to another region of the body (secondary site), surgery usually is not as effective anymore.^[10] Such a metastasized cancer is best treated in a combined way (multimodal).^[18] Chemotherapy is a treatment modality that employs chemical drugs to combat disease.^[13] This approach was pioneered by Paul Ehrlich, who synthesized a drug called Salvarsan to treat syphilis with a “magic bullet” in mind, a substance that explicitly targets the disease-causing pathogen.^[19,20] In cancer therapy, compared to surgery, chemotherapy is considered less precise since it also affects non-cancerous cells in the body. The subsequent chapter will delineate the process of cell division and the molecular mechanisms of chemotherapeutic drugs.

1.2. Cell Division and Modes of Action of Chemotherapeutic Agents

Our body consists of an incredibly large number of eukaryotic cells. Depending on their ability to proliferate, three types of cells can be differentiated: stable cells, permanent cells, and labile cells. Permanent cells are those that cannot regenerate. This group includes red blood cells, heart cells, and neurons, amongst others.^[21] Besides, stable cells are cells that multiply only when needed. Liver cells are an example of stable cells.^[22] Lastly, most cells in our body (e.g. epithelial skin cells, bone marrow) belong to the group of labile cells that continuously multiply and divide throughout life. This process is described by the eukaryotic cell cycle, which comprises four distinct phases: G1 phase, S phase (synthesis), G2 phase (interphase), and M phase (mitosis and cytokinesis).^[23]

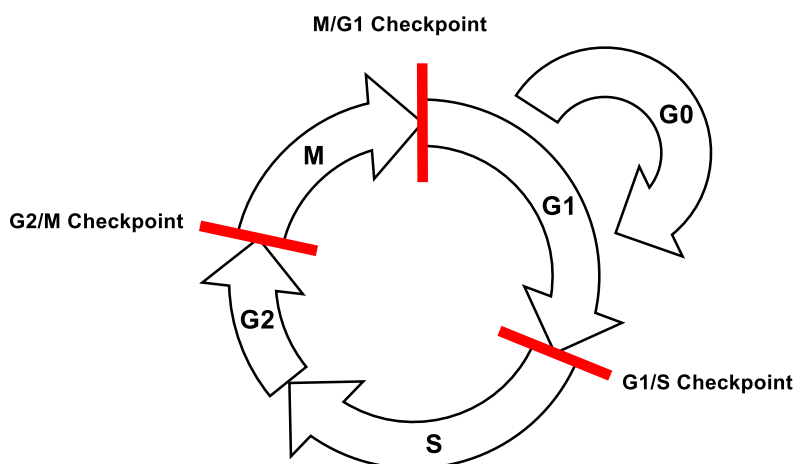


Figure 2: Schematic illustration of the eukaryotic cell cycle, including the checkpoints.

The activation of each phase depends on the proper progression and completion of the previous one. Stable cells that have temporarily or reversibly stopped dividing enter a state of quiescence known as the G0 phase, where they remain metabolically active but do not proliferate unless stimulated by appropriate extracellular signals. Beginning with the G1 phase, the cell fulfills its general purpose in the body while also extensively producing enzymes for DNA replication (e.g. helicase, topoisomerase, DNA polymerase) and DNA building blocks (nucleotides). During the S phase, DNA replication takes place. This process is very complex, and many specialized enzymes are involved.^[24] In a nutshell, the enzymes helicase and topoisomerase unwind the DNA, primase adds RNA primers (= starting sequences of nucleotides), DNA polymerase synthesizes new DNA strands by adding nucleotides to the primers. This process ensures that each new cell receives a flawless copy of the DNA. After DNA replication, in the G2 phase, the cell prepares the microtubule framework and other relevant proteins for the upcoming division. The final phase of the cell cycle, the M phase, consists of two tightly

coupled processes: mitosis, where the cell's nucleus divides, and cytokinesis, in which the cell's cytoplasm divides, forming two daughter cells.

In most cells, the coordination between different phases of the cell cycle depends on a system of checkpoints and feedback controls that prevent entry into the next phase until the events of the preceding phase have been completed.^[25] Furthermore, the cell has mechanisms to detect and repair damaged DNA. However, if the damage is extensive or irreparable, it can trigger cell cycle arrest (halting cell division) or initiate programmed cell death.

To prevent damaged or incomplete DNA from being passed on to daughter cells, there are three main checkpoints (see **Figure 2**): the G1/S checkpoint, the G2/M checkpoint, and the metaphase (mitotic) checkpoint.^[26] In mammalian cells, the G1/S checkpoint arrest is mediated by the protein p53, rapidly induced in response to damaged DNA.^[27] Loss of p53 function due to mutations prevents G1 arrest in response to DNA damage, resulting in the replication of damaged DNA and its transmission to daughter cells instead of being repaired. The inheritance of damaged DNA results in an elevated frequency of mutations and general instability of the cellular genome, which in turn contributes to cancer development. Towards the end of mitosis, there is another crucial cell cycle checkpoint that preserves the genome's integrity. This checkpoint oversees the alignment of chromosomes on the mitotic spindle, guaranteeing the accurate distribution of a complete set of chromosomes to the daughter cells. For instance, if one or more chromosomes fail to align correctly on the spindle, mitosis arrests at metaphase before segregating the newly replicated chromosomes to daughter nuclei.

Luckily this whole process is very efficient in correcting mistakes and avoiding uncontrolled growth of healthy cells. Cancer cells typically acquire their characteristic hallmarks through genomic changes. The viability of a cancer cell depends on multiple mutations in genes (such as oncogenes and tumor-suppressor genes) whose products play a crucial role in maintaining genomic stability in healthy cells.^[28] Proto-oncogenes are the non-mutated form of oncogenes. They code for proteins that function in signal transduction pathways, which stimulate cell growth and division. Mutations in proto-oncogenes usually result in increased proliferative activity. Tumor suppressor genes' products play a crucial role in signaling pathways that inhibit cell division. Mutations in tumor suppressor genes, such as TP53, can lead to the inactivation of their products, like the p53 protein. This can cause cancer cells to become insensitive to growth inhibitory signals, evade differentiation, and even avoid programmed cell death (apoptosis). It is unsurprising that TP53 is mutated in over 50% of human cancers, resulting in a loss of function in p53.^[29]

Most chemotherapeutic drugs affect either the DNA of the cell or the cell cycle itself in various ways, such as acting as DNA-modifying agents, anti-metabolites, mitotic inhibitors, or topoisomerase inhibitors.

DNA-modifying agents work by irreversibly changing the DNA molecule within a cell. This modification typically occurs at the guanine base, one of the four basic building blocks of DNA, although other bases can also be affected. This can disrupt the hydrogen bonding that is crucial for the DNA double helix structure and the accurate replication of DNA. Cancer cells, characterized by their rapid and uncontrolled division, are particularly vulnerable to agents that damage DNA because they have less time to repair the damage before entering the next phase of cell division.

Antimetabolites typically hinder the machinery responsible for DNA replication, either by introducing chemically modified nucleotides (e.g., 5-fluorouracil, 6-mercaptopurine) or by reducing the supply of deoxynucleotides required for DNA replication and cell proliferation (e.g., methotrexate, pemetrexed).^[30,31] They prevent these substances from being incorporated into DNA during the S phase of the cell cycle, thereby halting normal development and cell division.

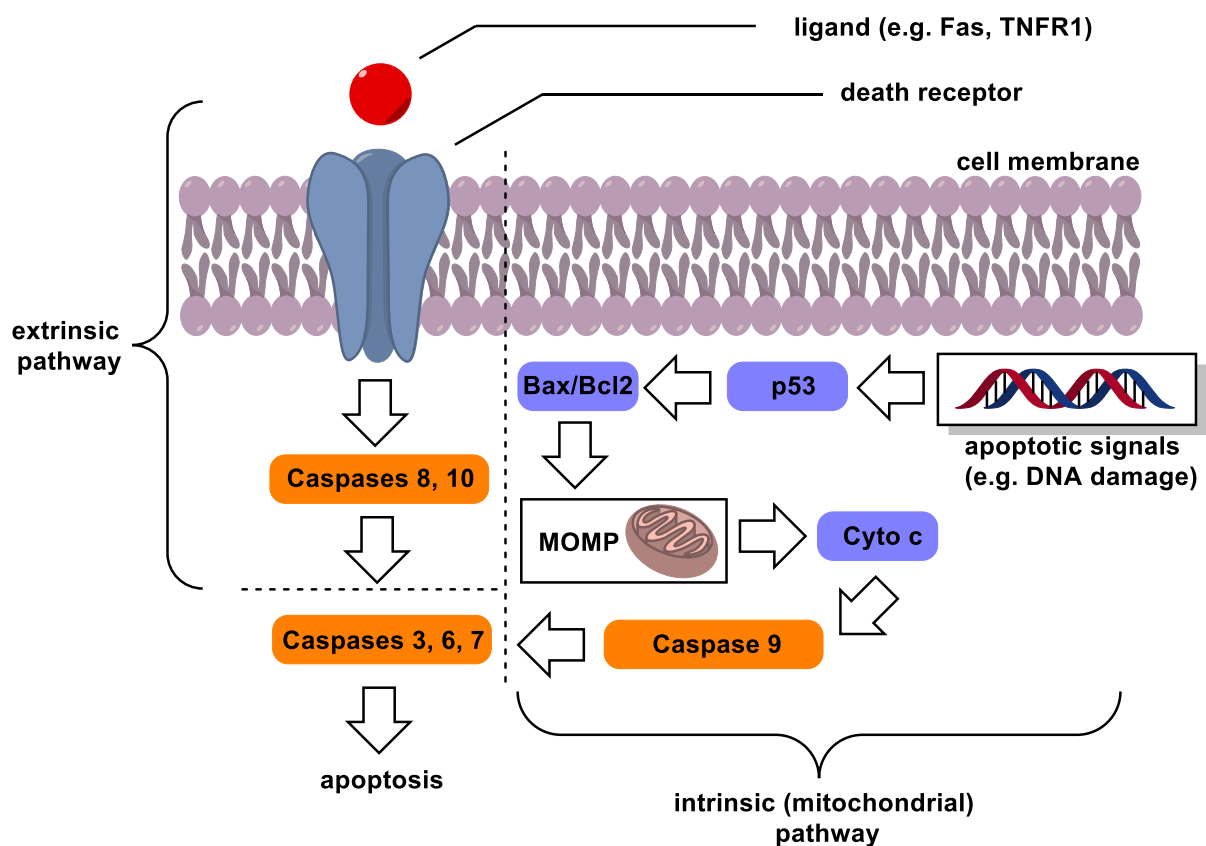
Mitotic inhibitors can work in two different ways: stabilizing microtubules or destabilizing them.^[32,33] Some mitotic inhibitors prevent microtubules from shortening, which is necessary for pulling chromosomes apart during M phase. By stabilizing microtubules, these drugs freeze the mitotic spindle in place, preventing the cell from completing mitosis. An example of a drug that works this way is paclitaxel (Taxol).^[34] Vincristine, on the other hand, is a mitotic inhibitor that prevents microtubule formation, hindering the cell's ability to proceed through mitosis.^[35]

Topoisomerase inhibitors are drugs that interfere with topoisomerases, enzymes essential for DNA replication during the S phase.^[36] Topoisomerase I inhibitors (like irinotecan and topotecan) disrupt DNA replication by causing single-strand breaks and are used against colorectal, ovarian, and lung cancer.^[37] Topoisomerase II inhibitors (such as etoposide and doxorubicin) prevent the repair of double-strand DNA breaks.^[38] They are effective against leukemia, lung, and testicular cancers.

As most common chemotherapeutics affect the cell cycle, rapidly growing cells are more susceptible. This results in a certain selectivity due to the increased proliferation of cancer cells. However, healthy cell types that also grow rapidly are also targeted, leading to several adverse effects such as myelosuppression, alopecia, and nausea, among others.^[39]

1.3. Controlled Cell Death: Apoptosis

Apoptosis is a process of programmed or controlled cell death.^[40] The development of cancer cells into a tumor is not solely due to uncontrolled proliferation but also to a decrease in the rate of cell death.^[41] Unlike the other major mechanism of cell death, necrosis, apoptosis can be actively carried out by the cell itself and is a relevant part of its metabolism. The progress and initiation of apoptosis, therefore, is a tightly controlled process and ensures that the cell disassembles without damaging neighboring tissues, which would result in small, localized inflammations as cytoplasm and cell organelles are released into the extracellular space.^[42,43] This is because once apoptosis has begun, it inevitably leads to the death of the cell. The two best-understood activation mechanisms are the intrinsic pathway and the extrinsic pathway.^[44]



Scheme 1: Simplified overview of the two main apoptosis induction pathways.

The intrinsic pathway (also known as the mitochondrial pathway) is initiated intracellularly as a response to apoptotic signals, whereas the extrinsic pathway is activated by death receptors located outside the cell and plays a crucial role in immune system functions.^[45] Since a common hallmark of cancers is the inactivation of the extracellular death receptors, the next paragraph focuses on the intrinsic pathway.^[46]

Apoptotic signals such as DNA damage, depleted growth factors, and oxidative stress all have an impact on the mitochondria and stimulate changes that result in mitochondrial outer

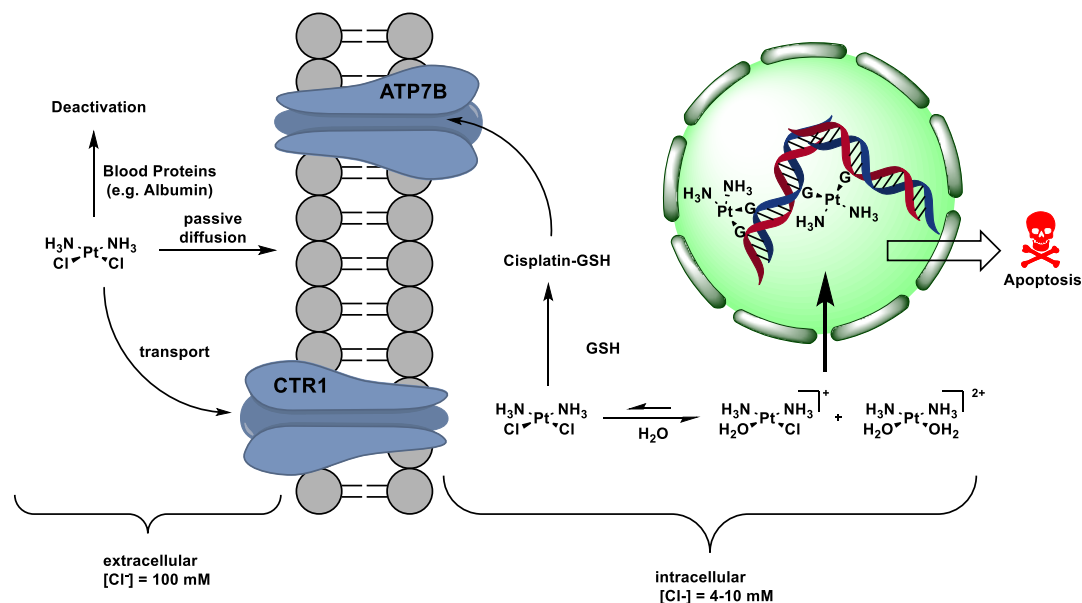
membrane permeabilization (MOMP).^[47] MOMP describes the opening of permeability transition (PT) pores located on the inner mitochondrial membrane (IMM). This process is accompanied by a sudden increase in IMM permeability, which allows ions and water to enter the matrix.^[48] As a result, there is a loss in mitochondrial transmembrane potential and swelling of the matrix.^[49] Consequently, the outer mitochondrial membrane ruptures, releasing pro-apoptotic proteins into the cell's cytoplasm. Additionally, in response to MOMP, vital proteins leak out of the mitochondria, causing the respiratory chain to cease and ATP production to stop, ultimately resulting in cell death.^[47,49] The liberation of the pro-apoptotic protein cytochrome c initiates a very complex signaling cascade of the major group of proteins involved in apoptosis, the caspases.^[50] The two simplified apoptosis pathways are illustrated in **Scheme 1**. The BCL-2 protein family regulates apoptosis, specifically mediating and controlling the events leading to MOMP.^[51] This family includes pro-apoptotic initiators (e.g. Bax, Bak, Puma) and anti-apoptotic inhibitors (e.g. BCL-2). Unfortunately, cancer cells have developed several mechanisms to evade apoptosis.^[52] In B-cell lymphoma, the protein BCL-2 is overexpressed, which promotes cell survival by inhibiting apoptosis.^[53]

1.4. Metallodrugs in Cancer Therapy (Au and Pt)

Although most clinically approved drugs for chemotherapy belong to the class of organic molecules, transition-metal complexes such as cisplatin and its derivatives are also frequently used and listed on the World Health Organization's list of Essential Medicines. However, in recent years, the use of cisplatin and its derivatives has become less dominant due to the emergence of resistant cancer types.^[54] The development and mechanism of action of cisplatin is well studied and will be briefly presented in the following:

When investigating the impact of an electromagnetic field on the proliferative activity of *E. coli* bacteria in 1965, Rosenberg *et al.* discovered that the platinum electrodes used in those experiments were not inert but instead reacted with the medium to form cis-diamminedichloridoplatinum(II).^[55,56] After these initial findings, further experiments revealed that this complex (later abbreviated with just cisplatin) also demonstrates antiproliferative activity in sarcoma 180 and leukemia L1210 in mice, ultimately leading to clinical approval in the USA by 1978.^[57] Regarding the cellular mechanism, cisplatin uptake into the cell is the first step. In theory, this can happen *via* passive diffusion or active transport; however, in the case of cisplatin, it was found that membrane proteins, particularly copper transporters (e.g., CTR1) or organic cationic transporters (OCT) 1-3, mediate the uptake inside the cell.^[58-61] Upon cellular uptake, cisplatin undergoes hydrolysis to form the mono- and di-aqua complexes. These complexes can then reach the nucleus. It is important to note that hydrolysis is inhibited in the blood due to the high chloride concentration (104 mM). However, inside the cell, the chloride concentration is significantly lower (4 mM – 10 mM). After hydrolysis and incorporation into the nucleus, the highly electrophilic complex interacts with the DNA strand. Having the highest basicity among the DNA bases, the N7 position of guanine and adenine is preferentially platinized.^[58] As a result, another DNA base can replace the remaining leaving group (chloride or H₂O), resulting in an irreversible crosslink between the DNA strands. Crosslinks primarily occur within the same DNA strand, resulting in 1,2 intrastrands, but 1,3 intrastrands or interstrands can also occur. However, it has been shown that 1,2 guanosine (GpG) crosslinks are the most common. Following the platination and crosslinking of the DNA, the strands adopt a bent structure. Upon recognition of damaged DNA, cells halt cell cycle progression at the G2/M phase and attempt to repair the damage with the nucleotide excision repair (NER) system to prevent replication of damaged DNA, which could otherwise lead to mutations. If the NER fails to repair the DNA, the cell is commanded programmed cell death (apoptosis). Cisplatin primarily targets DNA, but it can also interact with certain proteins to inhibit DNA repair mechanisms. It shall be noted here that only 5-10% of covalently bound cell-associated cisplatin is present in the DNA fraction. The remaining 75-85% of the drug is estimated to bind with proteins such as human serum albumin (HSA) in the blood and/or the thiol-containing peptide glutathione (GSH) inside the

cell.^[62–64] The resulting cisplatin-GSH adduct is then removed via export pumps during the cellular detoxification program. Overexpression of these pumps, including ATP7B, can lead to cisplatin resistance.^[65] The simplified mode of action of cisplatin is also visualized in **Scheme 2**.



Scheme 2: Simplified schematic overview of the molecular mechanism of cisplatin, including transport, decomposition and DNA cross-linking.

In order to overcome drug resistance related to cisplatin-like drugs, the anticancer properties of different metal complexes were evaluated. The aim was to identify compounds that could overcome certain drug resistances through different cell death mechanisms.^[65] The electronic properties of Au(III) were investigated in relation to those of Pt(II) due to their similar d^8 -configuration and square-planar geometry. However, it was discovered that Au(III) is not stable under physiological conditions and is quickly converted to Au(I). Hence, further research was conducted on linear Au(I) complexes. Auranofin is an early representative of such complexes. It is an orally active antirheumatic agent approved for treatment in 1985. It has also been tested in a phase II clinical study against chronic lymphocytic leukemia, among other conditions.^[66,67]

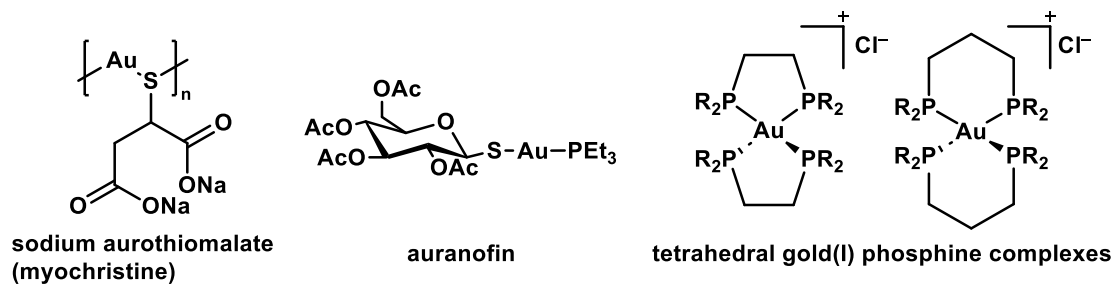
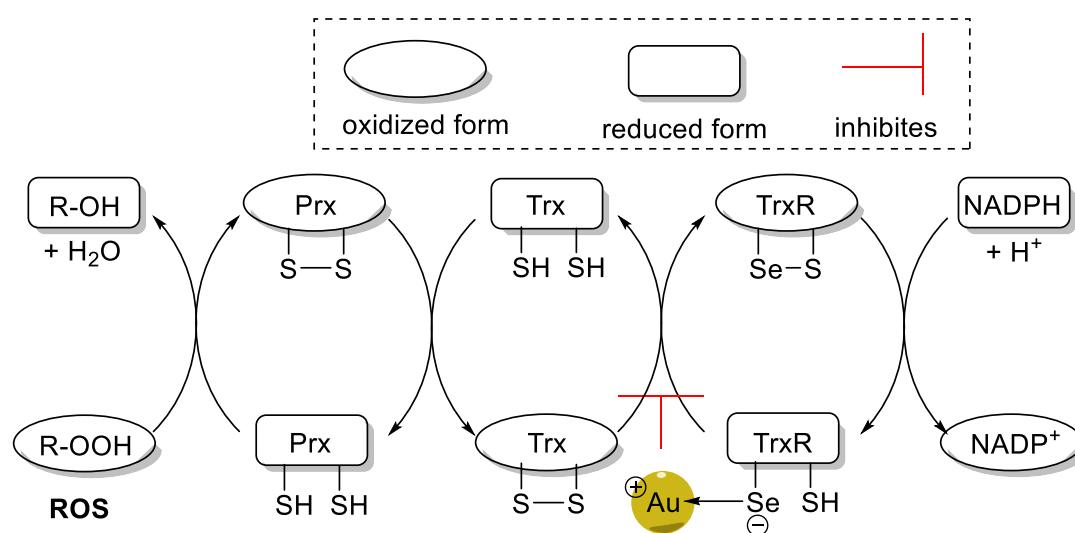


Figure 3: Molecular structures of gold(I) compounds with application in medicine.

After the discovery of auranofin, many Au(I) compounds were studied for medicinal purposes, including cytotoxic, antibacterial, antimalarial, and antioxidant activity.^[68] The use of gold derivatives against uncontrolled cell growth has gained prominence. It was found that the assumption that phosphine ligands are critical for cytotoxic activity is incorrect, and several ligands were investigated for this purpose.^[69] It shall be noted here that phosphines contain cytotoxic activity even without a metal. Furthermore, ligand-exchange reactions under physiological conditions have been found to limit the therapeutic potential of certain treatments due to severe side effects *in vivo*.^[70] To overcome this limitation, tetrahedral gold(I) complexes containing chelating bis-phosphines were developed through clever ligand design.^[71,72] **Figure 3** depicts the molecular structures of several gold(I) compounds that have medicinal applications.

Unlike many Pt-based drugs, gold(I)-compounds were found not to primarily target DNA-related molecules. Instead, many have a high affinity for proteins containing sulfur and selenium,^[73] such as thioredoxin reductase (TrxR) and glutathione peroxidase (GPx), which are often overexpressed in cancer cells.^[74] The inhibition of thioredoxin reductase (TrxR) is the most studied pathway hereof. TrxR is an enzyme that is part of the thioredoxin system and is responsible for the formation of reduced disulfide bonds.^[73,75] The thioredoxin system in mitochondria is briefly illustrated in **Scheme 3**. There are two known forms of the system: mitochondrial TrxR2 and Trx2, and cytosolic TxR1 and Trx1.^[76] Additionally, thioredoxin (Trx) acts as an antioxidant by reducing peroxiredoxin (Prx) and is critical to the survival of cancer cells. This is because levels of reactive oxygen species (ROS) in cancer cells are usually higher than in healthy cells, which leads to the accumulation of reactive oxygen species (ROS), eventually causing apoptosis through the mitochondrial pathway.^[75,77]



Scheme 3: Simplified Illustration of the antioxidant system in mitochondria. Selenophilic Au(I) inhibits the reduction from oxidized Trx by deactivating the enzyme TrxR, leading to a build-up of ROS in the mitochondria. Prx: peroxiredoxin; Trx: thioredoxin TrxR: thioredoxin reductase; ROS: reactive oxygen species.

1.5. Gold(I) Complexes bearing *N*-heterocyclic Carbenes (NHCs) in Medicinal Chemistry

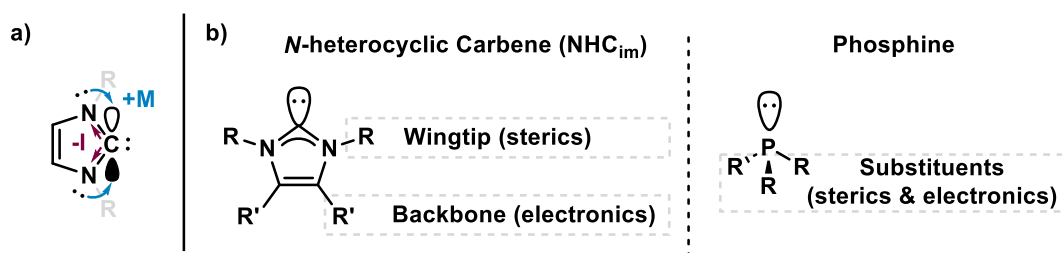
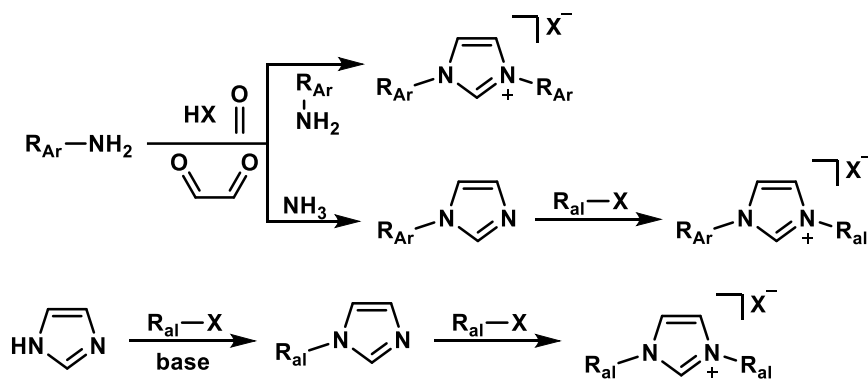


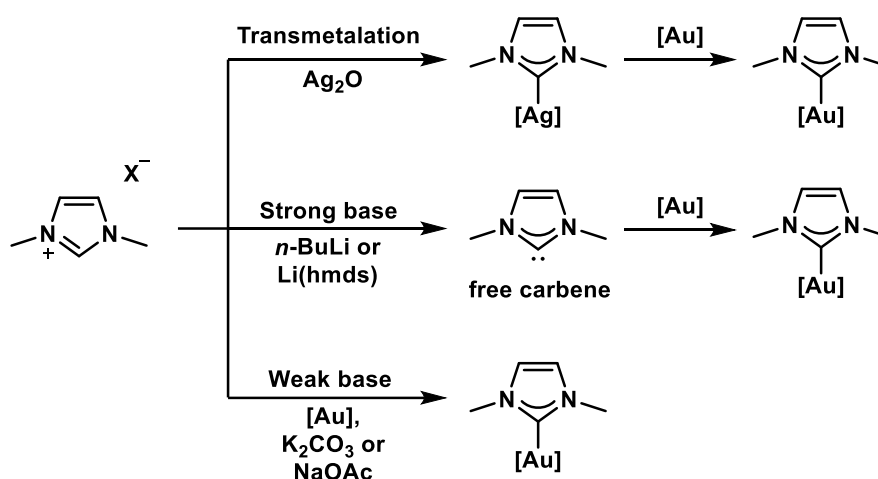
Figure 4: a) Stabilizing interactions on an Arduengo carbene; b) Structural comparison of two prominent ligands for transition metals: An imidazole-based *N*-heterocyclic carbene (NHC_{im}) and a classical phosphine.

An *N*-heterocyclic compound, or NHC, comprises a carbene atom incorporated into a heterocycle with at least one nitrogen atom and, optionally, one or more additional heteroatoms (typically sulfur, oxygen, or phosphorus).^[78] These heterocycles are usually five-membered rings. From the late 20th century, *N*-heterocyclic carbenes were used to stabilize transition metal complexes^[79–81]. In 1991, Arduengo *et al.* even reported the synthesis and crystallographic structure of metal-free imidazole-2-ylidene, demonstrating the persistency of this class of carbenes and coining the name Arduengo carbene.^[82] The success of NHCs can be attributed to the high covalent contribution to the M-NHC bond and their strong σ -donor ability. Compared to phosphines, NHCs show enhanced oxidation stability and more precise fine-tuning possibilities of their steric and electronic characteristics, as depicted in **Figure 4**.^[78] A prominent example is the second-generation Grubbs' olefin metathesis catalyst, where an Arduengo-type NHC substitutes a phosphine ligand on the ruthenium center.^[83] Furthermore, synthesizing NHC ligand precursors and the corresponding complexes is generally simple and versatile.^[84–87] The synthesis of some azolium salt precursors is briefly discussed in the following. Depending on the *N*-substituents of the final product, different synthetic routes are available.^[88] In general, alkyl substituents can readily be introduced in the imidazole system *via* *N*-alkylation with an alkyl-halide as electrophile.



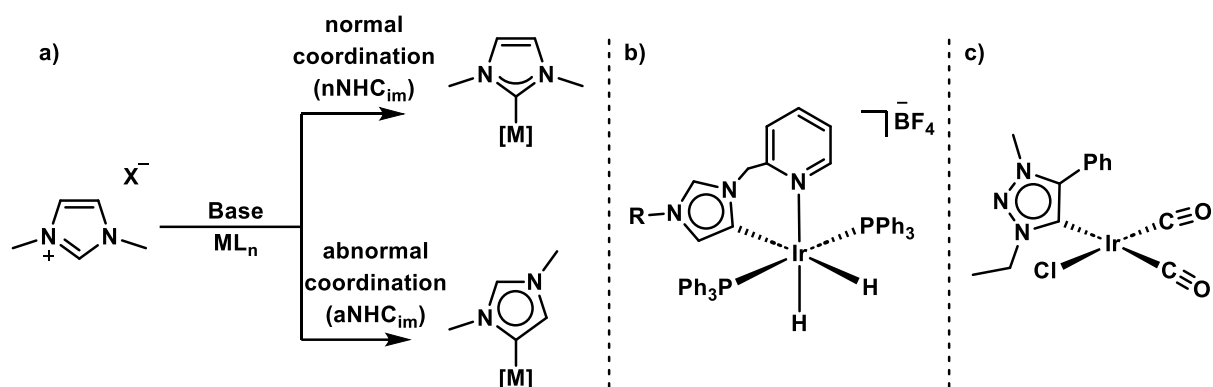
Scheme 4: Overview of synthetic strategies towards *N,N*-disubstituted imidazolium salts, a typical NHC precursor. R_{al} = aliphatic substituent; R_{Ar} = aromatic substituent.

To introduce aryl substituents into the imidazole framework, a condensation reaction of glyoxal, formaldehyde and either one or two aromatic amines is conducted.^[89] When only one aromatic amine is used, the monosubstituted imidazole can then further be *N*-alkylated, yielding a mixed alkyl/aryl imidazolium salt (**Scheme 4**). From the azolium salts, the respective transition-metal complexes can be obtained using different strategies. For Au(I) NHC complexes, the most employed strategies include the transmetalation route with Ag₂O and the weak base route with bases such as K₂CO₃, as depicted in **Scheme 5**.^[90] Nevertheless, the synthesis of Au(I) NHC complexes *via* the internal base route or a modified strong base route has been reported.^[91–93]



Scheme 5: Overview of synthetic routes towards Au(I) NHC_m complexes. Note that those routes are usually also applicable to other azolium salts besides imidazolium. hmnds = hexamethyldisilazide.

In the early 21st century Crabtree and co-workers discovered that besides the C2 carbon atom (between the two nitrogen atoms), the C5 position in the backbone of the imidazolium unit can readily be metalated *via* C-H activation.^[94] Imidazolylidenes with this unusual binding mode were later coined abnormal or mesoionic (aNHC or MIC) carbenes, while the Arduengo carbenes are considered normal carbenes (nNHC) as depicted in **Scheme 6**. 1,2,3-triazoles were already introduced in the beginning of this chapter and the first 1,2,3-triazolylidene transition-metal complexes were reported by Albrecht *et al.* in 2008.^[95,96] Besides the iridium carbonyl complex depicted in **Scheme 6c**), they also reported the synthesis and crystallographic structure of a dinuclear palladium complex and a rhodium complex with this new type of NHC ligand. Because the 1,2,3-triazole framework does not incorporate a carbon atom between two nitrogen atoms, the 1,2,3-triazolylidene ligand can only coordinate in an abnormal fashion and is considered exclusively a mesoionic carbene.^[97] Per definition, mesoionic compounds – the term stems from a combination of the two words mesomeric and zwitterionic – are dipolar heterocyclic structures, with both negative and positive charges being delocalized.^[98]



Scheme 6: a) Normal and abnormal coordination modes of an imidazolylidene to a metal; b) Crabtree *et al.* observed the first transition-metal complex with an abnormally coordinated imidazolylidene moiety: a cationic iridium complex.^[94] c) An iridium carbonyl complex with the mesoionic 1,2,3-triazolylidene ligand, one of several transition-metal complexes with this new ligand type, synthesized by Albrecht *et al.*

It is impossible to satisfactorily represent mesoionic compounds by any one mesomeric structure while following the octet rule, as they are not completely uncharged. A comparison of the NHCs and MICs of different ring sizes reveals that mesoionic carbenes exhibit enhanced σ -donation properties, which can be attributed to the diminished heteroatom stabilization observed in these systems (**Figure 5**).^[99,100] In contrast, the classical $nNHCs$ are more prone to π -backdonation in transition metal complexes.^[97]

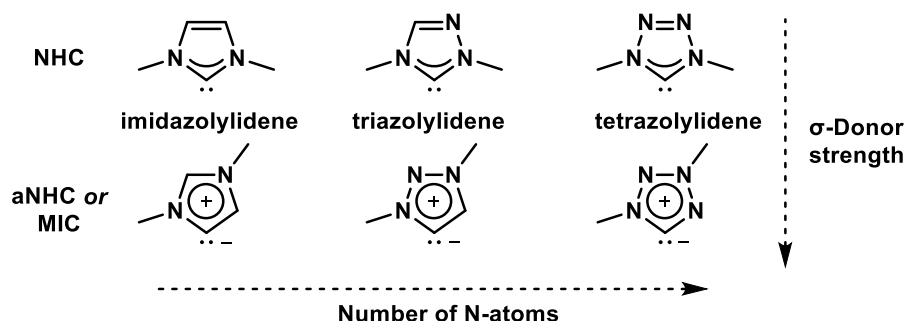


Figure 5: Comparison of different NHCs and aNHCs with respect to their number of heteroatoms and electronic properties.

Although initially exclusively employed in transition metal catalysis, the use of NHCs has also become more prominent in medicinal chemistry since 2004, especially with silver, gold, and ruthenium as a metal center.^[101–103] The use of gold(I) NHC complexes as antitumor agents was pioneered by the group of Berners-Price, where many mechanistic insights and structure-activity relationships of this new class of compounds were investigated.^[77,104–108] These pivotal studies demonstrated that Au(I) NHC complexes - showing characteristics of a delocalized lipophilic cation (DLC) - can selectively target the mitochondria of cancer cells, thereby inducing apoptosis (**Figure 6**). Subsequent studies substantiated the potential of TrxR as a molecular target for a range of other Au(I) complexes, especially those with a labile ligand on the gold center. This was validated by the Ott group, where a series of benzimidazole Au(I) complexes with NHC, phosphine, and chloride ligands were synthesized, and the main findings are briefly discussed in the following.^[109] As expected for the neutral chloro/NHC complex, the

more labile chloride ligand enhances ligand exchange, increasing TrxR inhibition. However, this complex was (due to the labile ligand) also less stable, which was investigated *via* the binding affinity towards serum albumin (a sulfur-containing protein in the blood). The cationic bis-NHC complex demonstrated augmented mitochondrial accumulation and cellular uptake, which is presumed to be attributed to its DLC character. Compared to the neutral NHC complex, the cationic species also exhibited a notable enhancement in cytotoxicity and improved stability toward serum albumin. Recently, we reported the synthesis and nanomolar antiproliferative activity of two mesoionic Au(I) bis-NHC_{trz} complexes.^[110] While selectively inducing apoptosis and overcoming common resistances against etoposide, cytarabine, daunorubicin, and cisplatin, we also demonstrated a synergistic effect in combination with daunorubicin. Also, in our case, the more lipophilic complex bearing mesityl wingtips was more active while both complexes only showed brief TrxR interaction and overcame resistances in several cell lines.

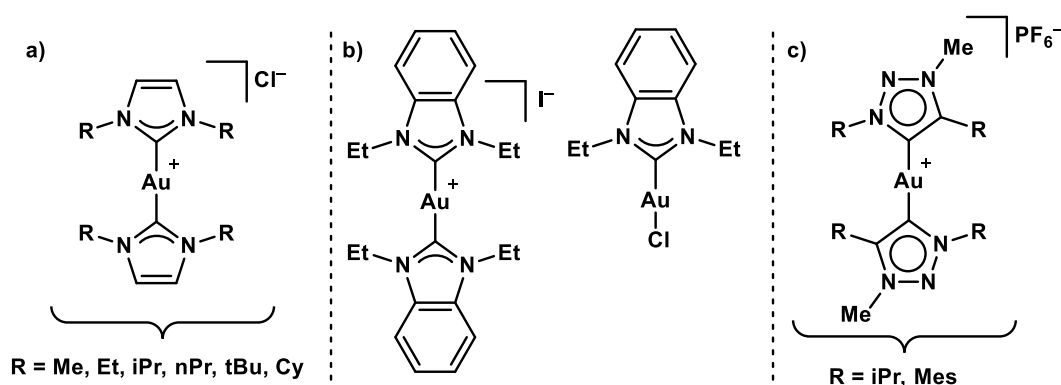


Figure 6: Overview of different Au(I) NHC complexes; besides the chloro complex from b), all shown complexes belong to the class of delocalized lipophilic cations.

In conclusion, it is crucial to guarantee sufficient stability of the Au(I) complexes to prevent undesired premature deactivation and metabolism. From the ligand perspective, NHCs are considered a sweet spot for ensuring the stability of the complexes while also retaining high activity. Furthermore, sterically demanding wingtips shield the gold and impede the attack of the nucleophilic thiol groups. **Figure 7** below summarizes these findings.

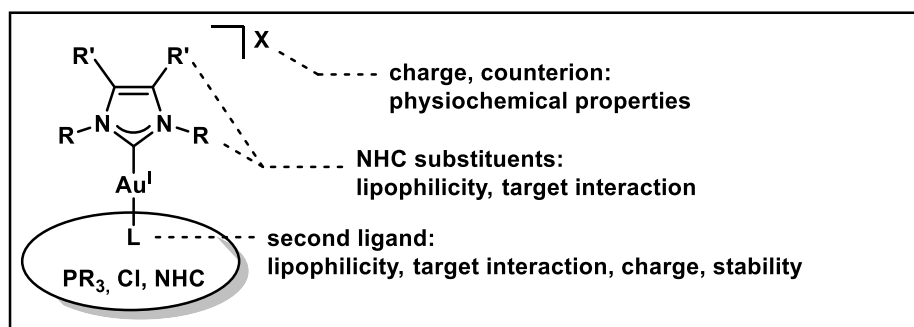
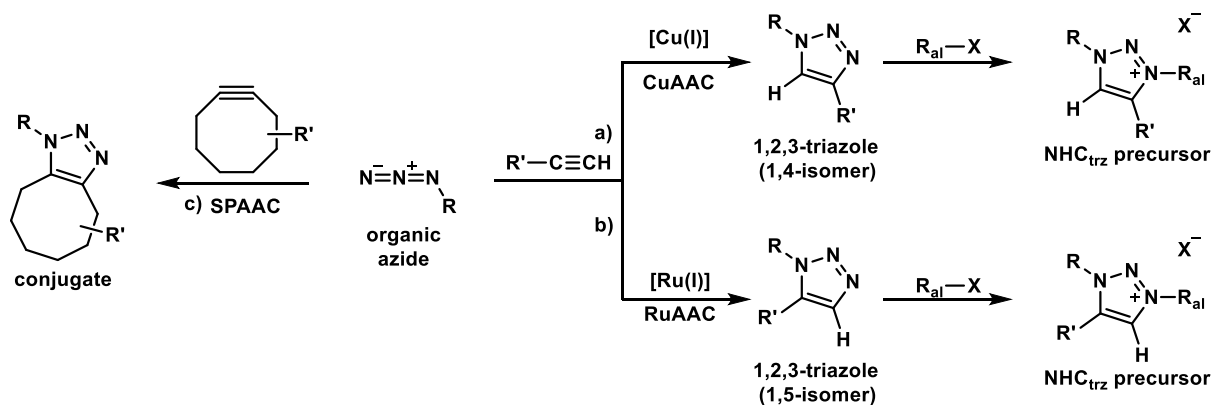


Figure 7: Relevant structural parameters of Au(I) NHC complexes to fine-tune chemical and biological properties for their application in medicinal chemistry.

1.6. Bioorthogonal Click-Chemistry and Other Bioconjugation Reactions

Sharpless et al. coined the term click-chemistry to describe a class of reactions that meet certain criteria. Namely, the reaction must be modular, wide in scope, give very high yields, generate only inoffensive by-products, and be stereospecific.^[111] This can be achieved by ensuring a high thermodynamic driving force of over 20 kJ/mol. Additionally, it is important to use a benign solvent, such as water, and a simple product isolation method, such as crystallization or distillation. The copper-catalyzed azide/alkyne cycloaddition (CuAAC) is a well-known example of click-chemistry. It has evolved from the Huisgen cycloaddition, which required high reaction temperatures and produced a mixture of 1,4- and 1,5-regioisomers of disubstituted 1,2,3-triazoles.^[112] The CuAAC reaction overcomes these limitations by allowing for moderate temperatures and selectively forming the 1,4-regioisomer.^[113,114] This is commonly called the 'click reaction' due to its prominence.^[115] However, other metal-free cycloaddition reactions, such as the strain-promoted azide/alkyne cycloaddition (SPAAC) and the tetrazine ligation, are also valuable tools in organic and bioorganic chemistry. **Scheme 7** provides an overview of the various azide/alkyne cycloaddition variants.

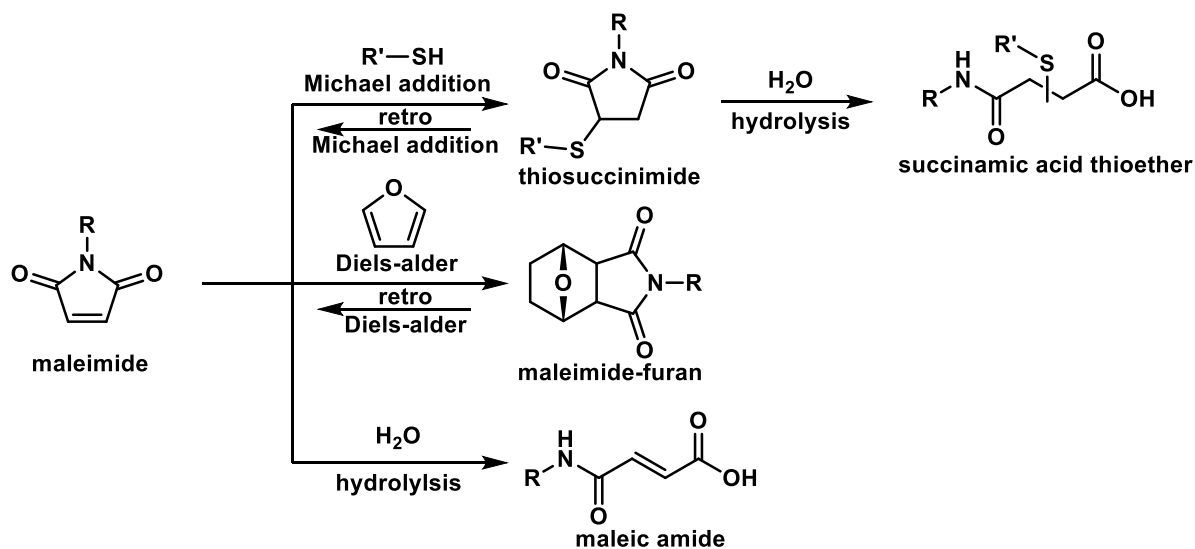


Scheme 7: Azide/alkyne cycloadditions reactions: a) Copper(I)-catalyzed cycloaddition, selectively yielding the 1,4-isomer; upon reaction with alkylation agents (e.g. MeI), the 1,2,3-triazole can be converted to a triazolium salt. c) Strain-promoted cycloaddition, often used for *in vivo* labeling/conjugation.

Click-chemistry has recently become particularly relevant in chemical biology. Sharpless et al. stated in their original paper that 'all searches must be restricted to molecules that are easy to make,' which also applies to the *in vitro* preparation or derivatization of drugs.^[111] Moreover, both reactions are bioorthogonal and only react with specific functional groups rather than amino acids or other biomolecules.^[116] However, it is important to note that copper ions can be toxic to cells. Therefore, the copper-free SPAAC variant is primarily used for *in vivo* labeling of probe molecules through bioconjugation.^[117,118] This is useful for investigating cellular processes, understanding mechanisms, and identifying potential new therapeutic applications.^[116,119–121] Interestingly, another relevant NHC precursor is the 1,2,3-triazolium salt that can be synthesized

from the copper-catalyzed alkyne/azide cycloaddition reaction (CuAAC),^[113] followed by *N*-alkylation at the N3-atom with an alkyl-halide, which is shown in Scheme 7.^[96] It shall be noted here that upon Ru catalysis (RUAAC), the 1,5-regioisomer of the 1,2,3-triazole is selectively formed, which can be further alkylated to also give a 1,2,3-triazolium salt with a different substitution pattern.^[122]

Besides bioorthogonal chemistry, there are various approaches to conjugate smaller molecules to (or even crosslink) large macromolecules like antibodies or peptides. One of the most prominent reactions for site-selective cysteine modification is the maleimide-sulfhydryl ligation, a Michael addition reaction between a thiol and a maleimide functionality.^[123] Even though the resulting thiosuccinimide adduct is prone to thiol exchange reactions or decomposition under physiological conditions, this reaction is still widely employed in chemical biology. Furthermore, the maleimide and the thiosuccinimide adduct readily undergo hydrolysis under physiological conditions, indicating a high base-lability of the maleimide unit. Therefore, when conducting chemical synthesis with molecules containing a maleimide group in basic conditions, protecting the maleimide functional group is necessary.^[124] Suitable protecting groups include furan derivatives. The protection then proceeds upon light heating *via* a Diels-alder reaction and the deprotection under strong heating in a vacuum *via* a retro Diels-alder reaction. Several reaction pathways from maleimide are depicted in **Scheme 8**.



Scheme 8: Reaction pathways from maleimide with different reagents.

1.7. Targeted Therapy: Oncology

Targeted therapy, also known as molecularly targeted therapy, is a major form of medical treatment for cancer.^[125] As a form of molecular medicine, targeted therapy inhibits the growth of cancer cells by disrupting specific molecules required for carcinogenesis and tumor growth rather than affecting all rapidly dividing cells as traditional chemotherapy does. Targeted cancer therapies are anticipated to be more effective and less harmful to normal cells than older forms of treatment. Many targeted therapies are a type of immunotherapy that uses immune mechanisms for therapeutic purposes developed in the field of cancer immunology.^[126,127] Another strategy to achieve targeted therapy is bioconjugation.^[128] As already presented in the previous chapter, bioconjugation is a chemical methodology used to create a stable covalent bond between two molecules, with at least one of them being a biomolecule. Depending on the targeting unit and drug type, several different classes of conjugates are differentiated: antibody-drug conjugates (ADCs),^[129] small molecule-drug conjugates (SMDCs)^[130,131] or antibody-oligonucleotide conjugates (AOCs),^[132,133] among others.^[134,135] All the aforementioned conjugates usually comprise three components: a targeting vector that ideally targets the cancer cell surface and may elicit a therapeutic response, a payload (=drug) that elicits the desired therapeutic response, and a linker that attaches the payload to the antibody (**Figure 8**). Different types of linkers can be used: cleavable and non-cleavable linkers.^[136] A common cleavable linker is ValCit, which is fragmented by the protease cathepsin in the cell's lysosome, releasing the drug from the targeting unit.^[137]

With ADCs, a (clinically approved) monoclonal antibody is used as a targeting vector. The drug-to-antibody ratio (DAR) indicates the level of payload loading on the ADC, where common values lie in the range between 2-6.^[138] Some examples of clinically approved ADCs include brentuximab vedotin (depicted in **Figure 8**):^[139] a CD30 targeting ADC to treat Hodgkin lymphoma, among others; trastuzumab-emtansine:^[140] a HER2+ targeting ADC for breast cancer treatment; inotuzumab ozogamicin:^[140] an ADC containing an antibody against CD22 to target acute lymphoblastic leukemia (ALL).

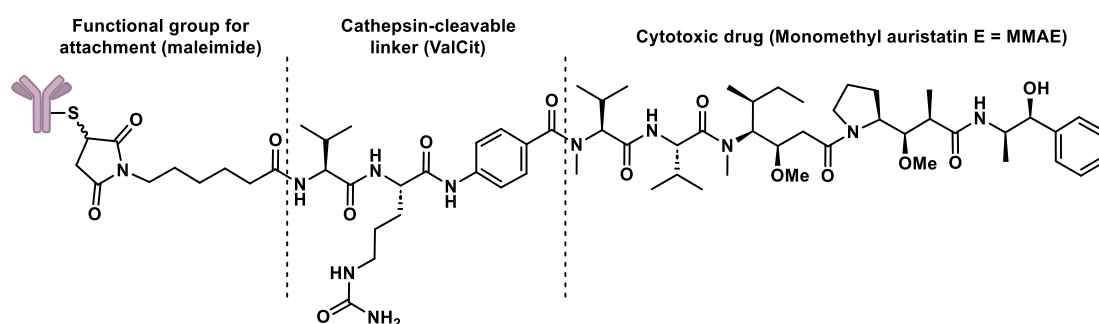


Figure 8: Simplified molecular structure of brentuximab vedotin, a typical antibody-drug conjugate (ADC). It has been available since 2011 under the name Adcetris®.

Although ADCs are currently the most researched conjugates, the targeting vector can also be a smaller molecule. One of the simplest examples of an SMDC is the conjugation of carbohydrates to the drug. Given that cancer cells have a higher energy demand than healthy cell lines, there is an increased uptake of sugars in cancer cells, which might lead to a selectivity increase towards cancer cells. This behavior is often referred to as the Warburg effect.^[141] Besides exploiting the Warburg effect, targeting the folate receptor is another effective way to achieve selectivity toward cancer cells.^[142] As an example, the experimental drug vintafolide, a targeted treatment for platinum-resistant ovarian cancer, was initially developed in 2011 but unfortunately could not surpass phase III clinical trials, and the development was thus stopped in 2014. At the same time, etarfolatide was developed to aid the therapeutic development as a folate-targeting imaging agent (**Figure 9**). Although not including a designated linker moiety, such targeted imaging agents are also becoming more interesting with the evolution of targeted therapy.^[143]

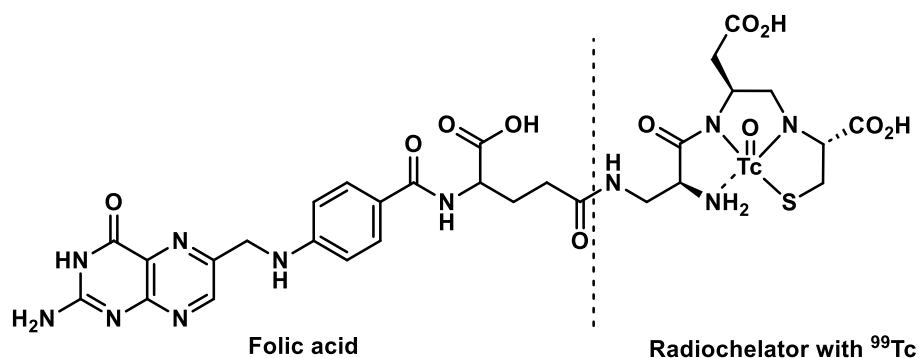


Figure 9: Etarfolatide; an experimental folate-targeting imaging agent used to identify cells that over-express the folate receptor.

1.8. NHC-Au(I) Complexes for Targeted Cancer Therapy: Frameworks and Examples

In addition to stability issues, many gold(I) NHC complexes also exhibit selectivity issues, which prevent the selective targeting of cancer cells or tissues. While some degree of selectivity may be achieved, it is typically not obtained through the rational targeting of specific over-expressed targets in cancer cells. Despite the well-established use of organic molecules in anticancer therapy, the number of inorganic complexes that employ a rational targeting approach to cancer cells remains limited. Several SMDCs based on the Au(I) NHC framework were developed and investigated to reduce adverse effects in cancer patients. In the following, a few examples of Au(I) NHC complexes reported in the literature are briefly discussed, and the molecular structures are depicted in **Figure 10** below.

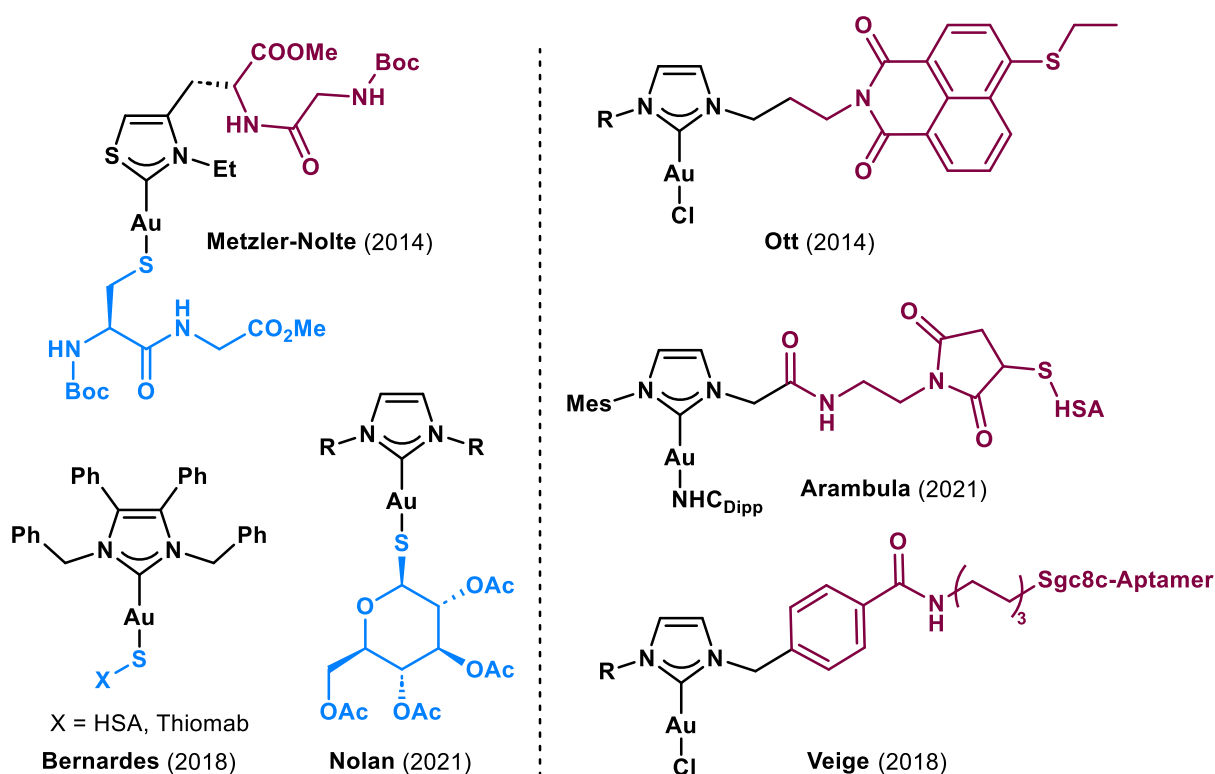


Figure 10: Selection of gold(I) NHC-based conjugates for targeted therapy; HSA = human serum albumin.^[144–149]

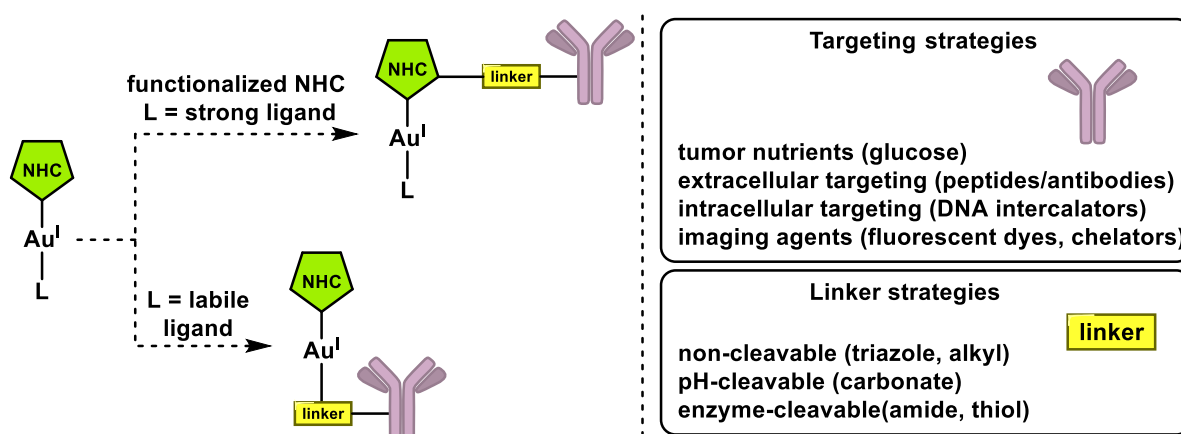
As a prominent example, researchers from the Veige group were the first to conduct a conjugation reaction between an Au(I) NHC complex and a leukemia-specific aptamer (sgc8c) *via* an amidation reaction.^[148] This resulted in the formation of a conjugate that exhibits specific recognition and internalization into leukemia cells without affecting other cells. Moreover, the researchers found that the conjugation of random aptamers resulted in a loss of selectivity and activity, indicating that sgc8c is the primary determinant of effective delivery.^[148] In a 2018 study, the group of Bernardes successfully conjugated an Au(I) NHC complex to

human serum albumin and the approved antibody thiomab (trastuzumab with an additional cysteine for site-specific modification).^[146] The conjugation was conducted via a free cysteine site on either albumin or the antibody. It is regrettable that no appreciable enhancement in selectivity or cytotoxicity was found compared to the Au(I) complex itself.

Intending to develop a potential anticancer drug with multiple modes of action, the group of Ott synthesized and investigated several naphthalimide conjugates of an Au NHC/chloro complex.^[145] Although the compounds were not suitable for fluorescence spectroscopy, it can be concluded that the conjugation of the gold complex (presumably targeting the TrxR enzyme) with the DNA intercalating naphthalimide moiety might be suitable for the design of nonrelated multimodal anticancer agents.

An example of a bis-NHC Au(I) complex that was pre-modified with a carboxylic acid on one of the NHC substituents and then post-conjugated to HSA using a maleimide functionality is reported by the group of Arambula (**Figure 10**).^[149] Interestingly, they have also reported a similar complex that shows non-covalent interactions with HSA by using a naphthalimide moiety (which is also a potent DNA intercalator) instead of maleimide. As a consequence of HSA conjugation, enhanced water solubility was observed for both complexes, although the covalently conjugated complex (also depicted in **Figure 10**) showed reduced cytotoxicity compared to the free complex.

To conclude, several small-molecule-drug-conjugates where the payload consists of a gold(I) NHC framework have already been reported. **Scheme 9** summarizes the targeting approaches for gold(I) NHC compounds.



Scheme 9: Schematic overview of different strategies for implementing a targeting approach into Au(I) NHC complexes

2. Objective

Given that cancer is a leading cause of mortality globally, the treatment of cancer represents a significant and pressing challenge in modern medicine. Among the various therapeutic modalities employed in cancer management, chemotherapy has emerged as a prominent approach. Unfortunately, the current utilization of chemotherapeutic agents is often accompanied by considerable adverse effects and the potential for the emergence of drug resistance in cancer cells. It is, therefore, imperative that new promising anticancer agents are identified. Given their distinctive and divergent characteristics from conventional organic drugs, metal complexes have garnered significant interest from the research community. While cisplatin and a handful of its derivatives have been approved for use as anticancer medications, ongoing research aims to develop superior alternatives.

It has become evident that the class of Au(I) NHC complexes (especially bis-NHC complexes) has become a prominent subject of interest within the field of new anticancer agents. This is due to their selective accumulation in mitochondria and high stability against thiols, which is usually not observed for neutral Au(I) NHC/chloro complexes. Recently, researchers have employed different strategies to functionalize complexes to enable targeted anticancer therapy with the Au(I) NHC framework. In our previous article, it was already proposed that this would be easily achievable with the 1,2,3-triazolylidene framework.^[110] Additionally, to extend the diversity of NHCs and potentially obtain new insights into structure-activity relationships, another new class of mesoionic NHCs, namely tetrazolylidenes, will be investigated for their application as ligands for Au(I) centers.

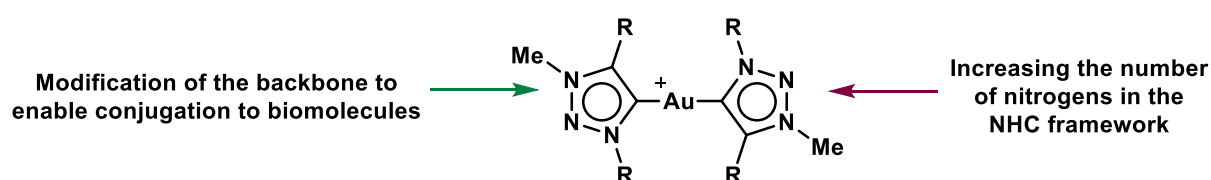


Figure 11: Aims of this thesis: modify the backbone of previously reported 1,2,3-triazolylidene-based Au(I) NHC complexes to enable bioconjugation and investigate other members of the NHC family as ligands for Au(I) complexes for application as anticancer agents.

This thesis presents the chemical synthesis of metal NHC complexes, with a particular focus on Au(I) bis-NHC complexes with mesoionic NHCs, and their potential as anticancer agents. The investigation encompasses the evaluation of their selectivity, stability, and antiproliferative activity. Furthermore, mechanistic studies are conducted to ascertain their suitability for further investigation, including *in vivo* studies. When showing promising properties in initial screening experiments, the complexes can be subjected to further conjugation with biomolecules to enhance their affinity for cancer cells or facilitate imaging and distribution studies.

3. Results: Publication Summaries

3.1. Exploiting click-chemistry: backbone post-functionalisation of homoleptic gold(I) 1,2,3-triazole-5-ylidene complexes

The article "Exploiting click chemistry: Backbone post-functionalization of homoleptic gold(I) 1,2,3-triazole-5-ylidene complexes" reveals a versatile framework for the post-functionalization of gold(I) bis-NHC complexes. This research is driven by the necessity to develop cancer treatments that are more selective and less harmful than current chemotherapy agents. As previously mentioned, conventional chemotherapy, exemplified by the extensively utilized drug cisplatin, frequently results in significant adverse effects and the emergence of drug resistance. Gold-based complexes, particularly those containing N-heterocyclic carbene (NHC) ligands, have recently attracted attention due to their straightforward synthesis and capacity for functionalization.

The synthesis of the ligand precursor is achieved by alkylation of the literature known 1,2,3-triazole bearing two mesityl substituents. To incorporate the versatile azide functionality in the backbone, the reaction of the triazole with a bifunctional iodoalkane is followed by the nucleophilic substitution with sodium azide. From there, the complexation reaction with potassium carbonate proceeded smoothly in high yields, giving the desired product.

The utilization of click chemistry allows us to undertake the post-functionalization of the gold complexes. Two principal techniques were utilized: copper-catalyzed azide-alkyne cycloaddition (CuAAC) and strain-promoted azide-alkyne cycloaddition (SPAAC). These methods permitted the attachment of various biologically relevant molecules to the gold complexes while maintaining their antiproliferative activity. Using an alkyne-modified sugar on the one hand and a substrate suitable for SPAAC, we demonstrated the simple approach as a proof-of-concept. To confirm the structure of the synthesized gold(I) complexes, a range of analytical techniques is employed, including nuclear magnetic resonance (NMR) spectroscopy, mass spectrometry (ESI-MS), and single-crystal X-ray crystallography. The crystal structure revealed that the azide-modified gold complex exhibits a linear geometry around the gold center, with bond lengths consistent with those observed in other gold(I) NHC complexes. These findings corroborate the successful synthesis and proper structural formation of the target complexes. From a medicinal perspective, this research offers considerable promise. The gold(I) complexes exhibited nanomolar antiproliferative effects on cancer cells, and the post-functionalization techniques afforded flexibility in modifying the complex without compromising its biological activity.

3.2. A new class of Gold(I) NHC Complexes with Proapoptotic and Resensitizing Properties towards Multidrug Resistant Leukemia Cells Over-expressing BCL-2

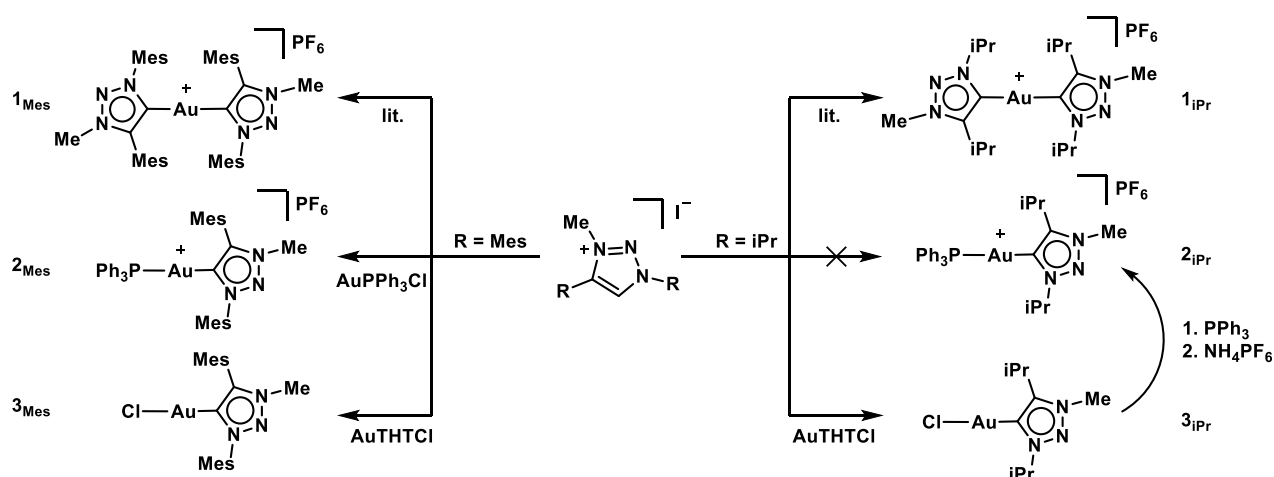
The article focuses on the synthesis and evaluation of novel gold(I) bis-tetrazolylidene complexes with promising proapoptotic and resensitizing properties, specifically targeting multidrug-resistant leukemia cells overexpressing BCL-2. The research is based on the premise that metal-organic gold(I) complexes have antiproliferative properties and seeks to address the challenges posed by cancer cells that develop resistance to common cytostatic drugs, such as doxorubicin. Au(I) complexes incorporating tetrazolylidenes (a rather uncommon type of NHCs) have barely been investigated. The chemical part of the study presents the synthesis pathways for the gold(I) complexes and their ligand precursors. While the ligand precursor with aliphatic substituents was synthesized according to a literature procedure, a new synthesis sequence was developed for the tetrazolium salt bearing aromatic wingtips. The importance of ligand design in ensuring the stability and reactivity of the complexes, particularly for medicinal applications, is also emphasized. Furthermore, the study examines the characterization of the complexes and ligand precursors *via* NMR, ESI-MS, elemental analysis, and HPLC, thereby confirming the successful synthesis and purity of the complexes. In particular, the methyl-substituted gold(I) complex was found to inhibit the growth of malignant cells and induce apoptosis selectively, with no signs of necrosis, even in drug-resistant cells. This finding is significant in that it represents a potential avenue for overcoming multidrug resistance, which is crucial for expanding treatment options for cancer patients. The study underscores the possibility that the complex may engage the mitochondrial pathway in apoptosis and target members of the BCL-2 family, thereby positioning it as a prospective therapeutic agent for resistant cancer cells. The biological evaluation of gold(I) complex 1 revealed a notable inhibition of cell proliferation and the induction of apoptosis in leukemia cells without signs of necrosis. The results of the flow cytometry analysis indicated that the complex effectively induced early apoptosis with minimal necrotic effects. Moreover, the complex demonstrated high efficacy in the low nanomolar range, with an IC_{50} value of 0.014 μ M, indicating its potential as a potent anti-cancer agent. The findings suggest that these complexes, particularly gold(I) complex 1, may serve as promising resensitizing agents for multidrug-resistant leukemia cells, offering a novel avenue for cancer treatment. The study's emphasis on overcoming drug resistance and minimizing side effects through targeted mechanisms of action establishes these gold complexes as valuable contributions to metallothrapeutics. Lastly, the gold(I) complex not only targets doxorubicin-resistant cells but also resensitizes them to doxorubicin, making it a promising therapeutic option for cancer recurrence.

4. Unpublished Results

This chapter presents an overview of the unpublished results of the doctoral thesis. The majority of the presented projects were conducted in collaboration with several partners who possess high expertise in the fields of medicine and biology/radiopharmacy. The author of this thesis made significant contributions to the chemical synthesis and characterization of the tested compounds. Additionally, the author conducted several biological and radiopharmaceutical assays during his training (Erasmus+) in early 2023.

4.1. Synthesis and antiproliferative effects of a series of Au(I) 1,2,3-triazolydene NHC/chloro and NHC/phosphine complexes

Following a pioneering study by the group of Ott, where a series of benzimidazolydene gold(I) complexes was investigated for their antiproliferative activity and molecular mechanism of action,^[150] this project aims to evaluate the properties of a series of 1,2,3-triazolydene based gold(I) complexes. Previously, we have demonstrated the high potential of the respective bis-NHC complexes for medicinal applications,^[110] where in this study, the synthesis and characterization, as well as the antiproliferative activity and DFT studies of a series of Au(I) 1,2,3-triazolydene complexes with a trans chloro- or phosphine-ligand are presented.



Scheme 10: Synthesis pathways to all gold(I) NHC/chloro and NHC/phosphine complexes from the respective ligand precursors.

The synthesis of all compounds is depicted in **Scheme 10**. For synthesizing the two heteroleptic Au(I) complexes, **2_{Mes}** and **3_{Mes}**, we followed the silver–route, using Ag₂O as a transmetalation agent and as an internal base. Variation of the stoichiometry of the reagents in our previously published synthetic procedure gave analytically pure **3_{Mes}** as indicated by NMR spectroscopy, ESI–MS, and elemental analysis. An additional variation of the gold(I) precursor from AuTHTCl to AuPPh₃Cl gave the pure NHC/Phosphine complex **2_{Mes}** as the only product. However, this rather straightforward approach did not apply to the synthesis of the two heteroleptic complexes containing iPr wingtip substituents. This is due to the observation that the equimolar reaction of AuTHTCl and Ag₂O with the triazolium salt yielded a mixture of **1_{iPr}** and **3_{iPr}**, as indicated by TLC, NMR, and ESI-MS. As the variation of the reaction time did not favor **3_{iPr}**, we then decided to exploit the stark difference in polarity between the neutral **3_{iPr}** and the cationic **1_{iPr}**, resulting in a modified procedure, where filtration over silica subsequent to the reaction removes all impurities and gives analytically pure **3_{iPr}** in good yields. Different from **2_{Mes}**, the synthesis of the heteroleptic **2_{iPr}** did not proceed as smoothly. The direct synthesis *via* the silver route using **iPr** and AuPPh₃Cl gives an indifferent mixture of products. After investigating

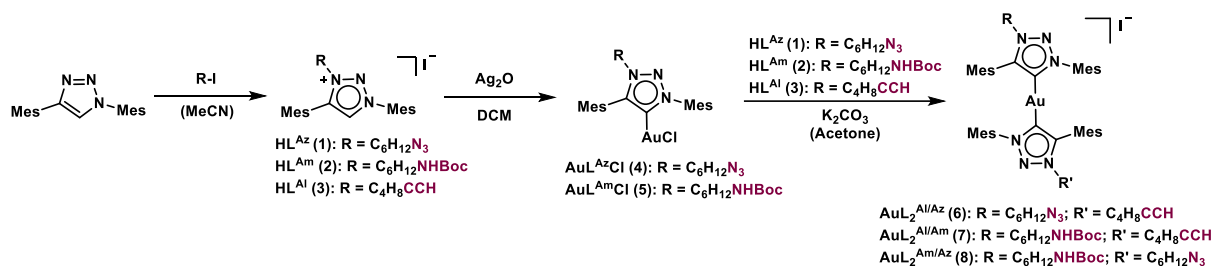
several possible approaches, the most promising reaction was the substitution of the weak chlorine ligand of **3_{iPr}** with PPh₃ in acetone in the presence of NH₄PF₆, as already described in the literature for imidazole-based complexes.^[106] This method finally yields compound **2_{iPr}** in high purity and good yields. The antiproliferative activity of the complexes was investigated via the MTT Assay in two human cancer cell lines. As previously shown, the activity of the compounds is strongly affected by the wingtip substituents and charge. Interestingly, when compared to the previously reported bis-NHC complexes **1_{Mes}** and **1_{iPr}**, the NHC/phosphine compounds **2_{Mes}** and **2_{iPr}** show identical activity in human ovarian cancer cells. However, in breast cancer cells, the phosphine-containing complexes show a significantly lower activity, for which we currently do not have an explanation. The NHC/chloro complexes **3_{Mes}** and **3_{iPr}**, on the other hand, displayed the lowest activity of the series. The respective IC₅₀ values are six to tenfold higher than the respective NHC/phosphine complexes. This might result from a lower stability towards nucleophiles and, thus, a faster decomposition in the cellular medium. The stability of the new complexes was evaluated in time-resolved NMR experiments in a deuterated PBS/DMSO mixture at 37°C, where none of the complexes showed signs of decomposition after 48 h. DFT studies were conducted to estimate the bond dissociation energy of the NHC-Au-L bond. The values are also found in **Table 1**. From the BDE values, it becomes clear that the removal of a NHC ligand from the gold is (as expected) the energetically most unfavorable. In contrast to a previous study,^[150] the removal of the phosphine ligand from the gold center is energetically more favorable than the removal of chlorine. To further evaluate the mechanism, TrxR affinity experiments are to be conducted. So far, it can be concluded that the trend previously found for benzimidazolylidene gold(I) complexes is also applicable to the respective 1,2,3-triazolylidene compounds.

Table 1: Bond dissociation energies and IC₅₀ values (μM) ± SD of the presented complexes in the human cancer cell lines A2780 (ovarian cancer) and MCF7 (breast cancer) after 48 h of incubation determined by the MTT assay. The hybrid functional, including dispersion and long-range correction wB97XD/gen, was used, and the def2-SVP basis set was applied for small atoms. For Au the aug-cc-pVDZ relativistic effective core potential (ECP) and its respective basis was utilized.

Compound	A2780 (ovarian)	MCF7 (breast)	BDE (DMSO) [kJ/mol]
1_{Mes} ^[110]	0.36 ± 0.09	0.084 ± 0.016	359.77
2_{Mes}	0.36 ± 0.07	2.52 ± 1.15	232.40
3_{Mes}	1.77 ± 0.6	14.7 ± 4.5	255.71
1_{iPr} ^[110]	1.30 ± 0.28	0.42 ± 0.11	301.17
2_{iPr}	1.34 ± 0.41	1.70 ± 0.59	217.16
3_{iPr}	10.3 ± 2.3	17.2 ± 4.1	252.46

4.2. Investigation of backbone-functionalized heteroleptic bis-NHC complexes

Following the incorporation of a reactive azide moiety into a symmetrical gold(I) bis 1,2,3-triazolylidene complex,^[151] the respective heteroleptic complexes with two different functional groups were considered the next step on the path to efficient, targeted therapy. Thus, in this project, three bis-NHC gold(I) complexes bearing azide, amine, and alkyne functional groups were synthesized, characterized, and evaluated for their potential as antiproliferative agents. The synthesis pathway to the heteroleptic complexes is shown in **Scheme 11**.



Scheme 11: Synthesis pathway to heteroleptic gold(I) bis-1,2,3-triazolylidene complexes with terminal functionalities.

For both ligand precursors, very good yields and straightforward product isolation by precipitation were achieved for the reaction in MeCN. The successful synthesis was verified by ¹H- and ¹³C-NMR spectroscopy, elemental analysis, and ESI-MS. Aimed to selectively synthesize the heteroleptic complexes without obtaining significant amounts of homoleptic by-products, we investigated several routes and obtained the best results for a two-step procedure via the intermediate Au(NHC)Cl species (often referred to as NHC/chloro or mono NHC complex). Hence, following the silver route (Ag₂O as a base), two novel gold(I) NHC/chloro complexes were synthesized from the ligand precursors. The resulting azide and amine (Boc-protected) complexes AuL^{Az}Cl and AuL^{Am}Cl were obtained in quantitative yields, and the synthesis is again verified by ¹H- and ¹³C-NMR spectroscopy, elemental analysis, and ESI-MS. Unfortunately, synthesizing the NHC/chloro complex from the HL^{Al} ligand precursor did not yield the desired product. This likely originates from the terminal alkyne functional group interacting with the transmetalation agent, forming an Ag/Au alkyne species, although this route has been successful for shorter spacers. Consequently, three heteroleptic bis-NHC gold complexes could be obtained by further reacting the two NHC/chloro complexes with the ligand precursors *via* the weak base route. For the synthesis of bis-NHC complexes **6** and **8**, complex **4** was reacted with the respective ligand. Complex **7** was obtained by reacting **5** with the alkyne functionalized ligand precursor **3**. The preliminary results of the apoptosis induction properties are presented in **Table 2** below. Interestingly, the azide-modified triazolium salt shows higher activity than

the two other ligand precursors. Similarly, the amine/azide-modified heteroleptic complex **9** displays reduced apoptosis induction potential compared to complexes **7** and **8**.

Table 2: Apoptosis induction potential of a series of 1,2,3-triazole based ligand precursors and gold(I) bis-NHC complexes. 72h incubation; DNA fragmentation *via* flow cytometry.

Compound	Nalm-6
HL ^{Az} (1)	< 0.5 μ M
HL ^{Am} (2)	0.5 μ M
HL ^{Al} (3)	0.5 μ M
AuL ₂ ^{Al/Az} (7)	0.1 μ M
AuL ₂ ^{Al/Am} (8)	0.1 μ M
AuL ₂ ^{Am/Az} (9)	0.5 μ M

4.3. Synthesis and antiproliferative effects of a series of Au(I) tetrazolylidene NHC/chloro complexes

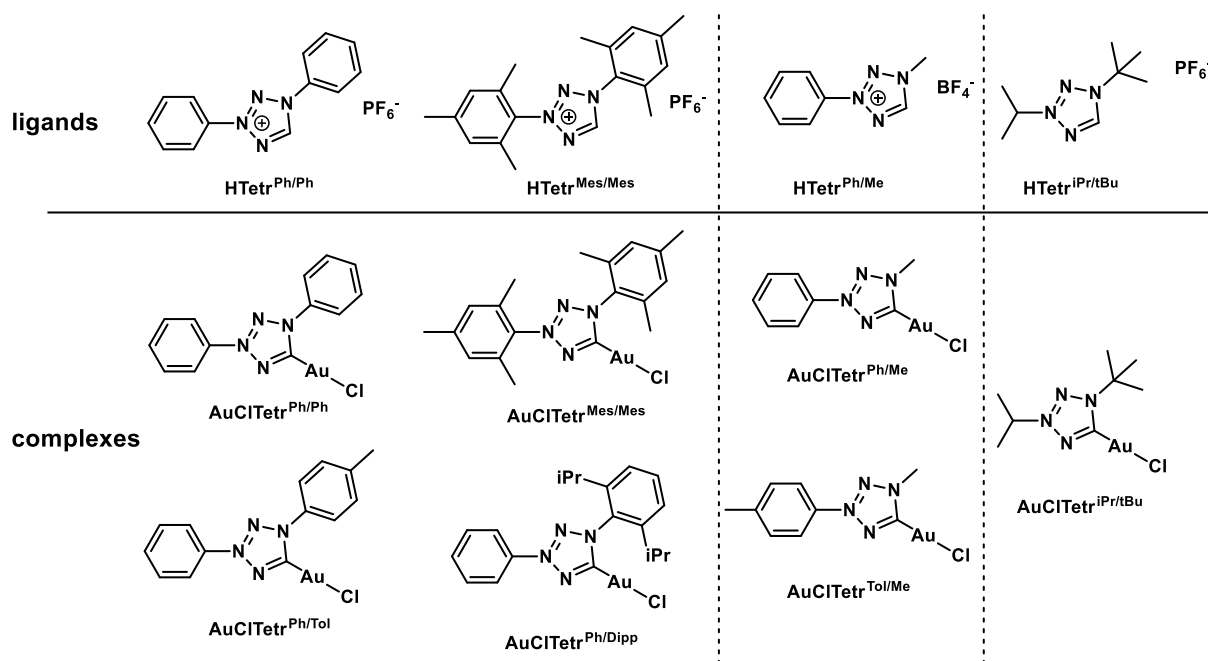


Figure 12: Overview of the synthesized gold(I) tetrazolylidene/chloro complexes.

The literature on tetrazolylidene gold complexes is relatively scarce.^[93,100,152] Therefore, a conclusive study revealing a possible structure-activity relationship of this unexplored class of compounds is of high interest. A series of Au(I) tetrazolylidene NHC/chloro complexes was synthesized, characterized, and investigated for their antiproliferative activity. As evident from **Figure 12**, the substituents on the tetrazole moiety are varied from aromatic to aliphatic. For each of the three different substitution patterns (aromatic/aromatic; aromatic/aliphatic, and aliphatic/aliphatic), a different synthetic pathway is necessary. Stability tests were conducted *via* NMR experiments, where none of the tested complexes showed signs of decomposition in wet DMSO-*d*⁶ at 37°C for up to 72 h. Considering the preliminary medicinal results, a few things can be concluded:

Firstly, for all tested ligands, low ligand toxicity was observed (the mesityl-substituted ligand precursor shows the highest antiproliferative activity in the high micromolar range). As previously demonstrated, this is not always the case for azolium salts in general.

Secondly, it seems to be the general trend that all compounds (including cisplatin and auranofin) are more active in ovarian cancer cells than in lung cancer cells. When comparing the antiproliferative effects of the gold(I) tetrazolylidene/chloro complexes to more established antiproliferative inhibitors like cisplatin and auranofin in the two human cancer cell lines, it becomes evident that the ones bearing two aryl substituents (especially Ph/Ph, Ph/Tol, and

Mes/Mes) have a comparable activity. Furthermore, those three compounds show significantly less activity in the non-cancerous VERO cells, potentially demonstrating a selectivity increase toward cancer cells. **Table 3** summarizes the results from the MTT assays. Additionally, the selectivity index (SI) was calculated for the two cancer cell lines. Again, the complexes with Ph/Ph, Ph/Tol, and Mes/Mes substituents significantly exceed the SIs for cisplatin and auranofin *in vitro*, making them promising candidates for chemotherapy with reduced adverse effects.

Table 3: MTT assay after 72 h incubation, n > 3, IC₅₀ in μM . SI: Selectivity index = $\text{IC}_{50}^{\text{non-cancerous}}/\text{IC}_{50}^{\text{cancerous}}$

Compound	A2780 (ovarian)	A549 (lung)	VERO (non- cancerous)	SI^{A2780}, SI^{A549}
Cisplatin	0.46 ± 0.12	6.07 ± 1.14	1.56 ± 0.33	3.40, 0.257
Auranofin	0.21 ± 0.03	7.14 ± 1.61	5.46 ± 1.71	26, 0.765
HTetr^{Ph/Ph}	42.71 ± 10.53	>100	>100	-
HTetr^{Mes/Mes}	13.05 ± 2.22	21.95 ± 5.59	47.27 ± 4.03	3.62, 2.15
HTetr^{Ph/Me}	>100	>100	>100	-
HTetr^{iPr/tBu}	>100	>100	>100	-
AuClTetr^{Ph/Ph}	0.35 ± 0.20	3.35 ± 0.39	25.87 ± 2.18	73.9 , 7.72
AuClTetr^{Ph/Tol}	0.34 ± 0.17	3.71 ± 0.77	21.48 ± 3.46	63.2 , 5.79
AuClTetr^{Ph/Dipp}	0.88 ± 0.12	13.34 ± 3.71	10.23 ± 3.23	11.6, 0.767
AuClTetr^{Mes/Mes}	0.23 ± 0.13	10.89 ± 1.15	19.95 ± 4.64	86.7 , 1.83
AuClTetr^{Ph/Me}	0.15 ± 0.03	27.22 ± 0.63	11.01 ± 2.95	73.4, 0.404
AuClTetr^{Tol/Me}	0.39 ± 0.24	24.44 ± 9.30	10.84 ± 1.67	27.8, 0.444
AuClTetr^{iPr/tBu}	0.27 ± 0.17	41.34 ± 14.61	22.47 ± 2.67	83.2, 0.544

4.4. Structure-activity relationship of a variety of antiproliferative azolium salts.

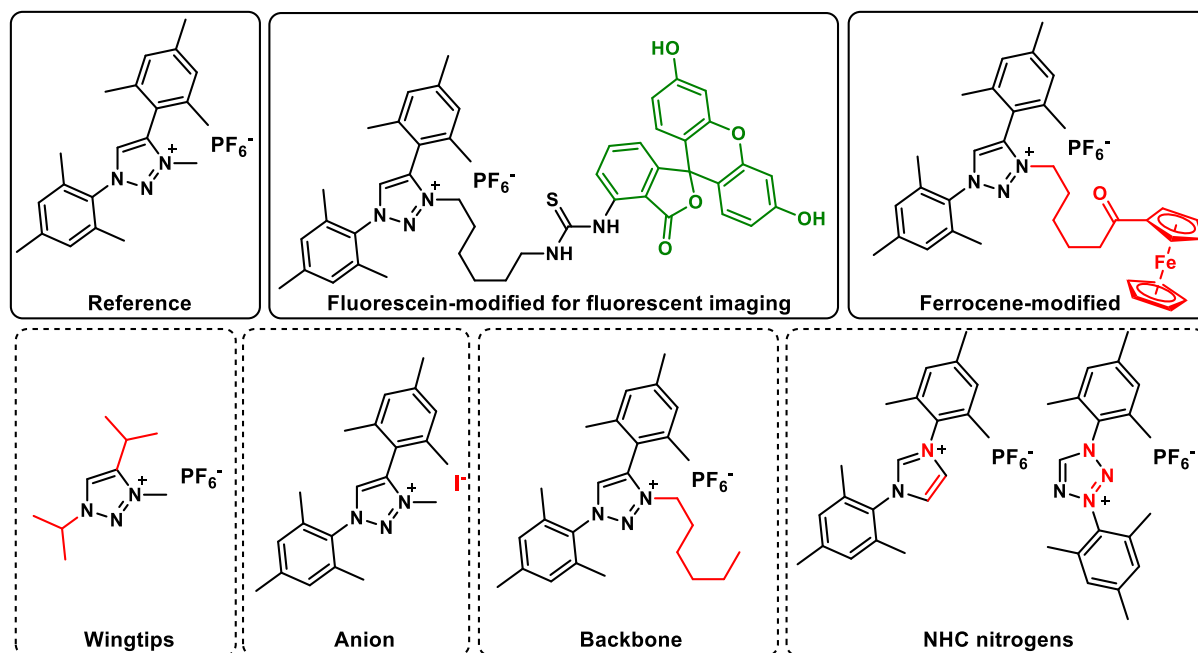


Figure 13: Overview of all synthesized azolium salts.

In previous experiments, it became evident that specific azolium salts also demonstrated a significant antiproliferative activity *in vitro* presumably *via* ROS generation.^[153–155] To further evaluate the structural features that favor a higher activity and to get insights into the mechanism of action, a series of azolium salts were synthesized and investigated with respect to their apoptosis induction in Nalm-6 cells (**Figure 13**). Some of the presented compounds are synthesized following procedures reported in the literature, while others were only obtained after multiple optimization iterations. Currently, the following trends can be observed from the preliminary apoptosis induction experiments in Nalm-6 cells (**Table 4**):

Firstly, the variation of the anion (PF₆ to I) and the reduction of the NHC nitrogens (1,2,3-triazole to imidazole) does not seem to significantly influence the activity in Nalm-6 cells. Secondly, alterations in the backbone and wingtips have a substantial effect: substituting the mesityl wingtips with *i*Pr leads to complete activity loss. Furthermore, the elongation of the backbone to a hexyl chain significantly increases the activity.

Thirdly, the elevation of the NHC nitrogens (1,2,3-triazole to tetrazole) with the combined relocation again leads to a completely diminished activity. Lastly, modifying the triazolium salt with ferrocene (potentially enhancing the ROS generation potential) slightly increased the apoptosis induction, although it was still less inferior than with just an aliphatic hexyl chain in the backbone. Further experiments with the fluorescein-modified triazolium salt aim toward the evaluation of the cellular distribution.

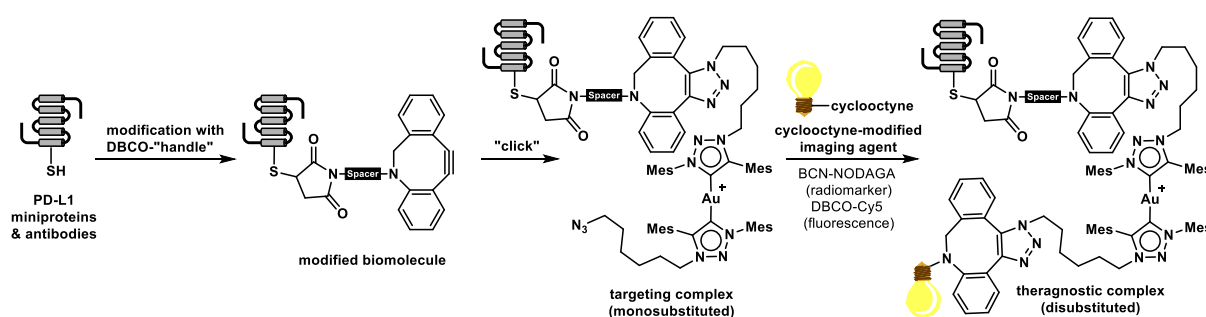
Table 4: Apoptosis induction potential of a series of azolium salts. 72h incubation; DNA fragmentation *via* flow cytometry.

Compound	Nalm-6
Fluorescein-modified	To be tested
Ferrocene-modified	< 0.5 μ M
Reference	1 μ M
Wingtips (iPr)	No activity
Anion (I⁻)	1 μ M
Backbone	< 0.05 μ M
Imidazole	1 μ M
Tetrazole	No activity

4.5. Bioconjugation of a homoleptic azide functionalized Au(I) 1,2,3-triazolydene complex with antibodies and miniproteins to enable targeted delivery for cancer therapy

With the development of new conjugates for targeted therapy in mind, we envisioned using the azide-functionalized gold bis-NHC framework for conjugation to various biomolecules and (radio-)markers for subsequent evaluation *in vitro* and *in vivo*.

Initially, with an ADC in mind, atezolizumab (and bevacizumab) was modified with DBCO-Maleimide to then further react with one of the terminal azides on the homoleptic gold(I) bis-NHC complex (**Scheme 12**). Unfortunately, this two-step approach led to low product concentrations of the ADC, rendering this pathway rather tedious. Several experiments were conducted to optimize the reaction *via* LC-MS, and for conjugate purification, membrane dialysis was found to be superior to amicon® filters. The complex was added in significant excess to avoid reactivity towards the second azide functionality and to ensure high conversion. Additionally, antibody precipitation was observed for high concentrations of the gold complex. To overcome both problems with the ADC, a PEG spacer can be incorporated between the complex and the antibody, leading to a significantly higher product concentration and reduced precipitation. The fluorescent dye DBCO Cy5 was used to label the ADC as verified by in-gel fluorescence, and a gradual accumulation of the ADC in A20 tumors was observed in the mouse model *in vivo* during IVIS imaging experiments. The radio-labeling of the ADC with ^{67}Ga using a BCN-NODAGA chelator was achieved, although the low yields during the ADC synthesis hindered the further optimization of the low radiochemical yields. **Scheme 12** highlights the conjugate synthesis, starting from the unmodified biomolecule.



Scheme 12: Synthetic steps for post-modifying a gold(I) bis-1,2,3-triazolydene complex, leading to a potentially theragnostic compound.

To increase the yields of the conjugate, instead of antibodies, the synthesis of a protein drug conjugate bearing a miniprotein (115 AA; 13 kDa) that targets PD-L1 was investigated. With the now obtained higher yields, the resulting theragnostic gold complexes were tested for their

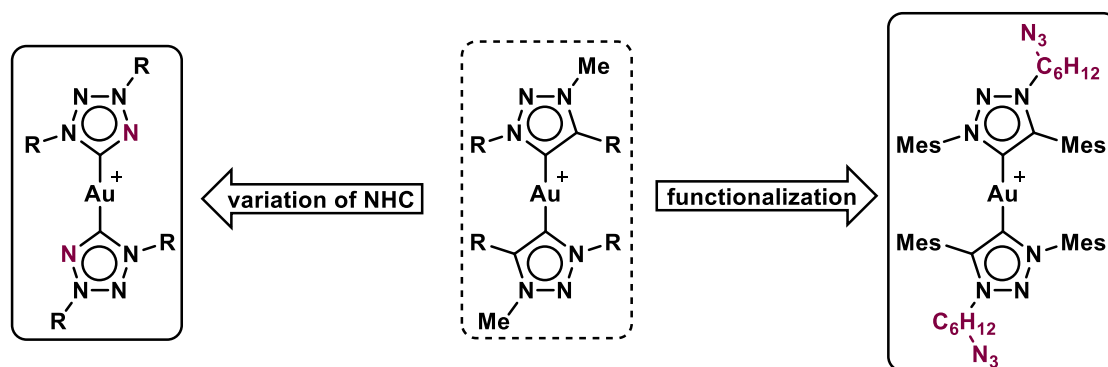
cellular viability in A20 cells (PD-L1 expressing B-cell lymphoma; mouse), where the conjugate (IC_{50} : 0.35 μ M in A20; 0.33 μ M in MC38) shows comparable antiproliferative activity than the isolated gold(I) bis-NHC complex (IC_{50} : 0.78 μ M in A20; 0.35 μ M in MC38). The conjugate was then successfully radiolabeled with ^{67}Ga , following the identical strategy mentioned above. Biodistribution studies in A20 cancer-inoculated mice demonstrated good tumor accumulation of the conjugate, although some off-target uptake was observed. Interestingly, conjugating the gold bis-NHC NODAGA fragment to the miniprotein changes the biodistribution pattern. While the tumor targeting is similar, the conjugate shows higher blood persistence and lower kidney uptake than the “gold-free” maleimide NODAGA-labeled miniprotein.

5. Conclusion and Outlook

This thesis describes the synthesis, characterization, and medicinal evaluation of a series of Au(I) NHC complexes as potential anticancer agents. Given the high stability of the Au-NHC bond, primarily bis-NHCs were employed to ensure sufficient stability under biological conditions. A significant emphasis is placed on the synthesis of Au(I) complexes, given their distinct mechanism of action in comparison to the current metallodrugs like cisplatin that may potentially facilitate the overcoming of current resistances. The complexes bearing a functional group allow for further bioconjugation, enabling the selective targeting of cancer cells. All suitable complexes are subjected to *in vitro* antiproliferative activity testing (MTT assays), and the most promising complexes undergo further investigation into their mechanism of action.

Modifying the 1,2,3-triazole ligand precursor with the terminal azide moiety represents a novel framework useful for post-modifying Au(I) bis-NHC complexes. In a proof-of-principle study, all complexes exhibit remarkable antiproliferative activity in human cancer cell lines, with IC₅₀ values that are several orders of magnitude lower than those of cisplatin in the tested cell lines. The post-functionalization of the presented framework with a modified biomolecule (peptide, antibody) in tandem with a clickable radio chelator or fluorescence marker thus resembles the next step on the path to theragnostic Au(I) complexes.

Besides the modification of existing ligands, another part of this thesis was the investigation of new NHC frameworks, of which the barely explored tetrazolylienes (NHC_{tetr}) were considered especially promising. The resulting Au(I) bis-NHC_{tetr} complexes have been demonstrated to be highly potent cytostatic agents, capable of inducing high apoptosis rates in a range of cancer cell lines, even at concentrations as low as the nanomolar range. The complex bearing mesityl substituents exert a markedly more potent effect on leukemia cells than previously investigated gold complexes. The selective and controlled induction of apoptosis was demonstrated *in vitro* without significant signs of necrosis. Mechanistic studies indicate that this class of complexes induces apoptosis via the mitochondrial pathway, which is consistent with the findings observed for other gold(I) NHC complexes. One target of particular interest is TrxR, which plays a direct role in regulating ROS levels. Given that the Au(I) tetrazolyliene complex elevates the ROS levels of the investigated cells, TrxR may represent a viable target. Furthermore, when the complex is combined with anthracyclines, apoptosis rates in the nanomolar range are observed in previously resistant cells. The occurrence of adverse effects associated with high concentrations of individual pharmaceutical agents can be diminished through the exploitation of such synergistic interactions.



Scheme 13: Visual summary of the outcomes of this thesis. Anions are omitted for clarity.

Besides the already published research, the presented unpublished results of this thesis are aimed at investigating the structure-activity relationships of azolium salts and different series of mesoionic gold(I) NHC complexes.

Further modifying the ligand-centered terminal azide functionality on the complex of the bifunctional triazole framework with antibodies and miniproteins on one side and imaging agents on the other side and consequently evaluating the resulting (potentially) theragnostic complexes *in vitro* and *in vivo* is achieved and poses a next big step towards targeted therapy with gold(I) NHC complexes.

Currently, the modification of the ligand backbone to host a cleavable linker (such as ValCit) and a maleimide and/or tetrazine functionality for effortless bioconjugation is conducted with promising preliminary results. Nevertheless, extensive *in vitro* and *in vivo* experiments are to be conducted to validate the advantages of the post-functionalization of the presented complexes and, thus, the therapeutic potential.

6. Reprint Permissions

- 6.1.1. **Richter, L. F.**, Marques, F., Correia, J. D., Pöthig, A., & Kühn, F. E. (2023). Exploiting click-chemistry: backbone post-functionalisation of homoleptic gold (i) 1, 2, 3-triazole-5-ylidene complexes. *Dalton Transactions*, 52(46), 17185-17192.

Authors contributing to RSC publications (journal articles, books or book chapters) do not need to formally request permission to reproduce material contained in this article provided that the correct acknowledgement is given with the reproduced material. If you are the author of this article you still need to obtain permission to reproduce the whole article in a third party publication with the exception of reproduction of the whole article in a thesis or dissertation.

- 6.1.2. Bannwart, F., **Richter, L. F.**, Stifel, S., Rueter, J., Lode, H. J., Correia, J. D., Kühn, F.E., & Prokop, A. (2024). A New Class of Gold (I) NHC Complexes with Proapoptotic and Resensitizing Properties towards Multidrug Resistant Leukemia Cells Overexpressing BCL-2. *Journal of Medicinal Chemistry*, 67 (17), 15494-15508.

This publication is licensed under CC-BY-NC-ND 4.0, meaning this is an open-access article under the terms of the Creative Commons Attribution License, which permits use and distribution in any medium, provided the original work is properly cited, the use is non-commercial, and no modifications or adaptations are made.

7. Bibliographic Data of First Author Publications

7.1. Royal Society of Chemistry (RSC)

Exploiting click-chemistry: backbone post-functionalisation of homoleptic gold(I) 1,2,3-triazole-5-ylidene complexes

Leon F. Richter,^a Fernanda Marques,^b João D. G. Correia,^b Alexander Pöthig,^c and Fritz E. Kühn^{a,*}

^aTechnical University of Munich, TUM School of Natural Sciences, Department of Chemistry and Catalysis Research Center, Molecular Catalysis, Lichtenbergstr. 4, 85748, Garching bei München, Germany. E-mail: fritz.kuehn@ch.tum.de

^bCentro de Ciências e Tecnologias Nucleares and Departamento de Engenharia e Ciências Nucleares, Instituto Superior Técnico, Universidade de Lisboa, CTN, Estrada Nacional 10 (km 139, 7), 2695-066 Bobadela LRS, Portugal

^cTechnical University of Munich, TUM School of Natural Sciences, Department of Chemistry; Catalysis Research Center, Lichtenbergstr. 4, 85748 Garching bei München, Germany

* corresponding author

Dalton Trans., **2023**,52, 17185-17192

Direct Link: <https://doi.org/10.1039/D3DT03052K>

7.2. American Chemical Society (ACS)

A New Class of Gold(I) NHC Complexes with Proapoptotic and Resensitizing Properties towards Multidrug Resistant Leukemia Cells Overexpressing BCL-2

Franziska Bannwart,^{a,b,*} Leon F. Richter,^c Simon Stifel,^c Johanna Rueter,^{a,b} Holger N. Lode,^d João D. G. Correia,^e Fritz E. Kühn,^{c,*} and Aram Prokop^{a,b,f,*}

^aDepartment of Pediatric Hematology/Oncology, Helios Kliniken Schwerin, Wismarsche Str. 393-397, 19055 Schwerin, Germany

^bDepartment of Human Medicine, MSH Medical School Hamburg, Am Kaiserkai 1, 20457 Hamburg, Germany

^cDepartment of Chemistry and Catalysis Research Center, Molecular Catalysis, Technical University of Munich, TUM School of Natural Sciences, Lichtenbergstr. 4, 85748 Garching bei München, Germany

München, Germany

^dDepartment of Pediatric Hematology/Oncology, University Medicine Greifswald, Ferdinand-Sauerbruch-Str. 1, 17475 Greifswald, Germany

^eCentro de Ciências e Tecnologias Nucleares and Departamento de Engenharia e Ciências Nucleares, Instituto Superior Técnico, Universidade de Lisboa, Bobadela, Lisbon, LRS 2695-066, Portugal

^fExperimental Oncology, Municipal Hospitals of Cologne, Ostmerheimer Str. 200, 51109 Cologne, Germany

* corresponding authors

§ equally contributing authors

Journal of Medicinal Chemistry, **2024**, 67 (17), 15494-15508.

Direct Link: <https://pubs.acs.org/action/showCitFormats?doi=10.1021/acs.jmedchem.4c01117&ref=pdf>

7.3. Elsevier

MULA, an affordable framework for multifunctional liquid automation in natural- and life sciences with a focus on hardware design, setup, modularity and validation

Leon F. Richter,[§] Wolfgang Büchele,[§] Alexander Imhof and Fritz E. Kühn*

Technical University of Munich, TUM School of Natural Sciences, Department of Chemistry and Catalysis Research Centre, Molecular Catalysis, Lichtenbergstr. 4, 85748, Garching bei München, Germany. E-mail: fritz.kuehn@ch.tum.de

* corresponding author

§ equally contributing authors

HardwareX., **2024**, 20

Direct Link: <https://www.sciencedirect.com/science/article/pii/S2468067224000750>

8. Complete List of Publications

8.1. Journal Articles (Peer-reviewed)

- 8.1.1. **Richter, L. F.**, Marques, F., Correia, J. D., Pöthig, A., & Kühn, F. E. (2023). Exploiting click-chemistry: backbone post-functionalisation of homoleptic gold (i) 1, 2, 3-triazole-5-ylidene complexes. *Dalton Transactions*, 52(46), 17185-17192. <https://doi.org/10.1039/D3DT03052K>
- 8.1.2. Bannwart, F., **Richter, L. F.**, Stifel, S., Rueter, J., Lode, H. J., Correia, J. D., Kühn, F.E., & Prokop, A. (2024). A New Class of Gold (I) NHC Complexes with Proapoptotic and Resensitizing Properties towards Multidrug Resistant Leukemia Cells Overexpressing BCL-2. *Journal of Medicinal Chemistry*, 67 (17), 15494-15508. <https://doi.org/10.1021/acs.jmedchem.4c01117>
- 8.1.3. **Richter, L. F.**, Büchele, W. R., Imhof, A., & Kühn, F. E. (2024). MULA, an affordable framework for multifunctional liquid automation in natural-and life sciences with a focus on hardware design, setup, modularity and validation. *HardwareX*, 20. <https://doi.org/10.1016/j.ohx.2024.e00581>
- 8.1.4. Sauer, M. J., **Richter, L. F.**, Offorjindu, J., Reich, R. M., & Kühn, F. E. (2024). Synthesis and characterization of Markó-type (NHC) Pt (dvtms) complexes and their evaluation in the hydrosilylation reaction of alkenes. *Journal of Organometallic Chemistry*, 1005, 122995. <https://doi.org/10.1016/j.jorganchem.2023.122995>
- 8.1.5. Schlachta, T. P., Sauer, M. J., **Richter, L. F.**, & Kühn, F. E. (2024). Formation of a diiron-(μ - η^1 : η^1 -CN) complex from acetonitrile solution. *Crystal Structure Communications*, 80(9). <https://doi.org/10.1107/S2053229624007058>
- 8.1.6. Schlachta, T. P., **Richter, L. F.**, & Kühn, F. E. (2024). Chiral imidazolium and triazolium salts as NHC and aNHC ligand precursors: A promising framework for asymmetric epoxidation catalysis. *Results in Chemistry*, 7, 101421. <https://doi.org/10.1016/j.rechem.2024.101421>
- 8.1.7. Büchele, W. R., Schlachta, T. P., Gebendorfer, A. L., Pamperin, J., **Richter, L. F.**, Sauer, M. J., Prokop, A. & Kühn, F. E. (2024). Synthesis, characterization, and biomedical evaluation of ethylene-bridged tetra-NHC Pd (ii), Pt (ii) and Au (iii) complexes, with apoptosis-inducing properties in cisplatin-resistant neuroblastoma cells. *RSC advances*, 14(15), 10244-10254. <https://doi.org/10.1039/d4ra01195c>

8.2. Conference Contributions

8.2.1. **International Conference of Coordination Chemistry (ICCC)**, Colorado (USA)

A new class of Gold(I) NHC Complexes with Proapoptotic and Resensitizing Properties towards Multidrug Resistant Leukemia Cells Over-expressing BCL-2

Authors: **Richter, L. F.**, Bannwart, F., Stifel, S., Rueter, J., Lode, H. J., Correia, J. D., Kühn, F.E., & Prokop, A. **2024**, Poster presentation.

8.3. Others

8.3.1. Using Microelectronics to Visualise Stereochemistry and Explain Chirality: an Interactive Model of Tartartic Acid; **published on Printables**: <https://www.printables.com/model/1026677-using-microelectronics-to-visualise-stereochemistr>

8.3.2. 3D Printing in Science; a Chemists Perspective; **submitted to PrusaResearch**

9. Figures, Schemes and Tables

Figure 1: Number of worldwide cancer incidences and deaths in 2022 ^[3]	9
Figure 2: Schematic illustration of the eucaryotic cell cycle, including the checkpoints.....	11
Figure 3: Molecular structures of gold(I) compounds with application in medicine.....	17
Figure 4: a) Stabilizing interactions on an Arduengo carbene; b) Structural comparison of two prominent ligands for transition metals: An imidazole-based N-heterocyclic carbene (NHC _{im}) and a classical phosphine.....	19
Figure 5: Comparison of different NHCs and aNHCs with respect to their number of heteroatoms and electronic properties.....	21
Figure 6: Overview of different Au(I) NHC complexes; besides the chloro complex from b), all shown complexes belong to the class of delocalized lipophilic cations.....	22
Figure 7: Relevant structural parameters of Au(I) NHC complexes to fine-tune chemical and biological properties for their application in medicinal chemistry.....	22
Figure 8: Simplified molecular structure of brentuximab vedotin, a typical antibody-drug conjugate (ADC). It has been available since 2011 under the name Adcetris®.....	25
Figure 9: Etarfolatide; an experimental folate-targeting imaging agent used to identify cells that over-express the folate receptor.....	26
Figure 10: Selection of gold(I) NHC-based conjugates for targeted therapy; HSA = human serum albumin. ^[145–150]	27
Figure 11: Aims of this thesis: modify the backbone of previously reported 1,2,3-triazolylidene-based Au(I) NHC complexes to enable bioconjugation and investigate other members of the NHC family as ligands for Au(I) complexes for application as anticancer agents.....	29
Figure 12: Overview of the synthesized gold(I) tetrazolylidene/chloro complexes.....	37
Figure 13: Overview of all synthesized azolium salts.....	39
Scheme 1: Simplified overview of the two main apoptosis induction pathways.....	14
Scheme 2: Simplified schematic overview of the molecular mechanism of cisplatin, including transport, decomposition and DNA crosslinking.....	17
Scheme 3: Simplified Illustration of the antioxidant system in mitochondria. Selenophilic Au(I) inhibits the reduction from oxidized Trx by deactivating the enzyme TrxR, leading to a build-up of ROS in the mitochondria. Prx: peroxiredoxin; Trx: thioredoxin TrxR: thioredoxin reductase; ROS: reactive oxygen species.....	18
Scheme 4: Overview of synthetic strategies towards N,N-disubstituted imidazolium salts, a typical NHC precursor. R _{al} = aliphatic substituent; R _{Ar} = aromatic substituent.....	19
Scheme 5: Overview of synthetic routes towards Au(I) NHC _{im} complexes. Note that those routes are usually also applicable to other azolium salts besides imidazolium. hm ₆ = hexamethyldisilazide.....	20
Scheme 6: a) Normal and abnormal coordination modes of an imidazolylidene to a metal; b) Crabtree et al. observed the first transition-metal complex with an abnormally coordinated imidazolylidene moiety: a cationic iridium complex. ^[95] ; c) An iridium carbonyl complex with the mesoionic 1,2,3-triazolylidene ligand, one of several transition-metal complexes with this new ligand type, synthesized by Albrecht et al.....	21
Scheme 7: Azide/alkyne cycloadditions reactions: a) Copper(I)-catalyzed cycloaddition, selectively yielding the 1,4-isomer; upon reaction with alkylation agents (e.g. MeI), the 1,2,3-triazole can be converted to a triazolium salt. c) Strain-promoted cycloaddition, often used for in vivo labeling/conjugation.....	23
Scheme 8: Reaction pathways from maleimide with different reagents.....	24
Scheme 9: Schematic overview of different strategies for implementing a targeting approach into Au(I) NHC complexes.....	28
Scheme 10: Synthesis pathways to all gold(I) NHC/chloro and NHC/phosphine complexes from the respective ligand precursors.....	33
Scheme 11: Synthesis pathway to heteroleptic gold(I) bis-1,2,3-triazolylidene complexes with terminal functionalities.....	35
Scheme 12: Synthetic steps for post-modifying a gold(I) bis-1,2,3-triazolylidene complex, leading to a potentially theragnostic compound.....	41
Scheme 13: Visual summary of the outcomes of this thesis. Anions are omitted for clarity.....	44

10. Literature

- [1] G. M. Cooper, D. Ganem, *Nat. Med.* **1997**, *3*, 1042.
- [2] D. P. Tabassum, K. Polyak, *Nat. Rev. Cancer* **2015**, *15*, 473–483.
- [3] “Global Cancer Observatory (GCO) Population World Factsheet,” can be found under <https://gco.iarc.who.int/media/globocan/factsheets/populations/900-world-factsheet.pdf>, **2022**.
- [4] “Global cancer burden growing, amidst mounting need for services,” can be found under <https://www.who.int/news/item/01-02-2024-global-cancer-burden-growing-amidst-mounting-need-for-services>, **2024**.
- [5] S. S. Hecht, D. K. Hatsukami, *Nat. Rev. Cancer* **2022**, *22*, 143–155.
- [6] “Why is cancer so hard to cure?,” can be found under <https://www.worldwidecancerresearch.org/news-opinion/2022/september/why-is-cancer-so-hard-to-cure/>, **2022**.
- [7] K. Bukowski, M. Kciuk, R. Kontek, *Int. J. Mol. Sci.* **2020**, *21*, 3233.
- [8] H. M. Coley, *Cancer Treat. Rev.* **2008**, *34*, 378–390.
- [9] E. S. Kim, *Lung Cancer Pers. Med. Curr. Knowl. Ther.* **2016**, 189–209.
- [10] L. Wyld, R. A. Audisio, G. J. Poston, *Nat. Rev. Clin. Oncol.* **2015**, *12*, 115–124.
- [11] R. Baskar, K. A. Lee, R. Yeo, K.-W. Yeoh, *Int. J. Med. Sci.* **2012**, *9*, 193.
- [12] E. Chu, A. C. Sartorelli, *Lange’s Basic Clin. Pharmacol.* **2018**, 948–976.
- [13] B. A. Chabner, T. G. Roberts Jr, *Nat. Rev. Cancer* **2005**, *5*, 65–72.
- [14] J. A. Collins, J. M. Blake, P. G. Crosignani, *Hum. Reprod. Update* **2005**, *11*, 545–560.
- [15] I. H. Abdulkareem, I. B. Zurmi, *Niger. J. Clin. Pract.* **2012**, *15*.
- [16] A. Huang, X. R. Yang, W. Y. Chung, A. R. Dennison, J. Zhou, *Signal Transduct. Target. Ther.* **2020**, *5*.
- [17] A.-M. Tsimberidou, *Cancer Chemother. Pharmacol.* **2015**, *76*, 1113–1132.
- [18] M. Alle, G. Sharma, S.-H. Lee, J.-C. Kim, *J. Nanobiotechnology* **2022**, *20*, 222.
- [19] P. Ehrlich, A. Bertheim, *Berichte der Dtsch. Chem. Gesellschaft* **1912**, *45*, 756–766.
- [20] S. Riethmiller, *Chemotherapy* **2005**, *51*, 234–242.
- [21] D. Schumacher, B. Karsten, J. P. Teifke, K. Wink, N. Osterrieder, *J. Gen. Virol.* **2002**, *83*, 1987–1992.
- [22] Y. Ni, Z. Zhang, L. Engelskircher, G. Verch, T. Tu, F. A. Lempp, S. Urban, *Sci. Rep.* **2019**, *9*, 1–14.

- [23] O. Fritsche, *Biologie Für Einsteiger: Prinzipien Des Lebens Verstehen*, Springer-Verlag, **2015**.
- [24] S. P. Bell, A. Dutta, *Annu. Rev. Biochem.* **2002**, *71*, 333–374.
- [25] G. M. Cooper, R. Hausman, *A Molecular Approach*, **2000**.
- [26] T. Enoch, C. Norbury, *Trends Biochem. Sci.* **1995**, *20*, 426–430.
- [27] J. Bartek, J. Lukas, *Curr. Opin. Cell Biol.* **2001**, *13*, 738–747.
- [28] P. K. Mandal, G. W. Collie, B. Kauffmann, I. Huc, *Acta Crystallogr. Sect. D Struct. Biol.* **2022**, *78*, 709–715.
- [29] M. Hollstein, D. Sidransky, B. Vogelstein, C. C. Harris, *Science* **1991**, *253*, 49–53.
- [30] G. J. Peters, C. L. Van der Wilt, C. J. A. Van Moorsel, J. R. Kroep, A. M. Bergman, S. P. Ackland, *Pharmacol. Ther.* **2000**, *87*, 227–253.
- [31] S. B. Kaye, *Br. J. Cancer* **1998**, *78*, 1–7.
- [32] N. Jiang, X. Wang, Y. Yang, W. Dai, *Mini Rev. Med. Chem.* **2006**, *6*, 885–895.
- [33] A. C. Henriques, D. Ribeiro, J. Pedrosa, B. Sarmiento, P. M. A. Silva, H. Bousbaa, *Cancer Lett.* **2019**, *440*, 64–81.
- [34] M. Markman, T. M. Mekhail, *Expert Opin. Pharmacother.* **2002**, *3*, 755–766.
- [35] M. Abal, J. M. Andreu, I. Barasoain, *Curr. Cancer Drug Targets* **2003**, *3*, 193–203.
- [36] B. K. Sinha, *Drugs* **1995**, *49*, 11–19.
- [37] Y. Pommier, *Nat. Rev. Cancer* **2006**, *6*, 789–802.
- [38] C. A. Felix, *Med. Pediatr. Oncol.* **2001**, *36*, 525–535.
- [39] Brianna, S. H. Lee, *Med. Oncol.* **2023**, *40*, 88.
- [40] A. Lawen, *Bioessays* **2003**, *25*, 888–896.
- [41] D. Hanahan, R. A. Weinberg, *Cell* **2000**, *100*, 57–70.
- [42] G. Majno, I. Joris, *Am. J. Pathol.* **1995**, *146*, 3.
- [43] P. Syntichaki, N. Tavernarakis, *EMBO Rep.* **2002**, *3*, 604–609.
- [44] K. C. Zimmermann, D. R. Green, *J. Allergy Clin. Immunol.* **2001**, *108*, S99–S103.
- [45] Z. Jin, W. S. El-Deiry, *Cancer Biol. Ther.* **2005**, *4*, 147–171.
- [46] N. Özören, W. S. El-Deiry, in *Semin. Cancer Biol.*, Elsevier, **2003**, pp. 135–147.
- [47] S. W. G. Tait, D. R. Green, *Nat. Rev. Mol. cell Biol.* **2010**, *11*, 621–632.
- [48] B. Wacquier, L. Combettes, G. Dupont, *Sci. Rep.* **2020**, *10*, 3924.
- [49] S. H. Suhaili, H. Karimian, M. Stellato, T.-H. Lee, M.-I. Aguilar, *Biophys. Rev.* **2017**, *9*,

443–457.

- [50] S. J. Korsmeyer, M. C. Wei, M. T. Saito, S. Weiler, K. J. Oh, P. H. Schlesinger, *Cell Death Differ.* **2000**, *7*, 1166–1173.
- [51] A. Burlacu, *J. Cell. Mol. Med.* **2003**, *7*, 249–257.
- [52] E. Hervouet, M. Cheray, F. M. Vallette, P.-F. Cartron, *Cells* **2013**, *2*, 545–573.
- [53] C. M. Adams, S. Clark-Garvey, P. Porcu, C. M. Eischen, *Front. Oncol.* **2019**, *8*, 636.
- [54] S. Kamer, B. M. Atasoy, *Princ. Pract. Mod. Radiother. Tech. Breast Cancer* **2013**, *478*, 49–57.
- [55] L. Kelland, *Nat. Rev. Cancer* **2007**, *7*, 573–584.
- [56] B. Rosenberg, L. Van Camp, T. Krigas, *Nature* **1965**, *205*, 698–699.
- [57] B. Rosenberg, L. Vancamp, J. E. Trosko, V. H. Mansour, *Nature* **1969**, *222*, 385–386.
- [58] T. C. Johnstone, K. Suntharalingam, S. J. Lippard, *Chem. Rev.* **2016**, *116*, 3436–3486.
- [59] S. Zhang, K. S. Lovejoy, J. E. Shima, L. L. Lagpacan, Y. Shu, A. Lapuk, Y. Chen, T. Komori, J. W. Gray, X. Chen, *Cancer Res.* **2006**, *66*, 8847–8857.
- [60] P. Abada, S. B. Howell, *Met. Drugs* **2010**, *2010*, 317581.
- [61] S. B. Howell, R. Safaei, C. A. Larson, M. J. Sailor, *Mol. Pharmacol.* **2010**, *77*, 887–894.
- [62] M. A. Fuertes, C. Alonso, M. Pe, **2003**, *103*.
- [63] M. Akaboshi, K. Kawai, Y. Ujeno, S. Takada, T. Miyahara, *Japanese J. cancer Res.* **1994**, *85*, 106–111.
- [64] M. Akaboshi, K. Kawai, H. Maki, K. Akuta, Y. Ujeno, T. Miyahara, *Japanese J. cancer Res.* **1992**, *83*, 522–526.
- [65] C. A. Rabik, M. E. Dolan, *Cancer Treat. Rev.* **2007**, *33*, 9–23.
- [66] C. Roder, M. J. Thomson, *Drugs R. D.* **2015**, *15*, 13–20.
- [67] M. Chaffman, R. N. Brogden, R. C. Heel, T. M. Speight, G. S. Avery, *Drugs* **1984**, *27*, 378–424.
- [68] M. Mora, M. C. Gimeno, R. Visbal, *Chem. Soc. Rev.* **2019**, *48*, 447–462.
- [69] S. J. Berners-Price, P. J. Sadler, in *Bioinorg. Chem.*, Springer, **1988**, pp. 27–102.
- [70] C. K. Mirabelli, R. K. Johnson, C. M. Sung, L. Faucette, K. Muirhead, S. T. Crooke, *Cancer Res.* **1985**, *45*, 32–39.
- [71] S. J. Berners-Price, P. J. Sadler, *Inorg. Chem.* **1986**, *25*, 3822–3827.
- [72] S. J. Berners-Price, C. K. Mirabelli, R. K. Johnson, M. R. Mattern, F. L. McCabe, L. F. Faucette, C.-M. Sung, S.-M. Mong, P. J. Sadler, S. T. Crooke, *Cancer Res.* **1986**, *46*,

5486–5493.

- [73] S. Gromer, S. Urig, K. Becker, *Med. Res. Rev.* **2004**, *24*, 40–89.
- [74] J. Chaudiere, A. L. Tappel, *J. Inorg. Biochem.* **1984**, *20*, 313–325.
- [75] A. Bindoli, M. P. Rigobello, G. Scutari, C. Gabbiani, A. Casini, L. Messori, *Coord. Chem. Rev.* **2009**, *253*, 1692–1707.
- [76] E. S. J. Arnér, A. Holmgren, *Eur. J. Biochem.* **2000**, *267*, 6102–6109.
- [77] P. J. Barnard, S. J. Berners-Price, *Coord. Chem. Rev.* **2007**, *251*, 1889–1902.
- [78] M. N. Hopkinson, C. Richter, M. Schedler, F. Glorius, *Nature* **2014**, *510*, 485–496.
- [79] H. Schönherr, H. Wanzlick, *Justus Liebigs Ann. Chem.* **1970**, *731*, 176–179.
- [80] W. A. Herrmann, K. Öfele, M. Elison, F. E. Kühn, P. W. Roesky, *J. Organomet. Chem.* **1994**, *480*, c7–c9.
- [81] W. Hermann, T. Weskamp, V. P. W. Bohm, *Adv. Organomet. Chem.* **2001**, *48*, 1–71.
- [82] A. J. Arduengo, R. L. Harlow, M. Kline, *J. Am. Chem. Soc.* **1991**, *113*, 361–363.
- [83] M. Scholl, T. M. Trnka, J. P. Morgan, R. H. Grubbs, *Tetrahedron Lett.* **1999**, *40*, 2247–2250.
- [84] R. A. Kelly, N. M. Scott, S. Díez-González, E. D. Stevens, S. P. Nolan, *Organometallics* **2005**, *24*, 3442–3447.
- [85] B. Liu, X. Ma, F. Wu, W. Chen, *Dalt. Trans.* **2015**, *44*, 1836–1844.
- [86] N. V Tzouras, F. Nahra, L. Falivene, L. Cavallo, M. Saab, K. Van Hecke, A. Collado, C. J. Collett, A. D. Smith, C. S. J. Cazin, *Chem. Eur. J.* **2020**, *26*, 4515–4519.
- [87] R. Visbal, A. Laguna, M. C. Gimeno, *Chem. Commun.* **2013**, *49*, 5642–5644.
- [88] M. G. Gardiner, C. C. Ho, *Coord. Chem. Rev.* **2018**, *375*, 373–388.
- [89] L. Hintermann, *Beilstein J. Org. Chem.* **2007**, *3*, 22.
- [90] E. A. Martynova, N. V. Tzouras, G. Pisanò, C. S. J. Cazin, S. P. Nolan, *Chem. Commun.* **2021**, *57*, 3836–3856.
- [91] S. Sen, Y. Li, V. Lynch, K. Arumugam, J. L. Sessler, J. F. Arambula, *Chem. Commun.* **2019**, *55*, 10627–10630.
- [92] S. Gaillard, A. M. Z. Slawin, S. P. Nolan, *Chem. Commun.* **2010**, *46*, 2742–2744.
- [93] W. F. Gabrielli, S. D. Nogai, J. M. McKenzie, S. Cronje, H. G. Raubenheimer, *New J. Chem.* **2009**, *33*, 2208–2218.
- [94] S. Gründemann, A. Kovacevic, M. Albrecht, J. W. R. Faller, H. Crabtree, *Chem. Commun.* **2001**, *1*, 2274–2275.
- [95] K. F. Donnelly, A. Petronilho, M. Albrecht, *Chem. Commun.* **2013**, *49*, 1145–1159.

- [96] P. Mathew, A. Neels, M. Albrecht, *J. Am. Chem. Soc.* **2008**, *130*, 13534–13535.
- [97] B. Schulze, U. S. Schubert, *Chem. Soc. Rev.* **2014**, *43*, 2522–2571.
- [98] W. Baker, W. D. Ollis, V. D. Poole, *J. Chem. Soc.* **1949**, 307–314.
- [99] S. C. Sau, P. K. Hota, S. K. Mandal, M. Soleilhavoup, G. Bertrand, *Chem. Soc. Rev.* **2020**, *49*, 1233–1252.
- [100] L. A. Schaper, X. Wei, P. J. Altmann, K. Öfele, A. Pöthig, M. Drees, J. Mink, E. Herdtweck, B. Bechlars, W. A. Herrmann, F. E. Kühn, *Inorg. Chem.* **2013**, *52*, 7031–7044.
- [101] C. A. Quezada, J. C. Garrison, M. J. Panzner, C. A. Tessier, W. J. Youngs, *Organometallics* **2004**, *23*, 4846–4848.
- [102] J. C. Garrison, C. A. Tessier, W. J. Youngs, *J. Organomet. Chem.* **2005**, *690*, 6008–6020.
- [103] I. Özdemir, A. Denizci, H. T. Öztürk, B. Çetinkaya, *Appl. Organomet. Chem.* **2004**, *18*, 318–322.
- [104] P. J. Barnard, M. V. Baker, S. J. Berners-Price, D. A. Day, *J. Inorg. Biochem.* **2004**, *98*, 1642–1647.
- [105] P. J. Barnard, M. V. Baker, S. J. Berners-Price, B. W. Skelton, A. H. White, *Dalt. Trans.* **2004**, 1038–1047.
- [106] M. V. Baker, P. J. Barnard, S. J. Berners-Price, S. K. Brayshaw, J. L. Hickey, B. W. Skelton, A. H. White, *J. Organomet. Chem.* **2005**, *690*, 5625–5635.
- [107] J. L. Hickey, R. A. Ruhayel, P. J. Barnard, M. V. Baker, S. J. Berners-Price, A. Filipovska, *J. Am. Chem. Soc.* **2008**, *130*, 12570–12571.
- [108] M. V. Baker, P. J. Barnard, S. J. Berners-Price, S. K. Brayshaw, J. L. Hickey, B. W. Skelton, A. H. White, *Dalt. Trans.* **2006**, 3708–3715.
- [109] R. Rubbiani, S. Can, I. Kitanovic, H. Alborzinia, M. Stefanopoulou, M. Kokoschka, S. Mönchgesang, W. S. Sheldrick, S. Wöflfl, I. Ott, *J. Med. Chem.* **2011**, *54*, 8646–8657.
- [110] J. F. Schlagintweit, C. H. G. Jakob, N. L. Wilke, M. Ahrweiler, C. Frias, J. Frias, M. König, E. M. H. J. Esslinger, F. Marques, J. F. MacHado, R. M. Reich, T. S. Morais, J. D. G. Correia, A. Prokop, F. E. Kühn, *J. Med. Chem.* **2021**, *64*, 15747–15757.
- [111] H. C. Kolb, M. G. Finn, K. B. Sharpless, *Angew. Chemie - Int. Ed.* **2001**, *40*, 2004–2021.
- [112] R. Huisgen, *Angew. Chemie Int. Ed. English* **1963**, *2*, 565–598.
- [113] V. V. Rostovtsev, L. G. Green, V. V. Fokin, K. B. Sharpless, *Angew. Chemie Int. Ed.* **2002**, *41*, 2596–2599.
- [114] C. W. Tornøe, C. Christensen, M. Meldal, *J. Org. Chem.* **2002**, *67*, 3057–3064.
- [115] J. E. Moses, A. D. Moorhouse, *Chem. Soc. Rev.* **2007**, *36*, 1249–1262.
- [116] J. M. Baskin, C. R. Bertozzi, *QSAR Comb. Sci.* **2007**, *26*, 1211–1219.

- [117] C. G. Gordon, J. L. MacKey, J. C. Jewett, E. M. Sletten, K. N. Houk, C. R. Bertozzi, *J. Am. Chem. Soc.* **2012**, *134*, 9199–9208.
- [118] J. A. Codelli, J. M. Baskin, N. J. Agard, C. R. Bertozzi, *J. Am. Chem. Soc.* **2008**, *130*, 11486–11493.
- [119] N. J. Agard, J. A. Prescher, C. R. Bertozzi, *J. Am. Chem. Soc.* **2004**, *126*, 15046–15047.
- [120] H. Wang, R. Wang, K. Cai, H. He, Y. Liu, J. Yen, Z. Wang, M. Xu, Y. Sun, X. Zhou, Q. Yin, L. Tang, I. T. Dobrucki, L. W. Dobrucki, E. J. Chaney, S. A. Boppart, T. M. Fan, S. Lezmi, X. Chen, L. Yin, J. Cheng, *Nat. Chem. Biol.* **2017**, *13*, 415–424.
- [121] X. Ning, J. Guo, M. A. Wolfert, G. Boons, *Angew. Chemie* **2008**, *120*, 2285–2287.
- [122] R. Maity, B. Sarkar, *JACS Au* **2022**, *2*, 22–57.
- [123] J. M. J. M. Ravasco, H. Faustino, A. Trindade, P. M. P. Gois, *Chem. - A Eur. J.* **2019**, *25*, 43–59.
- [124] C. Paris, O. Brun, E. Pedroso, A. Grandas, *Molecules* **2015**, *20*, 6389–6408.
- [125] H.-C. Wu, D.-K. Chang, C.-T. Huang, *J Cancer Mol* **2006**, *2*, 57–66.
- [126] Y. Lu, E. Segal, C. P. Leamon, P. S. Low, *Adv. Drug Deliv. Rev.* **2004**, *56*, 1161–1176.
- [127] G. Lipowska-Bhalla, D. E. Gilham, R. E. Hawkins, D. G. Rothwell, *Cancer Immunol. Immunother.* **2012**, *61*, 953–962.
- [128] F. M. Veronese, M. Morpurgo, *Farm.* **1999**, *54*, 497–516.
- [129] C. H. Chau, P. S. Steeg, W. D. Figg, *Lancet* **2019**, *394*, 793–804.
- [130] N. Krall, F. Pretto, W. Decurtins, G. J. L. Bernardes, C. T. Supuran, D. Neri, *Angew. Chemie Int. Ed.* **2014**, *53*, 4231–4235.
- [131] C. Zhuang, X. Guan, H. Ma, H. Cong, W. Zhang, Z. Miao, *Eur. J. Med. Chem.* **2019**, *163*, 883–895.
- [132] A. Mullard, *Nat Rev Drug Discov* **2022**, *21*, 6–8.
- [133] I. Dovgan, O. Koniev, S. Kolodych, A. Wagner, *Bioconjug. Chem.* **2019**, *30*, 2483–2501.
- [134] M. Alas, A. Saghaeidehkordi, K. Kaur, *J. Med. Chem.* **2020**, *64*, 216–232.
- [135] M. E. Wieder, D. C. Hone, M. J. Cook, M. M. Handsley, J. Gavrilovic, D. A. Russell, *Photochem. Photobiol. Sci.* **2006**, *5*, 727–734.
- [136] Z. Su, D. Xiao, F. Xie, L. Liu, Y. Wang, S. Fan, X. Zhou, S. Li, *Acta Pharm. Sin. B* **2021**, *11*, 3889–3907.
- [137] B. E. Toki, C. G. Cervený, A. F. Wahl, P. D. Senter, *J. Org. Chem.* **2002**, *67*, 1866–1872.
- [138] Y. Matsuda, B. A. Mendelsohn, *Chem. Pharm. Bull.* **2021**, *69*, 976–983.

- [139] A. Younes, U. Yasothan, P. Kirkpatrick, *Nat. Rev. Drug Discov.* **2012**, *11*, 19.
- [140] S. Verma, D. Miles, L. Gianni, I. E. Krop, M. Welslau, J. Baselga, M. Pegram, D.-Y. Oh, V. Diéras, E. Guardino, *N. Engl. J. Med.* **2012**, *367*, 1783–1791.
- [141] C. B. Thompson, K. H. Vousden, R. S. Johnson, W. H. Koppenol, H. Sies, Z. Lu, L. W. S. Finley, C. Frezza, J. Kim, Z. Hu, *Nat. Metab.* **2023**, *5*, 1840–1843.
- [142] M. Scaranti, E. Cojocar, S. Banerjee, U. Banerji, *Nat. Rev. Clin. Oncol.* **2020**, *17*, 349–359.
- [143] M. Srinivasarao, C. V Galliford, P. S. Low, *Nat. Rev. Drug Discov.* **2015**, *14*, 203–219.
- [144] A. Gutiérrez, M. C. Gimeno, I. Marzo, N. Metzler-Nolte, *Eur. J. Inorg. Chem.* **2014**, 2512–2519.
- [145] A. Meyer, L. Oehninger, Y. Geldmacher, H. Alborzinia, S. Wölfl, W. S. Sheldrick, I. Ott, *ChemMedChem* **2014**, *9*, 1794–1800.
- [146] M. J. Matos, C. Labão-Almeida, C. Sayers, O. Dada, M. Tacke, G. J. L. Bernardes, *Chem. Eur. J.* **2018**, *24*, 12250–12253.
- [147] M. Safir Filho, T. Scattolin, P. Dao, N. V Tzouras, R. Benhida, M. Saab, K. Van Hecke, P. Lippmann, A. R. Martin, I. Ott, S. P. Nolan, *New J. Chem.* **2021**, *45*, 9995–10001.
- [148] W. Niu, X. Chen, W. Tan, A. S. Veige, *Angew. Chemie - Int. Ed.* **2016**, *55*, 8889–8893.
- [149] S. Sen, M. W. Perrin, A. C. Sedgwick, V. M. Lynch, J. L. Sessler, J. F. Arambula, *Chem. Sci.* **2021**, *12*, 7547–7553.
- [150] R. Rubbiani, S. Can, I. Kitanovic, H. Alborzinia, M. Stefanopoulou, M. Kokoschka, S. Mönchgesang, W. S. Sheldrick, S. Wölfl, I. Ott, *J. Med. Chem.* **2011**, *54*, 8646–8657.
- [151] L. F. Richter, F. Marques, J. D. G. G. Correia, A. Pöthig, F. E. Kühn, *Dalt. Trans.* **2023**, *52*, 17185–17192.
- [152] A. Baschieri, R. Mazzoni, C. Cesari, S. Zacchini, L. Sambri, *Inorganica Chim. Acta* **2023**, 121472.
- [153] R. Wang, Y. Li, W. Dehaen, *Eur. J. Med. Chem.* **2020**, *207*, 112737.
- [154] I. Steiner, N. Stojanovic, A. Bolje, A. Brozovic, D. Polancec, A. Ambriovic-Ristov, M. R. Stojkovic, I. Piantanida, D. Eljuga, J. Kosmrlj, M. Osmak, *Radiol. Oncol.* **2016**, *50*, 280–288.
- [155] J. Song, J. Lv, J. Jin, Z. Jin, T. Li, J. Wu, *Int. J. Mol. Sci.* **2023**, *24*.

A New Class of Gold(I) NHC Complexes with Proapoptotic and Resensitizing Properties towards Multidrug Resistant Leukemia Cells Overexpressing BCL-2

Franziska Bannwart,* Leon F. Richter, Simon Stifel, Johanna Rueter, Holger N. Lode, João D. G. Correia, Fritz E. Kühn,* and Aram Prokop*



Cite This: *J. Med. Chem.* 2024, 67, 15494–15508



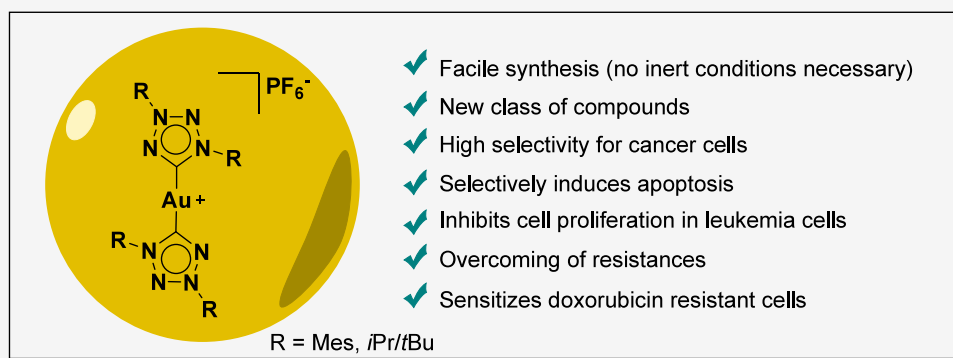
Read Online

ACCESS |

Metrics & More

Article Recommendations

Supporting Information



ABSTRACT: From previous studies, it is evident that metal–organic gold(I) complexes have antiproliferative activities. The aim of this study is not only to find new anticancer agents but also to overcome existing cytostatic resistance in cancer cells. The synthesis and medicinal evaluation of two cationic 1,3-disubstituted gold(I) bis-tetrazolyliene complexes **1** and **2** are reported. To determine apoptosis-inducing properties of the complexes, DNA fragmentation was measured using propidium iodide staining followed by flow cytometry. Gold(I) complex **1** targets explicitly malignant cells, effectively inhibiting their growth and selectively inducing apoptosis without signs of necrosis. Even in cells resistant to common treatments such as doxorubicin, it overcomes multidrug resistance and sensitizes existing drug-resistant cells to common cytostatic drugs. It is assumed that gold(I) complex **1** involves the mitochondrial pathway in apoptosis and targets members of the BCL-2 family, enhancing its potential as a therapeutic agent in cancer treatment.

INTRODUCTION

Following the fortuitous discovery of cisplatin in the 1960s by Rosenberg et al., the popularity of metallotherapeutic drugs and metal-based diagnostic agents grew rapidly.^{1,2} This was primarily due to their efficacy as anticancer chemotherapeutics.³ However, in some types of cancer, cells may develop resistance after initial treatment or persist despite treatment.^{4,5} Such resistance is either intrinsic or can be acquired during chemotherapy.⁶ Acquired cells may be resistant not only to the drug being treated but also cross-resistant to multiple cytostatic drugs. Mechanisms for the development of resistance include increased drug efflux, mutated drug targets, repair of DNA damage caused by cytostatic drugs, inactivation and metabolism of drugs and evasion of apoptosis.^{7,8} Overcoming drug resistance would positively impact patients' chances of recovery.⁶ The goal is either to find other effective treatments or to resensitize the resistant cells. The latter is the subject of current research and could significantly expand patient treatment options.⁹ For example, transport systems such as P-glycoprotein (PGP) or other ATP-binding cassette (ABC)

transport systems can be inhibited to minimize or eliminate drug efflux pathways.^{10,11} Besides resistance formation, a significant drawback of platinum-based medications is their lack of selectivity, which can result in severe negative effects due to their nonspecific mechanism of action and interaction with healthy cells, particularly those with high metabolism.¹² In recent years, researchers have shifted their focus to other metal-based drugs in order to discover more cancer-cell-specific mechanisms of action and reduce side effects. Various gold compounds have since been characterized and found to exhibit intriguing antiproliferative properties.^{13–16} Gold(I) complexes are especially being considered potential substitutes for the usual platinum-based agents due to their distinct and

Received: May 13, 2024
Revised: August 1, 2024
Accepted: August 15, 2024
Published: August 28, 2024



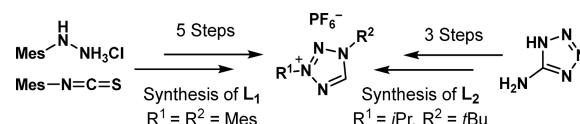
more targeted mode of action.^{17–19} Unlike platinum compounds, multiple biological studies have shown that most gold compounds make considerably weaker bonds with cellular DNA, which suggests a distinct, DNA-independent mode of action.¹⁷ Auranofin (AF) is an organogold complex already approved for the treatment of rheumatoid arthritis that has shown apoptotic effects on neuroblastoma cells in previous studies.²⁰ However, due to its significant side effects and low stability *in vivo*, it is now only considered a second choice. AF has been shown to selectively target the thioredoxin reductase (TrxR) system in cancer cells, affecting the formation of reactive oxygen species (ROS) in the cell.^{21,22} Unfortunately, gold complexes with labile ligands (such as AF) may irreversibly bind to transporter proteins such as human serum albumin (HSA) or antioxidants such as glutathione (GSH), preventing them from reaching the malignant cells *in vivo*.²³ Therefore, designing the ligand is crucial to balance the reactivity and stability of the resulting gold complexes.²⁴ Among the various types of ligands used to stabilize metal complexes, N-heterocyclic carbenes (NHCs) are particularly noteworthy. Generally, NHCs are defined as heterocyclic species that comprise a carbene carbon atom and one or more (usually 2) nitrogen atoms in the ring structure.²⁵ NHCs exhibit exceptional versatility as they can be effortlessly customized considering the steric arrangement of the substituents and the substituents themselves. This renders them an ideal ligand system for cancer-fighting metal complexes in medicinal chemistry.²⁶ Common variants of the NHC ligand type include imidazolyldenes (NHC_{im}) and triazolyldenes (NHC_{trz}), whereas other classes such as tetrazolyldenes (NHC_{tet}) are barely investigated. The group of Berners-Price conducted pioneering research on organometallic gold-NHC_{im} systems as potential anticancer agents.^{27,28} They reported a series of gold(I) bis-NHC_{im} complexes and correlated their antiproliferative properties with the permeabilization of the mitochondrial membrane, a key property in inducing cell apoptosis.^{29,30} Modica-Napolitano et al. additionally suggested that the cationic charge and relatively large lipophilic ligands found in these complexes are responsible for a phenomenon referred to as delocalized lipophilic cations (DLCs).³¹ DLCs offer a way to selectively target cancer cells by accumulating toxic substances in the mitochondria due to negative membrane potentials. However, not all gold(I) NHC complexes described in the literature specifically target mitochondria. An interesting exception is a cationic caffeine-based gold(I) bis-NHC complex that was found to be an efficient and selective DNA quadruplex-interacting agent.^{32,33} Recently, we published an extensive study on gold(I) bis-NHC_{trz} complexes that have been investigated for their antiproliferative effects on cancer cells and demonstrated the possibility of straightforward backbone functionalization.^{34,35} As mentioned above, NHCs containing numerous (>2) nitrogen atoms within the cycle are still under-investigated,^{34,36–38} especially those based on tetrazolyldenes and their corresponding metal complexes. Raubenheimer and co-workers were among the pioneers to report gold(I) carbene complexes based on 1,4-disubstituted tetrazolyldene species in a synthetic and structural study and to investigate the antiproliferative activity of a gold(I) NHC/Phosphine complex in a follow-up study.^{39,40} Unlike normal imidazole and abnormal triazole-based bis-NHC complexes, the abnormal tetrazolium-based ligands (1,3-substituted) have a different substitution pattern. This might benefit their

medicinal application because the gold center is more accessible for enzyme interactions. Within this framework, aimed at expanding the knowledge of these types of complexes and exploring their pharmacological properties, we describe herein two novel gold(I) bis-tetrazolyldene complexes and their ligand precursors and provide an extensive medicinal and mechanistic investigation.

RESULTS AND DISCUSSION

Synthesis and Characterization of gold(I) Complexes 1 and 2. First, we prepared the tetrazolium salts L₁ and L₂, following literature procedures with slight modification (Scheme 1). The diaryl-substituted tetrazolium salt is

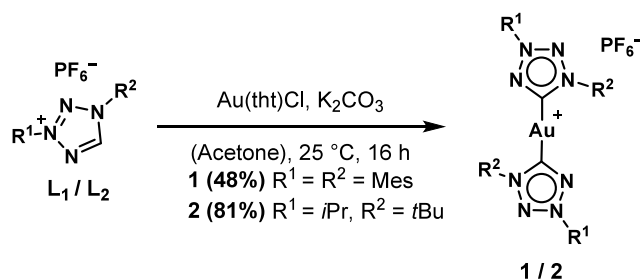
Scheme 1. Chemical Synthesis Pathways to the Ligand Precursors L₁ and L₂ from the Respective Starting Materials



accessible via a 5-step reaction pathway starting from mesityl hydrazine hydrochloride and mesityl isothiocyanate in a total yield of 15%.

The dialkyl-substituted tetrazolium salt is obtained from a 3-step reaction pathway starting from 5-amino tetrazole in a total yield of 23%. For the sake of comparison, we synthesized the complexes and ligand precursors in the form of the corresponding hexafluorophosphate salts. The synthesis of the gold(I) bis-tetrazolyldene complexes 1 and 2 was achieved via the weak base route using K₂CO₃ as the base in acetone (Scheme 2). This simple approach contrasts the previously

Scheme 2. Synthesis of the Gold(I) Bis-tetrazolyldene Complexes 1 and 2 from the Respective Ligand Precursors via the Weak Base Route Using K₂CO₃ in Acetone



reported synthetic pathways to 1,4-disubstituted gold tetrazolyldene complexes, allowing us to work under ambient noninert conditions and eliminating the need for strong bases and highly toxic alkylating agents.^{39,41} The complexes 1 and 2, the ligand precursors L₁ and L₂ and all synthetic intermediates were characterized by common chemical analytical techniques, including elemental analysis, ¹H-/¹³C NMR spectroscopy and thin layer chromatography. Furthermore, the ligand precursors and complexes were additionally characterized by electrospray-ionization mass spectrometry (ESI-MS). The most characteristic feature of the ligand precursors in the ¹H NMR spectrum is the highly deshielded tetrazolium proton at a chemical shift of 10.12 ppm (L₁) and 10.54 ppm (L₂), respectively. For the gold(I) complexes 1 and 2, the absence of this proton indicates a successful synthesis.

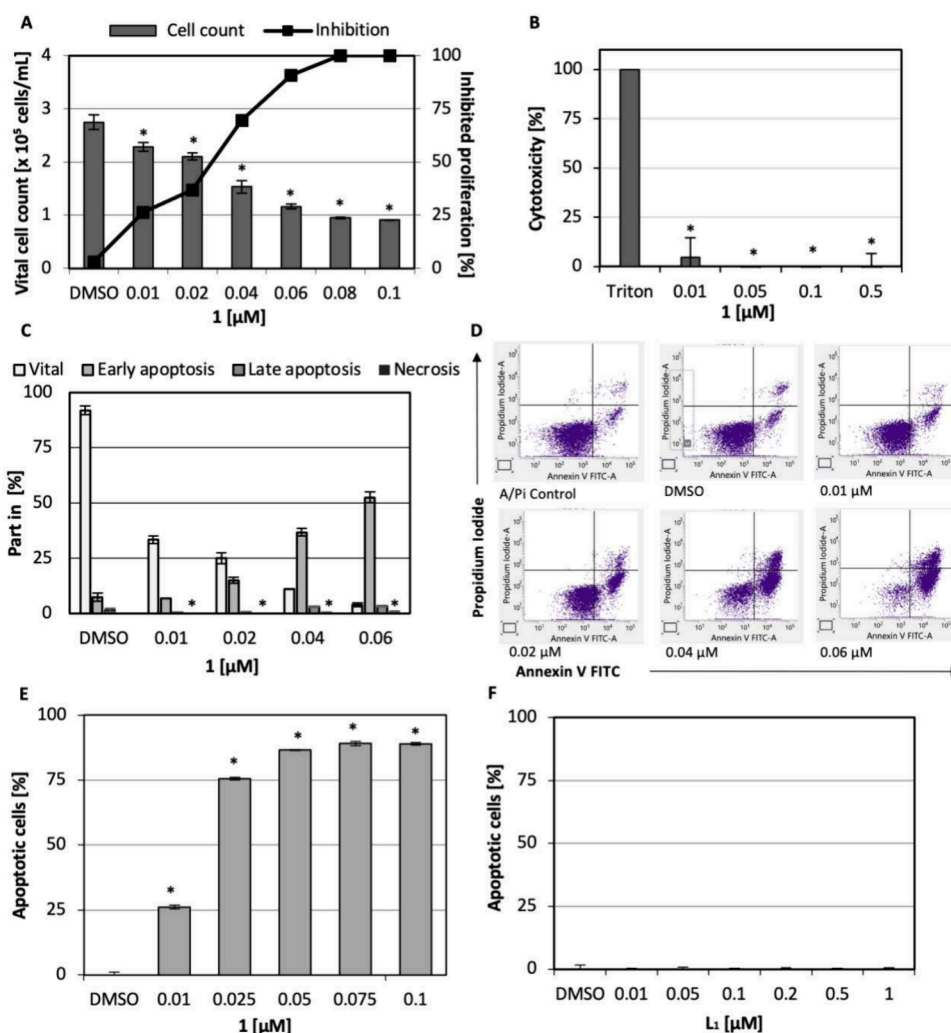


Figure 1. (A) After 24 h, the cell count of the Nalm-6 cells incubated with gold(I) complex **1** was measured. The cell count was significantly lower after 24 h of incubation with gold(I) complex **1**, compared to the DMSO control. * ($p < 0.05$) indicates a significant difference (t test) between the treated cells and the control cells (DMSO). (B) The extracellular LDH concentration was measured after 1 h of incubation with gold(I) complex **1** as a marker for necrosis and compared to the positive control treated with 2% v/v Triton-X 100 (Triton). There is no evidence for necrosis even at much higher concentrations than those used previously. (C) Annexin V FITC and PI double staining was conducted after 48 h of treatment with gold(I) complex **1** to distinguish between vital, early apoptotic, late apoptotic, and necrotic cells. Necrosis could be largely excluded. * ($p < 0.05$) indicates a significant difference (t test) between the cells incubated with gold(I) complex **1** and the Triton treated necrotic cells. (D) Representative images from the experiment in C. The dot plots show the dose-dependent change of the Annexin V FITC and PI signal in the cells treated with increasing concentrations of gold(I) complex **1**. (E,F) Nalm-6 cells were treated with gold(I) complex **1** (E) and the associated ligand L_1 (F) to investigate their apoptotic effects. After 72 h of treatment, DNA fragmentation was measured using flow cytometry. Complex **1** shows a significant induction of apoptosis compared to the DMSO control. * ($p < 0.05$) indicates a significant difference (t test) between treated Nalm-6 cells vs DMSO control. The IC_{50} value of the gold(I) complex **1** is $0.014 \mu\text{M}$, respectively. However, after treatment with L_1 , no apoptosis induction could be observed. All experiments were carried out in Nalm-6 cells in triplicates and the mean values \pm SD are shown.

Additionally, in the ^{13}C NMR spectrum of the gold(I) complexes, the typical Au-carbene peak appears quite far downfield shifted at 191.9 ppm (**1**) and 186.5 ppm (**2**), respectively. ESI-MS gives the expected m/z values for the cationic fragments of the ligand precursors and the gold(I) complexes. Furthermore, the purity of **1** and **2** was analyzed by high-pressure liquid chromatography (HPLC). The spectra and chromatograms can be found in the [Supporting Information](#).

Gold(I) Complex **1 Inhibits Cell Proliferation in Leukemia Cells.** To investigate the extent to which this new class of complexes inhibits the growth of Nalm-6 cells, leukemia cells were incubated with gold(I) complex **1**. The cell number of the treated cells was then measured (Figure 1A)

and showed a significant difference even at $0.01 \mu\text{M}$ compared to the DMSO control. At the time of measurement after 24 h, a reduction in the number of cells can already be seen at $0.08 \mu\text{M}$, indicating the onset of apoptosis, but in any case, an inhibition of proliferation.

Gold(I) Complex **1 Is Not a Trigger for Necrosis.** The question of whether an agent triggers apoptosis or necrosis (early, uncontrolled cell death), can be answered by measuring the release of lactate dehydrogenase (LDH) in the cell culture media after treatment with the test substance. For this purpose, Nalm-6 cells were incubated with gold(I) complex **1** and after 1 h, LDH was measured using a photometric assay (Figure 1B). After treatment of the cells with gold(I) complex **1**, 100% of the cells are still vital and no LDH has leaked out. The

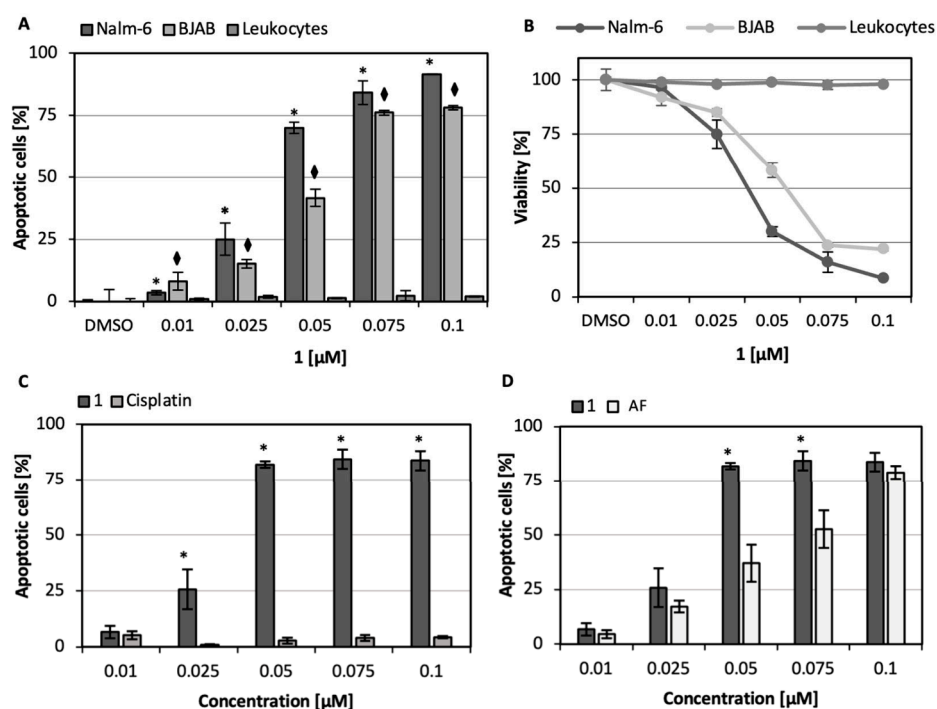


Figure 2. (A) Gold(I) complex **1** was tested on Nalm-6 and BJAB cells in comparison to healthy human leukocytes (*ex vivo*). Gold(I) complex **1** is significantly selective and hardly induces apoptosis on healthy leukocytes. * and ◆ ($p < 0.05$) indicate significant differences (t test) between treated nonproliferative healthy human leukocytes vs treated Nalm-6 and BJAB, respectively. (B) From the experiment described in A, the viability of Nalm-6 and BJAB cells was calculated in comparison to human healthy leukocytes. (C) Gold(I) complex **1** was tested on Nalm-6 cells in comparison to the conventional cytostatic drug cisplatin. While treatment with gold(I) complex **1** results in high apoptosis rates, the same concentration of cisplatin shows almost no effect on the Nalm-6 cells. * ($p < 0.05$) indicates a significant difference (t test) between Nalm-6 cells treated with gold(I) complex **1** vs treatment with cisplatin. (D) Gold(I) complex **1** and the conventional gold-containing drug AF were tested on Nalm-6 cells. Gold(I) complex **1** shows a 2-fold higher apoptosis rate in the low concentration range ($0.05 \mu\text{M}$). * ($p < 0.05$) indicates a significant difference (t test) between Nalm-6 cells treated with gold(I) complex **1** vs treatment with AF. In all experiments three replicates each were examined and the mean values \pm SD are shown.

results were compared to cells treated with 2% Triton-X 100, which served as a positive control. The concentrations investigated were deliberately chosen to be higher in order to investigate a wider therapeutic range, and even in concentrations up to $0.5 \mu\text{M}$ (30–40 times higher than the IC_{50}) there are no indications for necrosis. Another way to obtain information about potential necrosis is staining with Annexin V FITC (A) and Propidium Iodide (PI). The selective staining of the dyes can be used to differentiate between vital cells (A–/PI–), early apoptosis (A+/PI–) and late apoptosis (A+/PI+) or rather necrosis (A–/PI+). For this purpose, Nalm-6 cells were incubated with different concentrations of gold(I) complex **1**. The results show pronounced early apoptosis, while only very few cells are already in the late apoptosis stage and hardly any cells show signs of necrosis (Figure 1C,D).

Gold(I) Complexes 1 and 2 Exhibit Proapoptotic Properties in the Low Nanomolar Range. Previously, we have noticed a strong difference in pharmacologic activity for different wingtip (R) substituents on bis-NHC gold(I) complexes.³⁴ Therefore, we have again synthesized a ligand precursor with lipophilic aromatic mesityl groups (L_1) and another precursor with more flexible and less lipophilic *i*Pr and *t*Bu substituents (L_2). To evaluate the efficacy of apoptosis induction, gold(I) complexes **1** and **2** were incubated on B-lymphoblastic leukemia (B-ALL) cells (Nalm-6). The cells were stained with Propidium Iodide after 72 h of incubation and apoptosis was analyzed using a modified cell cycle analysis

by flow cytometry (Figure 1E, and SI). Apoptosis was detected after treatment with both complexes (Figure 1E, and SI), gold(I) complex **1** with an IC_{50} of $0.014 \mu\text{M}$ and **2** with an IC_{50} of $0.017 \mu\text{M}$, which indicates a very high efficacy at already low concentrations. The two complexes differ only in their ligands and both ligands were tested for their own apoptotic effect on Nalm-6 cells (Figure 1F and SI). No apoptosis induced by the treatment of the cells with L_1 or L_2 could be detected. Thus, gold appears to play an essential role in apoptosis induction by the examined metal complexes.

As the IC_{50} values of complex **1** and **2** are comparable, they appear to be effective at a similar concentration. However, in our recent article, we previously focused on the more lipophilic complex (with Mes wingtips).³⁴ For better comparability, the focus for further experiments was placed on gold(I) complex **1**.

Gold(I) Complex 1 Shows High Selectivity for Cancer Cells. The selective efficacy of gold(I) complex **1**, was tested on healthy human leukocytes *ex vivo* (generated by a member of the research group) and compared to Nalm-6 cells and Burkitt lymphoma (BJAB) cells. DNA fragmentation as a marker for apoptosis was measured after treatment with gold(I) complex **1** by flow cytometry (Figure 2A,B). Gold(I) complex **1** shows effective potency on the leukemia and lymphoma cells (Nalm-6 and BJAB) whereas there is no or very little apoptosis induction on the healthy human leukocytes, even at relatively high concentrations, such as $0.1 \mu\text{M}$ (Figure 2A,B) which indicates a high selectivity of the compound for malignant cells. However, this is an *ex vivo*

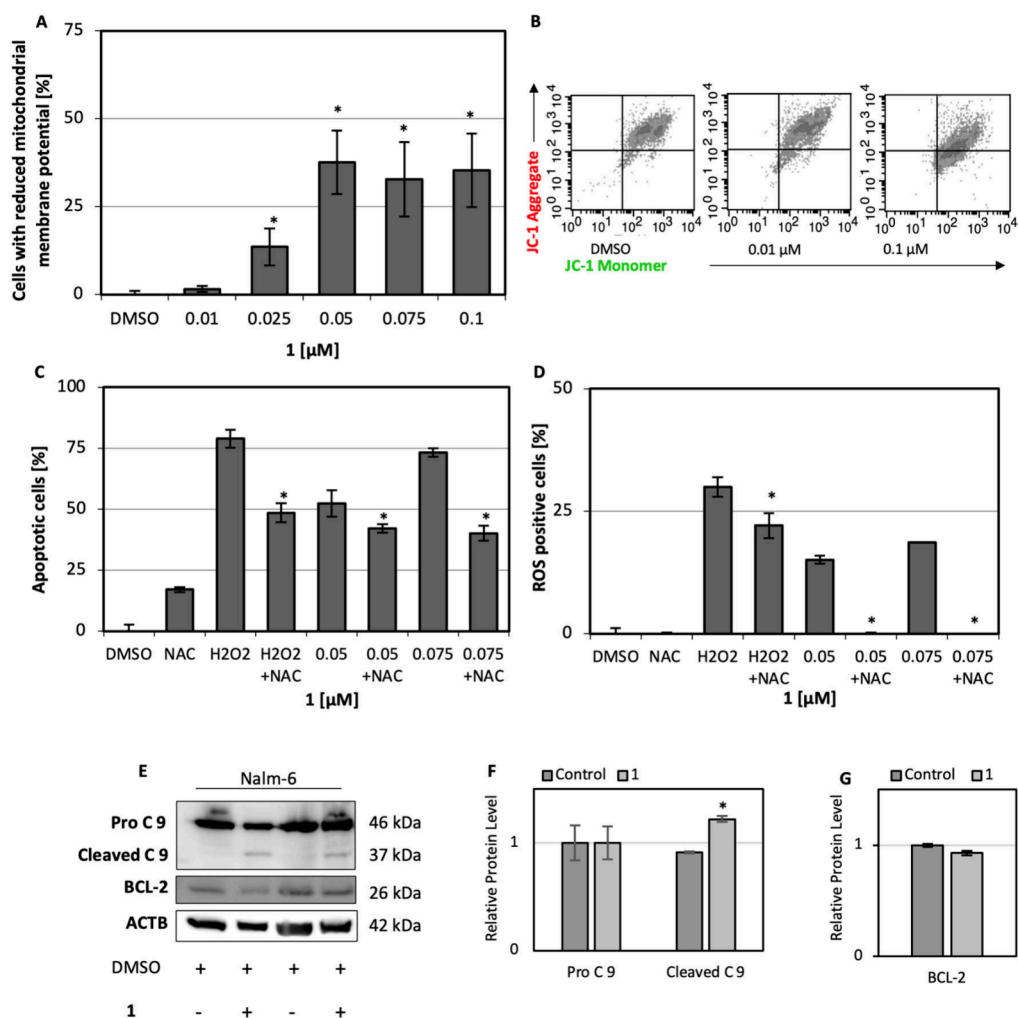


Figure 3. Apoptosis induction by the gold(I) complex 1 is mediated via the mitochondrial and reactive oxygen species (ROS) pathway. (A) A significant change in MOMP could be detected after 48 h of treatment with gold(I) complex 1 using the JC-1 dye and was interpreted in relation to the DMSO control. * ($p < 0.05$) indicates a significant difference (t test) between gold(I) complex 1 treatment vs DMSO control. (B) Representative images from the experiment in A. The density dot plots show the dose-dependent change of the JC-1 aggregate and JC-1 monomer signal in the cells treated with increasing concentrations of gold(I) complex 1. Color gradients show the density of events and go from light gray (low density) to dark gray (high density of events). (C) The cells treated with *N*-acetylcysteine (NAC) showed significantly lower apoptosis rates compared to the samples without NAC. Therefore, the induction of apoptosis by gold(I) complex 1 seems to be ROS-dependent. The DNA fragmentation was analyzed 72 h after incubation with gold(I) complex 1 and the control substances by flow cytometry. Hydrogen peroxide (H_2O_2), known to react ROS positive in cells, was used as a positive control. The values are expressed in relation to the DMSO control. * ($p < 0.05$) indicates a significant difference (t test) between cells treated with gold(I) complex 1 vs treatment with 1 and NAC. (D) ROS positive cells could be detected 5 h after treatment with gold(I) complex 1 using CellRox staining. The ROS levels could be significantly inhibited with the ROS inhibitor NAC. H_2O_2 was used as a positive control. * ($p < 0.05$) indicates a significant difference (t test) between cells treated with gold(I) complex 1 vs treatment with 1 and NAC. (E) Representative Western Blot images of Nalm-6 cells incubated with gold(I) complex 1 and harvested after 24 h for protein expression analysis. The antibodies for procaspase 9 and BCL-2 were tested, and β -actin (ACTB) was used as housekeeping protein to ensure equal protein loading. An increased cleavage of procaspase 9 in treated Nalm-6 cells could be detected. (F) Semiquantitative analysis of procaspase 9 and cleaved caspase 9 protein bands showing an increased cleaved caspase 9 protein level. * ($p < 0.05$) indicates a significant difference (t test) between the DMSO control and cells treated with gold(I) complex 1. (G) Semiquantitative analysis of BCL-2 showing a decreased protein level due to the treatment with gold(I) complex 1. The density of the target protein bands was quantified and normalized by the density of the corresponding ACTB protein band. The results are expressed relative to the DMSO control. All experiments were carried out in Nalm-6 cells in triplicate, and the mean values \pm SD are shown.

experiment that can only give an indication of how the compound will behave *in vivo*. Nevertheless, it is an important indication for a selective anticancer agent that these complexes, at least *in vitro* or *ex vivo*, induce apoptosis almost exclusively in tumor cells and not in nonproliferative healthy leukocytes.

Gold(I) Complex 1 Is More Effective than Common Metal Complexes on Leukemia Cells. To compare the efficacy of gold(I) complex 1 with cisplatin, Nalm-6 cells were

treated with both agents and examined for apoptosis via DNA fragmentation using flow cytometry (Figure 2C). There is a significant difference between the two metal complexes, with gold(I) complex 1 showing significantly higher apoptosis rates than cisplatin at the same concentration. Cisplatin appears to have little or no response on the Nalm-6 leukemia cells in the concentration range studied. According to this experiment, gold(I) complex 1 could have clinical relevance, especially in

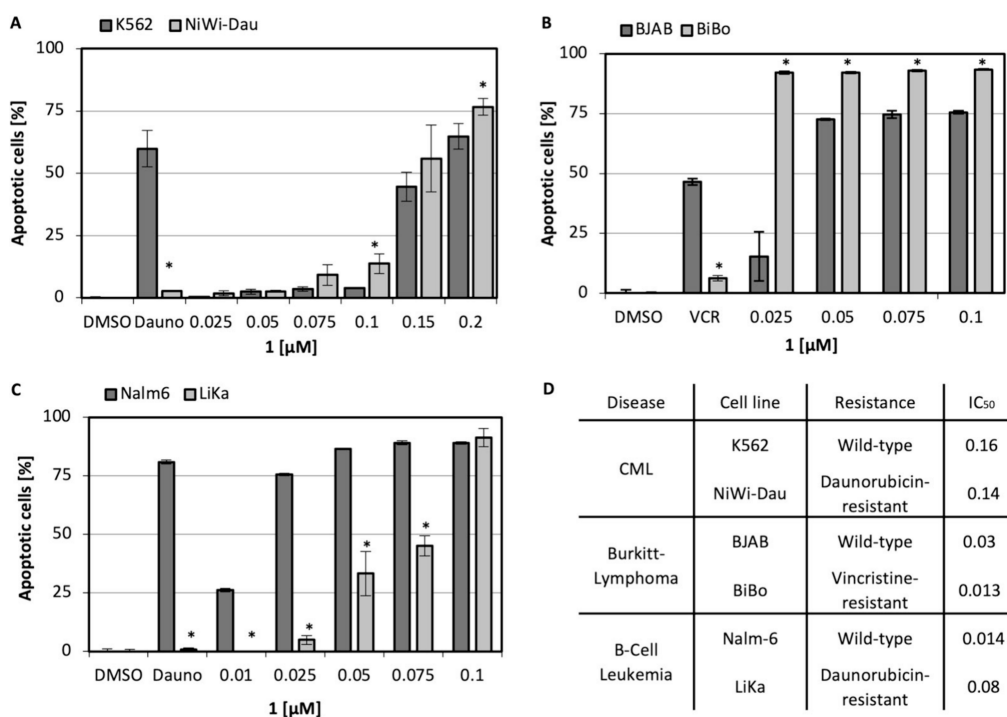


Figure 4. (A) Gold(I) complex **1** was tested on chronic myeloid leukemia (CML) K562 cells and on the daunorubicin-resistant K562 cell line NiWi-Dau. Daunorubicin (Dauno) was applied in the concentration of 2 μM. Gold(I) complex **1** overcomes the resistance and is equally effective on the resistant cells. (B) Gold(I) complex **1** was tested on BJAB cells and on vincristine (VCR)-resistant cells (BiBo). Vincristine was applied in the concentration of 6 μM. Significantly higher levels of apoptosis were achieved in the VCR-resistant cells by the treatment with gold(I) complex **1** than in the wild-type cells, indicating that resistance has been overcome. (C) Gold(I) complex **1** was tested on Nalm-6 cells and on the daunorubicin-resistant Nalm-6 cell line LiKa. Daunorubicin was applied in the concentration of 56 nM. The wild-type Nalm-6 cells were significantly more responsive to treatment with gold(I) complex **1** than the daunorubicin-resistant LiKa cells. * ($p < 0.05$) indicates a significant difference (t test) between wild-type cells and the resistant cell line treated with gold(I) complex **1**. Three replicates were examined and the mean values of three replicates \pm SD are shown. (D) IC₅₀ values of the cell lines (A–C) treated with the gold(I) complex **1**.

comparison with conventional cytostatic drugs of similar substance classes. Cisplatin has been shown to interact with DNA, therefore circular dichroism (CD) spectroscopy with calf thymus DNA (CT-DNA) was conducted to analyze the interaction of gold(I) complex **1** with DNA. However, the results indicate that gold(I) complex **1** (and **2**) do not interact with DNA in contrast to cisplatin (see SI). Treatment of Nalm-6 cells with gold(I) complex **1** and AF (Figure 2D) shows that the novel gold compound has an even higher apoptotic effect at low concentrations compared to AF. Side effects that occur with the clinical use of AF and other metal complexes, could be prevented, or at least minimized at low doses.

The Apoptosis Triggered by Gold(I) Complex **1 Proceeds via the Mitochondrial Pathway.** To analyze whether apoptosis induced by gold(I) complex **1** proceeds via the mitochondrial pathway, Nalm-6 cells were treated with the gold(I) complex **1** for 48 h and stained with the dye 5,5',6,6'-tetrachloro-1,1',3,3'-tetra-ethylbenz-imidazolyl-carbocyanine iodide (JC-1). Depending on the mitochondrial outer membrane potential (MOMP), the emission maximum of the fluorescent signal changes and the depolarization of the mitochondria is characterized by a shift from red (JC-1 aggregates) to green (JC-1 monomers) fluorescence that can be measured by flow cytometry. The change in MOMP is an important event of the intrinsic apoptotic pathway and initiates pore formation and Cytochrome C efflux from the mitochondrial matrix into the cytosol. The mitochondrial apoptosis pathway appears to play an important role in the

mechanism of action of gold(I) complex **1**, because a dose-dependent decrease in the MOMP could be observed (Figure 3A). A reduced membrane potential can be seen in the treated cells by the change in the detected JC-1 signal from red toward green (Figure 3B). MOMP reduction can occur through the oligomerization of the proapoptotic B-cell lymphoma 2 (BCL-2) family members BCL-2 associated X protein (BAX) and BCL-2 Antagonist/Killer (BAK). However, the formation of reactive oxygen species (ROS) can also cause such a membrane potential change. Other metal-based cytostatic drugs, such as cisplatin, have been shown to induce ROS in the cell.⁴ To detect ROS and ROS-induced apoptosis via DNA fragmentation, Nalm-6 cells were incubated with gold(I) complex **1** combined with 1.5 h by pretreatment with *N*-acetylcysteine (NAC), a ROS inhibitor. It has been shown that cells treated with only gold(I) complex **1** had significantly higher apoptosis levels than those treated with **1** (Figure 3C). In addition to this indirect detection of apoptosis with ROS involvement, ROS positive cells can also be detected directly using CellRox Green staining. Nalm-6 cells were treated with gold(I) complex **1** and the corresponding controls were inhibited with NAC. The measurement revealed a significantly higher ROS level in the cells treated with gold(I) complex **1** alone compared to the cells additionally treated with NAC (Figure 3D), suggesting that gold(I) complex **1** affects the presence of ROS.

Treatment with Gold(I) Complex **1 Leads to Activation of Procaspase 9.** After initiation of the mitochondrial apoptotic pathway, apoptotic protease activating

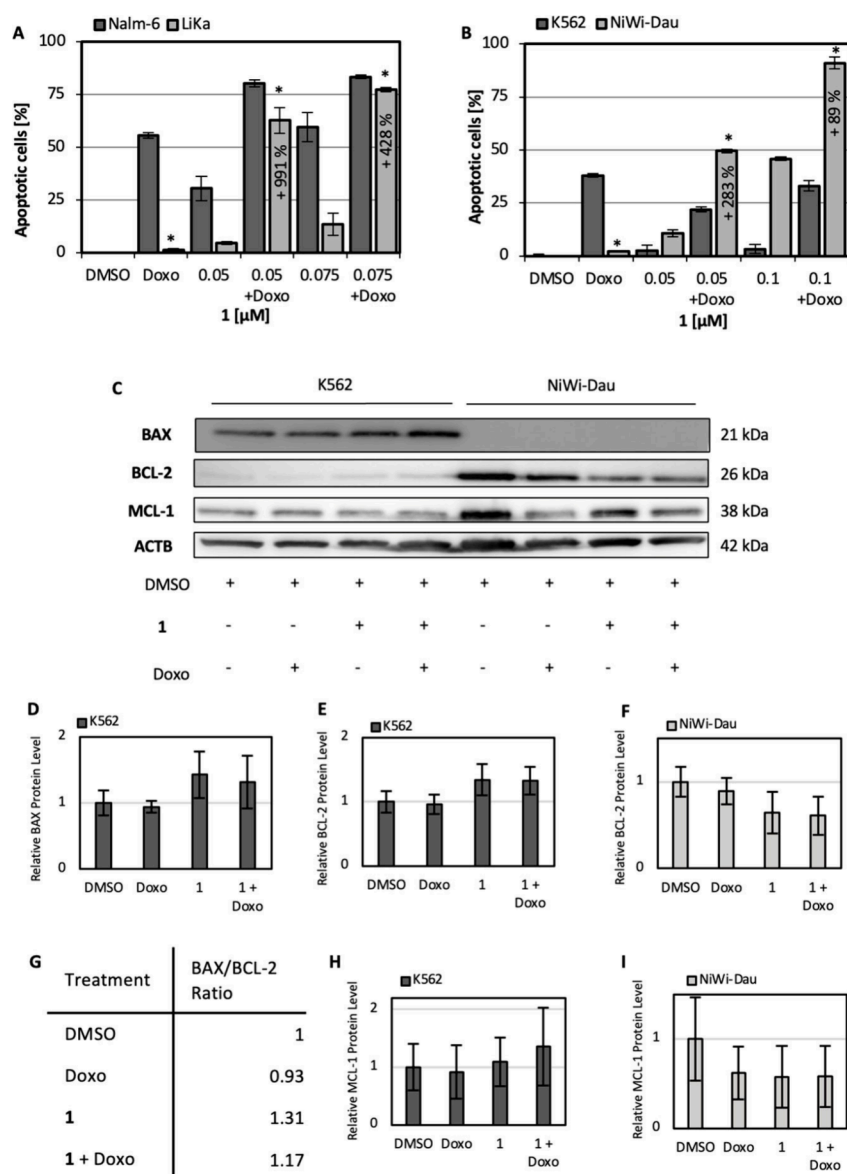


Figure 5. Important mitochondrial apoptosis targets are addressed by gold(I) complex **1**. (A) Potential synergistic effects of gold(I) complex **1** and doxorubicin were tested on Nalm-6 and LiKa cells, the latter are coreistant to doxorubicin. (B) Potential synergistic effects of gold(I) complex **1** and doxorubicin (Doxo) were tested on K562 and NiWi-Dau cells, the latter showing coreistance to doxorubicin. The resistant cells show significant synergistic effects compared to the cells treated with gold(I) complex **1** and with doxorubicin alone. **1** resensitizes NiWi-Dau cells to doxorubicin. In both cell lines (A,B), synergistic effects of **1** with doxorubicin were observed, especially in the doxorubicin coreistant cell lines NiWi-Dau (A) and LiKa (B). * ($p < 0.05$) indicates a significant difference (t test) between cells treated with gold(I) complex **1** and doxorubicin alone, each versus treatment with both. (C) K562 and doxorubicin-resistant NiWi-Dau cells were incubated with gold(I) complex **1**, doxorubicin and the combination of both and harvested after 24 h for Western Blot analysis. The antibodies against BCL-2, BAX and MCL-1 were tested and β -actin (ACTB) was used as housekeeping protein to ensure equal protein loading. (D–F,H,I) The semiquantitative evaluation of the relative protein level of BAX (D) in K562 cells, BCL-2 in K562 (E) and NiWi-Dau cells (F) and MCL-1 in K562 (H) and NiWi-Dau cells (I) treated with gold(I) complex **1** is shown. The protein levels of BCL-2 (F) and MCL-1 (I) are downregulated in NiWi-Dau cells by gold(I) complex **1** and doxorubicin, whereas the BAX level is upregulated in K562 cells (D). Three independent passages were tested, one of them is presented above. The density of the target protein bands was quantified and normalized by the density of the corresponding ACTB protein band and the results are expressed relative to the DMSO control. No significant differences could be detected, but a trend can be seen. In all experiments the mean values of three replicates \pm SD are shown. (G) The BAX/BCL-2 ratio in K562 cells was determined and calculated from the previous Western blotting results. A change in the ratio in favor of BAX can be seen, suggesting a proapoptotic metabolic situation in these cells.

factor 1 (APAF-1) proteins build an apoptosome mediated by Cytochrome C release. procaspase 9 can bind to this structure, dimerize and then be activated to caspase 9. Activated (cleaved) caspase 9 can then activate effector caspases to initiate the final stage of apoptosis. Twenty-four h after treatment of Nalm-6 cells with gold(I) complex **1**, a cleavage from procaspase 9 can be detected by Western Blot. A cleaved

caspase 9 protein band can be detected at 37 kDa in cells incubated with gold(I) complex **1** (Figure 3E). Quantitative analysis of the protein bands indicates that the level of cleaved caspase 9 is significantly increased after treatment with gold(I) complex **1** compared to untreated cells (Figure 3F). In addition, a slightly downregulated BCL-2 protein level was detected in Nalm-6 cells treated with gold(I) complex **1**

(Figure 3E,G). It is therefore thought that the apoptosis induced by this compound involves the mitochondrion via activation of caspases. Apoptosis induced by gold complexes via (indirect) activation of caspases has been the subject of previous research and may be related to the induction of ROS upstream.⁴²⁻⁴⁵ Previous knowledge is supported by the results presented here.

Overcoming Multidrug Resistant Cells by Gold(I) Complex 1, Despite BCL-2 Overexpression. Overcoming multidrug resistance in cancer (cells) is an important part of the search for novel agents. To investigate whether gold(I) complex 1 has resistance overcoming properties, various cytostatic-resistant cell lines were tested for apoptosis induction. Therefore, chronic myeloid leukemia (CML) cells (K562) and daunorubicin-resistant K562 cells (NiWi-Dau), Burkitt lymphoma cells (BJAB) and vincristine-resistant BJAB cells (BiBo) as well as B-lymphoblastic leukemia cells (Nalm-6) and daunorubicin-resistant Nalm-6 (LiKa) cells were treated with gold(I) complex 1 and examined for DNA fragmentation using flow cytometry. NiWi-Dau cells show increased expression of the antiapoptotic protein BCL-2 and significant downregulation of the pro-apoptotic protein BAX. This altered expression pattern of both anti- and pro-apoptotic proteins probably contributes significantly to resistance to daunorubicin and other anthracyclines. Because the gold(I) complex 1 is as effective in the BCL-2 overexpressing NiWi-Dau cells as in the wild-type cell line (Figure 4A,D), it can be assumed that the complex has an impact on the BCL-2 pathway and is able to overcome multidrug resistance in the examined cells. In addition, the pro-apoptotic protein BAX does not seem to play a major role in the induction of apoptosis by gold(I) complex 1 because the same rate of apoptosis can occur in cells that show hardly any BAX expression level (NiWi-Dau cells). Vincristine-resistant BJAB cells (BiBo cells) are also characterized by an overexpression of BCL-2. The rate of gold(I) complex 1-induced apoptosis in the resistant BiBo cell line is significantly higher than in the wild-type cells, also compared by their IC_{50} values (Figure 4B,D). At a concentration of 0.025 μ M, more than 90% of the resistant cells are already in a determined stage of cell death, while less than 25% of the BJAB cells are in apoptosis. These almost 4-fold higher results suggest that gold(I) complex 1 exerts an influence on BCL-2-dependent apoptosis and has a BCL-2 regulatory function. Again, it can be seen that 1 induces apoptosis in cytostatic-resistant cells and thus overcomes multidrug resistance.

Daunorubicin-resistant (and coresistant to doxorubicin) Nalm-6 cells (LiKa) exhibit an overexpression of P-Glycoprotein (PGP), which is one potential reason for their resistance behavior. PGP is part of an unspecific ejection mechanism of the cell through which, for example, cytostatic drugs can be ejected from the tumor cell. The level of apoptotic cells induced by treatment with gold(I) complex 1 is significantly lower in the LiKa cells compared to Nalm-6 (Figure 4C,D). This indicates that the increased expression of PGP in the resistant cells leads to increased elimination of gold(I) complex 1. The gold(I) complex 1 thus appears to be a substrate of PGP.

Gold(I) Complex 1 Sensitizes Doxorubicin-Resistant Cells to Doxorubicin. To enhance the efficacy of conventional cytostatic drugs, it can be tested whether novel agents have synergistic effects with them. A synergistic effect is defined as the apoptosis rate of cells treated with two agents

simultaneously being higher than the sum of the apoptosis rates of the individually treated cells.⁴⁶ For this purpose, cells were treated with 1 and the cytostatic drug doxorubicin and DNA fragmentation as a marker for apoptosis was measured by flow cytometry. No synergistic effect was observed in the simultaneous treatment of the wild-type cell lines Nalm-6 (Figure 5A) and K562 (Figure 5B) with gold(I) complex 1 and doxorubicin, as the effect of both substances at the same time does not exceed the sum of the effects of the two individual substances. The daunorubicin-resistant cell lines LiKa and NiWi-Dau show a coresistance against other anthracyclines like doxorubicin. However, if the doxorubicin-resistant associated cell lines (LiKa and NiWi-Dau) are treated with gold(I) complex 1 and doxorubicin, a distinct synergistic effect can be demonstrated (Figure 5A and B). Comparing the apoptosis rate of the synergy on the wild-type Nalm-6 cells with the rate on the resistant LiKa cells, it is apparent that the resistance cannot be completely overcome. Nevertheless, a closer look at the treated LiKa cells reveals a significant synergistic effect (Figure 5A). At a concentration of 0.05 μ M, an enormous increase in efficiency of +991% can be observed due to the combination with doxorubicin (Figure 5A). Although the relative apoptosis rate does not exceed that of the wild-type cell line, the initially doxorubicin-resistant LiKa cells are significantly sensitized to doxorubicin (Figure 5A). The synergistic effect is even more apparent when considering the K562 cells and the doxorubicin-resistant NiWi-Dau cells (Figure 6B). The synergistic effect on NiWi-Dau cells is highly significant in the experiment with the anthracycline and gold(I) complex 1 at both concentrations tested. Not only the synergy and the sensitization of the resistant cells are remarkable (Figure 5B). The apoptosis rate of NiWi-Dau cells in the synergy experiment significantly exceeds the rate of apoptotic K562 cells at the same concentrations and moreover the initial doxorubicin-resistant cells are again sensitized to doxorubicin (Figure 5B).

In summary, the combinations of the two compounds, namely the conventional drug doxorubicin and the novel gold(I) complex 1, result in high apoptosis rates in the low nanomolar range and sensitize previously resistant cells. Side effects caused by high concentrations of individual drugs can be reduced or even avoided through synergistic effects.

Gold(I) Complex 1 Influences the BAX/BCL-2 Ratio. As described above, gold(I) complex 1 is involved in apoptosis induction via the mitochondrion. The semiquantitative analysis of protein expression by Western Blotting can provide further information about the exact signaling pathways that are targeted. Of particular interest here is the mechanism of sensitization of the doxorubicin-resistant NiWi-Dau cells. An important aspect of the intrinsic apoptosis pathway is the interplay between BAX and its antiapoptotic counterpart BCL-2. Various gold complexes have been investigated for their proapoptotic effects in previous studies. These gold complexes were often directed against a target of the BCL-2 family.^{47,48} To analyze the expression of different key proteins in K562 and NiWi-Dau cells, these cells were incubated for 24 h with the gold(I) complex 1, doxorubicin and the combination of both, respectively. Examining the protein level of BAX in NiWi-Dau cells, no protein band for the BAX protein can barely be seen (Figure 5C). In addition, a significant increase in the BCL-2 protein level can be observed in NiWi-Dau cells compared to the wild-type cell line K562. Treatment with gold(I) complex 1 and the combination of 1 and doxorubicin leads to an

increased expression of BAX in K562 cells (Figure 5D), compared to untreated K562 cells (DMSO control).

The BCL-2 protein level, on the other hand, is almost constant or increases slightly when treated with gold(I) complex **1** (Figure 5E). However, BCL-2 expression is relatively low in K562 cells, compared to NiWi-Dau. By treating the doxorubicin-resistant cells with gold(I) complex **1** and with **1** and doxorubicin, a reduced expression of BCL-2 can be detected (Figure 5F), which presumably shifts the ratio back in favor of the pro-apoptotic protein. However, due to high standard deviation, the proteins levels differ not statistically significant from each other, but nevertheless a clear trend can be seen. The ratio of BAX/BCL-2 in K562 cells was found to change in favor of BAX when treated with **1** and with **1** and doxorubicin (Figure 5G). The shift in this ratio could lead to an increased presence of pro-apoptotic proteins in the cell and facilitate apoptotic events. In NiWi-Dau cells, no ratio can be formed due to the barely visible BAX protein band, but it can be assumed that the BAX/BCL-2 ratio in these cells in general is clearly shifted in favor of the antiapoptotic protein due to the strongly increased BCL-2 protein level. Furthermore, from the results (Figure 5C and D) it can be concluded that treatment with gold(I) complex **1** as well as with **1** and doxorubicin in K562 cells seems to favor apoptosis induction possibly through an increased BAX protein level. In NiWi-Dau cells, on the other hand, no or barely any BAX protein band can be detected even after treatment, so it can be assumed that apoptosis occurs in these cells almost independently of BAX. The significantly increased BCL-2 level in NiWi-Dau cells compared to K562 (Figure 5E and F) cells is reduced by treatment with the gold(I) complex **1** and the combination of **1** and doxorubicin (Figure 5C,F). The formation of the BAX/BCL-2 ratio is not possible in these cells due to the absence of BAX. However, the relative BCL-2 protein level decreases by about 32% in the NiWi-Dau cells treated with doxorubicin compared to treatment with **1** and doxorubicin. Due to high standard deviation the difference between the doxorubicin and the doxorubicin + **1** treated cells not statistically significant. The gold(I) complex **1** attacks exactly where the cell has developed mechanisms to escape apoptosis: it leads to a reduced amount of antiapoptotic proteins such as BCL-2, which is probably partly the cause of resistance. Therefore, the reduced BCL-2 protein levels may possibly play a crucial role in overcoming resistance in the daunorubicin-resistant K562 (NiWi-Dau) cells. BCL-2 as an important antiapoptotic protein can therefore be down-regulated by the novel gold(I) complex **1** and is eligible for a potential target of **1**. Gold(I) complex **1** thus joins the family of gold complexes that have a pro-apoptotic effect on the BCL-2 family.

BCL-2 Family as Possible Targets of Gold(I) Complex

1. Another important antiapoptotic protein of the BCL-2 superfamily is Myeloid-cell-leukemia-1 protein (MCL-1), which is also a promising anticancer target. Targeted therapies can target cancer cells more specifically and reduce the potential side effects of chemotherapeutic drugs.⁶ It is already known that gold complexes target MCL-1.⁴⁹ In NiWi-Dau cells, an increased expression level of MCL-1 can be observed compared to K562 cells (Figure 5C). In K562 cells, no effect of gold(I) complex **1** on the expression of MCL-1 protein levels could be demonstrated (Figure 5H). Due to the treatment with gold(I) complex **1**, doxorubicin or the combination, a reduction in MCL-1 protein levels compared to DMSO

control can be observed in NiWi-Dau cells (Figure 5I). However, the quantification revealed no significant reduction, but a trend.

In summary, treatment with gold(I) complex **1** reduced the protein levels of mitochondrial antiapoptotic proteins such as BCL-2 and MCL-1, particularly in the anthracycline-resistant NiWi-Dau cells. These results give a clear indication of the mechanism of action of gold(I) complex **1** and confirm the suspicion of apoptosis with mitochondrial involvement. Nevertheless, the significant synergistic effect of gold(I) complex **1** and doxorubicin could not be explained at the protein level.

As cancer cells develop resistance to conventional cytostatic drugs after relapse, the search for drugs to overcome this resistance has expanded. The approach of resensitizing resistant cells to the respective cytostatic drug has already been taken up in previous studies. The discovery that gold(I) complex **1** resensitizes doxorubicin-resistant cells, allowing conventional cytostatic drugs to induce apoptosis in the cells again, is an important discovery in the treatment of cancer relapse. Further research is underway to investigate the mechanisms of resensitization. This includes sensitization with epigenetic modifiers.⁵⁰ Another approach is to identify the resistance mechanism of the cell and to combat the modified target with a specific targeted therapy.⁵¹ In the NiWi-Dau cells tested here, the reduction of BCL-2 protein levels was found to be a particularly interesting target for resensitization with gold(I) complex **1**. Drug efflux systems such as PGP also play a role in the development of resistance of cancer cells to cytostatic drugs. For example, Huang et al. have described the influence of the ABCB1 transporter on cytostatic resistance and how it can be inhibited to resensitize cells.⁵² It is therefore conceivable that gold(I) complex **1** blocks drug efflux transporters and thus prevents the elimination of doxorubicin.

CONCLUSION

The novel gold(I) complex **1** is a highly potent complex that induces high apoptosis rates in various cancer cell lines even in the low nanomolar range. The complex investigated here has a much more potent effect on leukemia cells than previously investigated gold complexes.^{34,53-58} Gold(I) complex **1** is already effective at about one fiftieth of the IC₅₀ compared to other potent gold complexes (with an IC₅₀ of approximately 0.5 μM).³⁴ Selective, controlled induction of cell death in tumor cells *in vitro* was demonstrated without detectable signs of necrosis. In particular, selective induction of apoptosis is of high clinical relevance, as it is essential to find potent anticancer agents that do not affect healthy cells. In comparison to conventional metal complexes such as cisplatin, which is clinically used as a cytostatic agent, and AF, which has also shown antiapoptotic properties, the gold(I) complex has been shown to be more effective. Mechanistically, it can be assumed that the versatile gold(I) complex **1** induces apoptosis via the mitochondrial pathway, which is in line with other gold complexes already investigated.⁵⁹ A long-discussed target of gold complexes in general is TrxR, which has a direct influence on the ROS level of the cell.⁶⁰ As gold(I) complex **1** increases the ROS level of the investigated cells, TrxR might be a potential target. Gold(I) complex **1** is not only highly effective in inducing apoptosis in cancer cells, but it is also particularly promising in overcoming multidrug resistance. Treatment with the gold(I) complex **1** can overcome existing multidrug

resistance and moreover sensitize the previously resistant cells to the cytostatic drug. Again, evidence for a mitochondrial mechanism of action was found at the protein level and the BCL-2 family, in particular BCL-2 and MCL-1, may be important targets for 1.

However, it must be considered that these experiments are *in vitro* tests that would have to be tested *in vivo* to further clarify their efficacy. Based on the experiences with metal complexes that are already used clinically in anticancer therapy, such as cisplatin, the application of gold(I) complex 1 could also lead to some side effects. The extent to which the possible lower application dose could lead to a reduction in these potential side effects has to be evaluated in future studies. Furthermore, gold(I) complex 1 was tested exclusively on leukemia and lymphoma cells in the experiments performed here. However, previous studies with gold complexes have shown high efficacy on solid tumors.^{61,62} It may therefore be interesting to test gold(I) complex 1 on solid tumor cells as well.

EXPERIMENTAL SECTION

General Remarks and Synthesis. All reagents were purchased from commercial suppliers and used without further purification. NMR spectra were recorded on a Bruker AVANCE DPX 400 (¹H NMR, 400.13 MHz; ¹³C NMR, 100.53 MHz). Chemical shifts are reported in parts per million and referenced to the residual signal of the deuterated solvent (acetonitrile-*d*₃; 1.94 ppm, (CD₃)₂SO; 2.50 ppm). Elemental analyses (C/H/N) were performed by the microanalytical laboratory at Technische Universität München. ESI-MS data were acquired on a Thermo Fisher UltiMate 3000. Analytical reversed-phase HPLC-HESI-MS (heated ESI-MS) was performed on an UltiMate 3000 UHPLC focused chromatographic system (Dionex) connected to an LCQ Fleet mass spectrometer (Thermo Scientific) equipped with a C18 column (Hypersil GOLD aQ, 150 mm × 2.1 mm, 3 μm). 1-*tert*-Butyl,3-*iso*-propyl-tetrazolium perchlorate was prepared according to a literature procedure from commercially available 5-aminotetrazole.^{63–65} The identity and purity (>95%) of all biologically studied compounds were confirmed by analytical HPLC in conjunction with elemental analysis and NMR spectroscopy.

N-2-Dimesitylhydrazine-1-carbothioamide (1a). In a 100 mL round-bottom flask, 1.45 g of 2,4,6-trimethylphenylhydrazine (7.77 mmol, 1.00 equiv) are suspended in 40 mL of diethyl ether. Subsequently, a mixture of 1.38 g of 2-isothiocyanato-1,3,5-trimethylbenzene (7.77 mmol, 1.00 equiv) and 2.20 mL of TEA (15.9 mmol, 2.04 equiv) in 15 mL of diethyl ether are added slowly. The reaction mixture is stirred for 1 h at 40 °C reflux. After the reaction time, the mixture is cooled to 0 °C and the precipitate is filtered and washed sequentially with cold diethyl ether (2 × 15 mL) and ethanol (1 × 20 mL). The crude residue is recrystallized with ethanol (56 mL) to obtain 1.52 g 1a (4.64 mmol, 60%) as a white crystalline solid. ¹H NMR (400 MHz, (CD₃)₂SO, 294 K): δ [ppm] = 9.33 (s, 1H, H_{SCNHC}), 9.22 (s, 1H, H_{NHNHC}), 6.85 (s, 2H, CH), 6.77 (s, 2H, CH), 6.73 (s, 1H, H_{NHNHC}), 2.30 (s, 6H, CH_{3,0-mes}), 2.23 (s, 3H, CH_{3,p-mes}), 2.18 (m, 9H, CH_{3,op-mes}). ¹³C NMR (101 MHz, (CD₃)₂SO, 303 K): δ [ppm] = 179.8 (s, C_{NCSN}), 140.6 (s, C_{ar}), 136.2 (s, C_{ar}), 135.3 (s, C_{ar}), 134.9 (s, C_{ar}), 131.4 (s, C_{ar}), 129.3 (s, C_{ar}), 128.1 (s, C_{ar}), 20.6 (s, CH₃), 20.2 (s, CH₃), 18.6 (s, CH₃), 18.4 (s, CH₃). EA (%): calcd C 69.68, H 7.69, N 12.83, S 9.79; found C 69.65, H 7.73, N 12.70, S 9.26. R_f = 0.11 (DCM) [UV].

Mesityl-(3-mesityl-1,2,3,4-oxatriazolium-5-yl)-amide (1b). In a 50 mL round-bottom flask, 1.00 g 1a (3.05 mmol, 1.00 equiv) is suspended in 18 mL ethanol and the suspension is cooled to -10 °C. The cold suspension is acidified with conc HCl_(aq) (1 mL) to pH 2 and 3.60 mL of an aqueous sodium nitrite solution (1M, 1.50 equiv) are added slowly. After stirring for 1 h at 25 °C, the reaction mixture is filtered, and the filtrate is subsequently alkalinized with solid sodium carbonate to pH 11. After cooling overnight at 4 °C, the precipitate is

filtered and washed with an excess amount of water (3 × 15 mL). After drying *in vacuo*, 808 mg of mesityl-(3-mesityl-1,2,3,4-oxatriazol-3-ium-5-yl)-amide 1b (2.50 mmol, 82%) is obtained as a light orange solid. ¹H NMR (400 MHz, (CD₃)₂SO, 295 K): δ [ppm] = 7.21 (s, 2H, CH), 6.81 (s, 2H, CH), 2.34 (s, 3H, CH_{3,p-mes}), 2.18 (s, 9H, CH_{3,op-mes}), 2.07 (s, 6H, CH_{3,p-mes}). ¹³C NMR (101 MHz, (CD₃)₂SO, 294 K): δ [ppm] = 142.7 (s, C_{NCON}), 133.3 (s, C_{ar}), 131.2 (s, C_{ar}), 130.7 (s, C_{ar}), 130.3 (s, C_{ar}), 129.6 (s, C_{ar}), 128.4 (s, C_{ar}), 128.3 (s, C_{ar}), 20.8 (s, CH₃), 20.4 (s, CH₃), 17.9 (s, CH₃), 16.1 (s, CH₃). EA (%): calcd C 70.78, H 6.88, N 17.38, O 4.96; found C 69.39, H 6.97, N 16.63, S 1.97. R_f = 0.36 (DCM) [UV].

1,3-Dimesityltetrazolium-5-olate (1c). In a pressure tube, 781 mg 1b (2.42 mmol, 1.00 equiv) are dissolved in 18 mL ethanol and alkalinized with NaOH_(aq) (10 M, 3 mL) to pH 9. After stirring for 2 days at 90 °C reflux, the reaction mixture is allowed to reach 25 °C and is subsequently diluted with 30 mL of water. The formed precipitate is filtered, washed with water (2 × 10 mL), and dried *in vacuo* to obtain 742 mg 1c (2.30 mmol, 95%) as an orange solid. ¹H NMR (400 MHz, (CD₃)₂SO, 294 K): δ [ppm] = 7.18 (s, 2H, CH), 7.14 (s, 2H, CH), 2.37 (s, 3H, CH_{3,p-mes}), 2.33 (s, 3H, CH_{3,p-mes}), 2.14 (s, 6H, CH_{3,0-mes}), 2.11 (s, 6H, CH_{3,0-mes}). ¹³C NMR (101 MHz, (CD₃)₂SO, 294 K): δ [ppm] = 159.8 (s, C_{NCON}), 141.7 (s, C_{ar}), 140.6 (s, C_{ar}), 135.5 (s, C_{ar}), 133.9 (s, C_{ar}), 133.6 (s, C_{ar}), 129.4 (s, C_{ar}), 129.2 (s, C_{ar}), 127.9 (s, C_{ar}), 20.8 (s, CH₃), 20.7 (s, CH₃), 17.1 (s, CH₃), 16.3 (s, CH₃). EA (%): calcd C 70.78, H 6.88, N 17.38, O 4.96; found C 70.66, H 6.85, N 17.21. R_f = 0.05 (DCM); 0.79 (EtOAc) [UV].

1,3-Dimesityltetrazolium-5-thiolate (1d). In a 50 mL round-bottom flask, 896 mg 1c (2.78 mmol, 1.00 equiv) are suspended in 10 mL toluene. After the addition of 1.18 g Lawesson's reagent (2.92 mmol, 1.05 equiv), the reaction mixture is stirred for 3 days at 120 °C reflux. After the reaction time, the reaction mixture is transferred to a separation funnel and washed with a saturated sodium hydrogen carbonate solution (3 × 20 mL). The combined organic phases are dried over MgSO₄, and the solvent is removed *in vacuo*. The crude residue is further purified by recrystallization with ethyl acetate (16 mL) to obtain 520 mg 1d (1.54 mmol, 55%) as yellow solid. ¹H NMR (400 MHz, (CD₃)₂SO, 294 K): δ [ppm] = 7.24 (s, 2H, CH), 7.17 (s, 2H, CH), 2.37 (s, 3H, CH_{3,p-mes}), 2.35 (s, 3H, CH_{3,p-mes}), 2.14 (s, 6H, CH_{3,0-mes}), 2.07 (s, 6H, CH_{3,0-mes}). ¹³C NMR (101 MHz, (CD₃)₂SO, 294 K): δ [ppm] = 175.3 (s, C_{NCON}), 142.4 (s, C_{ar}), 141.3 (s, C_{ar}), 135.3 (s, C_{ar}), 134.0 (s, C_{ar}), 132.3 (s, C_{ar}), 129.4 (s, C_{ar}), 129.0 (s, C_{ar}), 20.8 (s, CH₃), 20.8 (s, CH₃), 17.1 (s, CH₃), 16.3 (s, CH₃). EA (%): calcd C 67.42, H 6.55, N 16.55, S 9.47; found C 67.15, H 6.68, N 16.46, S 9.21. R_f = 0.94 (EtOAc) [UV].

1,3-Dimesityltetrazolium Hexafluorophosphate (L₁). In a 25 mL round-bottom flask, 457 mg 1d (1.35 mmol, 1.00 equiv) are dissolved in 2 mL of conc HNO_{3(aq)} and the reaction mixture is stirred for 2 h at 100 °C reflux. After the reaction time, the solution is filtered over Celite into a solution of 330 mg ammonium hexafluorophosphate (2.03 mmol, 1.50 equiv) in water (2.5 mL). After cooling to 4 °C, the precipitate is filtered and washed with water (3 × 2 mL). For further purification the product is dissolved in a small amount of acetonitrile and precipitated by addition of diethyl ether to obtain 370 mg L₁ (0.82 mmol, 61%) as a white solid. ¹H NMR (400 MHz, CD₃CN, 294 K): δ [ppm] = 10.12 (s, 1H, H_{tetr}), 7.28 (s, 4H, CH), 2.43 (s, 3H, CH_{3,p-mes}), 2.42 (s, 3H, CH_{3,p-mes}), 2.17 (s, 6H, CH_{3,0-mes}), 2.16 (s, 6H, CH_{3,0-mes}). ¹³C NMR (101 MHz, (CD₃)₂SO, 294 K): δ [ppm] = 152.1 (s, C_{NCON}), 143.8 (s, C_{ar}), 143.3 (s, C_{ar}), 134.7 (s, C_{ar}), 134.5 (s, C_{ar}), 131.4 (s, C_{ar}), 130.2 (s, C_{ar}), 128.8 (s, C_{ar}), 128.0 (s, C_{ar}), 124.0 (s, C_{ar}), 20.9 (s, CH₃), 20.9 (s, CH₃), 17.3 (s, CH₃), 17.0 (s, CH₃). EA (%): calcd C 50.45, H 5.12, N 12.39, F 25.20, P 6.85; found C 50.61, H 4.84, N 12.59. R_f = 0.10 (DCM) [UV].

General Procedure for the Synthesis of 1,3-Substituted Tetrazol-5-ylidene gold(I) Bis-NHC Complexes. The respective proligand (2.00 equiv), the gold precursor chloro-(tetrahydrothiophene)gold(I) (1.00 equiv) and the weak base potassium carbonate (6.00 equiv) are weighed in a glass vial and suspended in 4 mL of acetone. After stirring for 16 h, the solvent is

removed *in vacuo*. The crude residue is suspended in a small amount of dichloromethane and filtered over Celite. Subsequently, the filtrate is concentrated *in vacuo* (1 mL).

Bis-(1,3-dimesityltetrazol-5-ylidene)gold(I) Hexafluorophosphate (1). The general procedure for 1,3-substituted tetrazolylidene gold(I) bis-NHC complexes is applied, using 70 mg of the proligand L₁ (155 μmol, 2.00 equiv). The crude product is further dissolved in a small amount of DCM and purified by column chromatography (20 × 200 mm, 6.7 g Silica, DCM → DCM/MeOH 97:3) to obtain 35.4 mg of the product 1 (37.1 μmol, 48%) as a white solid. ¹H NMR (400 MHz, CD₃CN, 294 K): δ [ppm] = 7.21 (s, 4H, CH), 7.14 (s, 4H, CH), 2.48 (s, 6H, CH_{3,p-mes}), 2.40 (s, 6H, CH_{3,p-mes}), 2.04 (s, 12H, CH_{3,o-mes}), 1.83 (s, 12H, CH_{3,o-mes}). ¹³C NMR (101 MHz, CD₃CN, 295 K): 191.9 (s, C_{tetr}), 144.5 (s, C_{ar}), 143.7 (s, C_{ar}), 138.7 (s, C_{ar}), 135.7 (s, C_{ar}), 135.5 (s, C_{ar}), 133.0 (s, C_{ar}), 131.6 (s, C_{ar}), 130.8 (s, C_{ar}), 130.7 (s, C_{ar}), 118.3 (s, C_{ar}), 21.5 (s, CH₃), 21.3 (s, CH₃), 17.6 (s, CH₃), 17.3 (s, CH₃). EA (%): calcd, C 47.80, H 4.65, N 11.74, Au 20.63, P 3.24, F 11.94; found, C 48.13, H 4.76, N 11.35. R_f = 0.17 (DCM/MeOH = 97:3) [UV]. ESI-MS (*m/z*): [1-PF₆]⁺ calcd, 809.33; found, 809.27.

Bis-(1-tert-Butyl,3-iso-propyl-tetrazol-5-ylidene)gold(I) Hexafluorophosphate (2). The general procedure for 1,3-substituted tetrazolylidene gold(I) Bis-NHC complexes is applied, using 70 mg of the proligand L₂ (223 μmol). The crude perchlorate salt is further purified by filtration over Celite into a solution of ammonium hexafluorophosphate (27.2 mg, 167 μmol, 1.50 equiv) in water and acetone (4 mL, H₂O/acetone = 1:1). After removing the acetone under reduced pressure, the product is extracted with dichloromethane (3 × 6 mL) and the combined organic phases are dried over MgSO₄. The solvent is removed *in vacuo* to obtain the product 2 is obtained as a slightly yellow solid with a yield of 61.2 mg (90.2 μmol, 81%). Crystals suitable for SC-XRD were grown by slow diffusion of Et₂O into a solution of 2 in MeCN at 20 °C.

¹H NMR (400 MHz, CD₃CN, 294 K): δ [ppm] = 5.15 (hept, ²J = 6.7 Hz, 2H, CH), 1.91 (s, 18H, CH_{3,t-butyl}), 1.69 (s, 6H, CH_{3,o-isopropyl}), 1.68 (s, 6H, CH_{3,o-isopropyl}). ¹³C NMR (101 MHz, CD₃CN, 295 K): 186.5 (s, C_{tetr}), 65.0 (s, C_{t-butyl}), 60.9 (s, CH), 30.7 (s, C_{t-butyl}), 21.7 (s, C_{isopropyl}). EA (%): calcd C 28.33, H 4.75, N 16.52, Au 29.03, P 4.57, F 16.80; found C 28.60, H 4.80, N 16.29. R_f = 0.66 (DCM/MeOH = 10:2) [UV]. ESI-MS (*m/z*): [2-PF₆]⁺ calcd, 533.24; found, 533.17.

Used Cell Lines and Cultivation of Cells. The cell lines used were grown in RPMI 1640 medium (Gibco, Invitrogen, Karlsruhe, Germany) and cultivated at 37 °C with 5% CO₂. The medium was supplemented with 10% (v/v) heat-inactivated fetal bovine serum (FBS; Merck KGaA, Darmstadt, Germany) and 1% (v/v) penicillin streptomycin (ThermoFisher Scientific Inc., Waltham, USA). The cells are splitted twice a week and transferred to 75 cm² cell culture flasks at a concentration of 0.5 × 10⁵ cells/mL. In preparation for experiments, the suspension cells are prepared the day before in a concentration of 3 × 10⁵ cells/mL and standardized growth conditions are ensured. On the day of performance, the suspension cells are seeded at a concentration of 1 × 10⁵ cells/mL in 12-well plates in 2 mL of RPMI 1640 medium. Different concentrations of gold complexes and cytostatic drugs are added to the cells depending on the test being performed and incubated for different lengths of time, as described in the following sections. The gold complexes are dissolved in dimethyl sulfoxide (DMSO; Serva Electrophoresis GmbH, Heidelberg, Germany) in stock solutions with a concentration of 40 mM. A DMSO control with the highest concentration of the corresponding test substance, not exceeding 0.5%, is added to each test preparation.

The suspension cells B-lymphocyte leukemia cells (Nalm-6), B-lymphoma cells (BJAB) and chronic myeloid leukemia cells (K562) are used, as well as associated, specially generated, multidrug-resistant cell lines.

Measurement of Cell Concentration and Viability. The CASYCell Counter and Analyzer System (OMNI Life Science GmbH, Bremen, Germany) is used to measure the cell concentration, inhibition of proliferation and viability induced by the compounds

under investigation. There is a specific setting for each cell line used. 100 μL of the cell suspension are resuspended after 24 h in 10 mL CASYton (ready to use isotonic saline solution) and measured. The cell count of the treated cells with DMSO is taken as the maximum.

Determination of DNA Fragmentation. In the late phase of apoptosis, DNA fragmentation can be observed as a final process. Therefore, the cells incubated with gold compound are centrifuged after 72 h (5900g, 5 min, 4 °C) and then resuspended in 200 μL 2% (v/v) formaldehyde (Carl Roth GmbH, Karlsruhe, Germany). After 30 min incubation on ice, the cells are centrifuged (370g, 5 min, 4 °C), resuspended in 180 μL 2:1 (v/v) ethanol/1× PBS (Merck KGaA, Darmstadt, Germany; ThermoFisher Scientific Inc., Waltham, USA) and incubated again for 15 min on ice. After washing, 50 μL RNase A Solution (10 mg/mL in 1× PBS; VWR International GmbH, Darmstadt, Germany) is added to eliminate the RNA and incubated at 37 °C for 30 min. The cells are then centrifuged again (370g, 5 min, 4 °C) and stained with 200 μL 1× PBS containing 50 μg/μL propidium iodide (PI). PI is a DNA intercalating dye and allows the identification of cells with hypodiploid DNA. The experiment is quantified via flow cytometry (FACS Lyric, Becton Dickinson GmbH, Heidelberg, Germany), the data evaluation was performed by Cell Quest software. The IC₅₀ values determined to compare potency on different cell lines were obtained using the QuestGraph IC₅₀ Calculator (AAT Bioquest, Inc., <https://www.aatbio.com/tools/ic50-calculator>).

Exclusion of Necrosis via the Lactate Dehydrogenase (LDH) Outflow. The exclusion of necrosis is measured via the lactate dehydrogenase (LDH) release after one hour. For this purpose, Nalm-6 cells are seeded at a concentration of 1 × 10⁵ cells/mL in RPMI 1640 medium without FBS and treated for one hour with the gold compound at different concentrations. The LDH assay (Roche Molecular Systems Inc., Rotkreuz, Switzerland) was performed according to the manual. As a positive control, Nalm-6 cells were treated with 2% v/v Triton X-100 (Merck KGaA, Darmstadt, Germany) and defined as 100% cytotoxicity. DMSO control results are subtracted from all measured results to avoid possible background signals.

Differentiation between Late and Early Apoptosis and Necrosis via Annexin V/Propidium Iodide Staining. The Annexin-V-Fluos staining kit (Roche, Mannheim, Germany) can be used to determine the different stages of apoptosis and necrosis. Annexin-V dye binds to phosphatidylserine, which is normally localized on the inner membrane of the cell and migrates to the outside of the membrane during early apoptosis. Only then can the dye bind; it cannot pass through the membrane. PI cannot pass through the intact membrane either. Late apoptosis leads to permeabilization of the membrane and thus to the entry of PI dye, which can now intercalate with the DNA. If an isolated PI signal is found, this indicates necrosis. Nalm-6 cells are centrifuged 48 h after treatment with the gold compounds (8000 rpm, 5 min, 4 °C) and resuspended in 100 μL Annexin/PI staining solution. After incubation for 10–15 min, 200 μL incubation buffer is added and the cells are quantified using flow cytometry and Cell Quest software.

Interaction with CT-DNA by Circular Dichroism (CD) Spectroscopy. One mg of CT-DNA (Sigma-Aldrich) was dissolved in 7.58 mL of PBS buffer (10 mM phosphate buffer, 140 mM NaCl, 3 mM KCl, pH 7.4 at 25 °C) to obtain a 200 μM (in base pairs) solution. The solution was then diluted 1:2 and quantified by UV-vis spectroscopy by ε (260 nm) = 13,200 mol⁻¹ dm³ cm⁻¹ to give the actual concentration in DNA base pairs. The respective stock solution of the complexes was prepared by dissolving an adequate amount of the complexes (to achieve double the target concentration) in 1 mL DMSO and diluting it with 49 mL PBS buffer. For a blank measurement, 500 μL of the stock DNA solution was mixed with 500 μL of a mixture of DMSO and PBS (1:50). For the experiments with the complexes, 500 μL of the DNA stock solution was mixed with 500 μL of the complex stock solution. All CD spectra were collected on a Jasco J-810 spectrometer in the range of 230 to 320 nm with a measuring velocity of 100 nm/min, and a data point interval of 0.1 nm. Final DMSO concentrations remained below 1%.

CellRox. Reactive oxygen species (ROS) are formed in the cell during oxidative cell stress and can thus initiate cell death pathways. These ROS can be stained and detected using CellROX Green Reagent (ThermoFisher Scientific Inc., Waltham, USA). The procedure was according to the manual with slight modifications. 30% H₂O₂ was used as a positive control instead of TBHP. The fluorescence signal from stained ROS is measured by flow cytometry.

Measurement of the Mitochondrial Outer Membrane Potential (MOMP). The permeabilization of the mitochondrial outer membrane leads to a change in MOMP and initiates the apoptosis cascade.

5,5',6,6'-Tetrachloro-1,1',3,3'-tetra-ethylbenzimidazolyl-carbocyanine iodide (JC-1) is a dye used to detect the reduced MOMP. The cells are incubated for 48 h with the compound to be analyzed. The cells are then centrifuged (800g, 5 min, 4 °C) and the pellet is resuspended in phenol free RPMI medium. After addition of 6.25 μL JC-1 (ThermoFisher Scientific Inc., Waltham, USA), the cells are incubated (30 min, 37 °C) and then centrifuged (1500g, 5 min, 4 °C). The pellet is resuspended in 1x PBS and the percentage of cells with reduced MOMP is measured using flow cytometry and Cell Quest software.

Protein Extraction and Western Blotting. The analysis of protein expression was performed with cells treated for 24 h with the gold compound. Control cells were incubated with DMSO. Proteins were extracted from the cells by lysis in RPIA lysis buffer (50 mM Tris HCl, 150 mM NaCl, 1% Triton X-100, 0.1% SDS, 1 mM EDTA, pH 7.4) supplemented with protease inhibitors (Roche, Mannheim, Germany). The lysates were then incubated on ice (60 min) and centrifuged (12,000g, 30 min, 4 °C). The total protein in the supernatant was stored at -80 °C for Western blot analysis. The Bicinchoninic acid assay (BCA; Thermo Scientific, Rockford, USA) was used to determine the protein concentration of the samples in order to determine the loading volume required with 40 μg protein. The concentration was calculated and quantified using a standard curve of bovine serum albumin (BSA). Forty μg protein were diluted with 4x Laemmli sample buffer (12% SDS, 25% glycerol, 150 mM Tris HCl, 0.03% bromophenol blue, 20% β-mercaptoethanol) and denatured (5 min, 95 °C). The single proteins were separated on 12% acrylamide gels by gel electrophoresis using the Laemmli running buffer (Serva, Heidelberg, Germany). The proteins were then transferred to nitrocellulose membranes using Towbin transfer buffer (Serva, Heidelberg, Germany). The membranes were stained with Ponceau red to check the uniform protein loading. After blocking in 5% (m/v) skim milk in PBST (1x PBS, 0.05% Tween-20), primary antibodies were diluted in 5% BSA in PBST and incubated on the membrane for two hours at room temperature. The following primary antibodies were used: anticaspase 9 (R&D Systems, Minneapolis, USA), anti-MCL-1, anti-BCL2, anti-BAX (Proteintech Europe, Manchester, UK), and anti-β-actin (Sigma, St. Louis, USA). After washing three times in 1x PBST, the corresponding secondary antibody was incubated for two hours at room temperature. As secondary antibodies, antimouse IgG, antirabbit IgG and antigoat IgG (Promega, Madison, USA) were diluted in 5% skim milk in PBST. After washing again three times in PBST, the membranes were detected using the ECL Western Blotting Detection Reagent (GE Healthcare, Chicago, USA) and the Super Signal West Pico Chemiluminescent Substrate (Thermo Scientific, Rockford, USA). The images were captured using the Imager Chemi Premium System (VWR, Pennsylvania, USA). The densitometric analysis was performed with the VWR Image Capture Software (software version; VWR, Pennsylvania, USA) and the signal intensity of the target protein bands was normalized to the signal intensity of the housekeeping protein ACTB.

Isolation of Healthy Human Leukocytes. Human healthy leukocytes were isolated to investigate the selectivity of the compounds in proliferative cells. The blood from which the white blood cells were taken was made available to us by the coauthor Aram Prokop. 40 mL human blood was diluted in 14 mL RPMI 1640 medium (containing 20% (v/v) heat inactivated FBS and 1% (v/v) penicillin streptomycin). To each 5 mL of blood suspension, 4 mL of

Lymphosep (sucrose–epichlorohydrin copolymer) lymphocytes separation solution (Biowest, Nuaille, France) was added to create a separation with buffy coat using a concentration gradient. The suspension is centrifuged (2000 rpm, 18 min, 18 °C). Leukocytes are then transferred from the buffy coat into a 50 mL tube and dissolved 1:1 in RPMI medium and centrifuged again (2000 rpm, 5 min, 18 °C). The cell pellet is resuspended in 10 mL RPMI medium (20% FBS) and the cells are seeded in 12-well plates at a concentration of 3 × 10 cells/mL.

Statistical Analysis. The data collected was run in triplicate. The standard deviation (SD) was calculated and is shown in the figures as error bars. To assess the significance of the results, a two-tailed *t* test was performed with an accepted significance at *p* ≤ 0.05. The mean values of the results ± SD are shown in the figures and the significance is marked with an asterisk (*). The graphs and statistics were generated using Microsoft Office Excel.

■ ASSOCIATED CONTENT

SI Supporting Information

The Supporting Information is available free of charge at <https://pubs.acs.org/doi/10.1021/acs.jmedchem.4c01117>.

NMR spectra, MS spectra, and HPLC chromatograms, as well as biological assays (PDF)

Molecular formula strings file containing the SMILE structures of 1 and 2 (CSV)

■ AUTHOR INFORMATION

Corresponding Authors

Franziska Bannwart – Department of Human Medicine, MSH Medical School Hamburg, 20457 Hamburg, Germany; Department of Pediatric Hematology/Oncology, Helios Kliniken Schwerin, 19055 Schwerin, Germany; orcid.org/0009-0007-3344-1602; Phone: (+49) 385 520 6397; Email: franziska.bannwart@medicalschooll-hamburg.de

Aram Prokop – Department of Human Medicine, MSH Medical School Hamburg, 20457 Hamburg, Germany; Department of Pediatric Hematology/Oncology, Helios Kliniken Schwerin, 19055 Schwerin, Germany; Experimental Oncology, Municipal Hospitals of Cologne, 51109 Cologne, Germany; Phone: (+49) 385 520 6396; Email: aram.prokop@helios-gesundheit.de; Fax: (+49) 385 520 2704

Fritz E. Kühn – Department of Chemistry and Catalysis Research Center, Molecular Catalysis, Technical University of Munich, TUM School of Natural Sciences, 85748 Garching bei München, Germany; orcid.org/0000-0002-4156-780X; Phone: (+49) 89 289 13096; Email: fritz.kuehn@ch.tum.de

Authors

Leon F. Richter – Department of Chemistry and Catalysis Research Center, Molecular Catalysis, Technical University of Munich, TUM School of Natural Sciences, 85748 Garching bei München, Germany

Simon Stifel – Department of Chemistry and Catalysis Research Center, Molecular Catalysis, Technical University of Munich, TUM School of Natural Sciences, 85748 Garching bei München, Germany

Johanna Rueter – Department of Human Medicine, MSH Medical School Hamburg, 20457 Hamburg, Germany; Department of Pediatric Hematology/Oncology, Helios Kliniken Schwerin, 19055 Schwerin, Germany

Holger N. Lode – Department of Pediatric Hematology/Oncology, University Medicine Greifswald, 17475 Greifswald, Germany

João D. G. Correia – Centro de Ciências e Tecnologias Nucleares and Departamento de Engenharia e Ciências Nucleares, Instituto Superior Técnico, Universidade de Lisboa, Lisbon, LRS 2695-066, Portugal; orcid.org/0000-0002-7847-4906

Complete contact information is available at:
<https://pubs.acs.org/10.1021/acs.jmedchem.4c01117>

Author Contributions

Franziska Bannwart and Leon F. Richter contributed equally; **Franziska Bannwart**: Conceptualization, Data Curation, Formal analysis, Investigation, Project administration, Validation, Visualization, Writing – Original Draft, Writing – Review & Editing; **Leon F. Richter**: Conceptualization, Data Curation, Formal analysis, Investigation, Project administration, Validation, Visualization, Writing – Original Draft, Writing – Review & Editing; **Simon Stifel**: Investigation; **Johanna Rueter**: Investigation, Supervision, Writing – Review & Editing; **Holger N. Lode**: Supervision, Writing – Review & Editing; **João D. G. Correia**: Funding acquisition, Resources, Supervision, Writing – Review & Editing; **Fritz E. Kühn**: Funding acquisition, Resources, Supervision, Writing – Review & Editing; **Aram Prokop**: Funding acquisition, Resources, Supervision, Writing – Review & Editing; All authors have read and agreed to the published version of this article.

Notes

The authors declare no competing financial interest.

ACKNOWLEDGMENTS

F.B., J.R., and A.P. gratefully thank the Foundation Blankenheimerdorf ev (Blankenheim, Germany), the Foundation David (Cologne, Germany), the Dr. Kleist Foundation (Berlin, Germany), and the Koch-Foundation (Berlin, Germany) for financial support. Also, they thank the pharmacy of the Helios Clinics Schwerin, Germany, for providing the cytostatic drugs for their experiments. J.D.G.C. thanks Fundação para a Ciência e Tecnologia” (FCT, Portugal) for funding through projects UIDP/04349/2020 and PTDC/QUI-OUT/3854/2021. L.F.R. thanks Melanie Hoffmann and Dr. Aras Kartouzian for their valuable input and experimental support.

ABBREVIATIONS

A, Annexin V FITC; ABC, ATP-binding cassette; ACTB, β -actin; AF, auranofin; APAF-1, apoptotic protease activating factor-1; BAK, BCL-2 antagonist/killer; BAX, BCL-2 associated X protein; BCL-2, B-cell-lymphoma 2; BSA, bovine serum albumin; B-ALL, B-lymphoblastic leukemia; CD, circular dichroism; CML, chronic myeloid leukemia; CT-DNA, calf thymus DNA; Dauno, daunorubicin; DLCs, delocalized lipophilic cations; DMSO, dimethyl sulfoxide; Doxo, doxorubicin; ESI-MS, electrospray ionization mass spectrometry; FBS, fetal bovine serum; GSH, glutathione; HPLC, high pressure liquid chromatography; HSA, human serum albumin; H₂O₂, hydrogen peroxide; JC-1, 5,5',6,6'-tetrachloro-1,1',3,3'-tetra-ethylbenzimidazolyl-carbocyanine iodide; LDH, lactate dehydrogenase; MCL-1, myeloid cell leukemia-1; MOMP, mitochondrial outer membrane potential; NAC, N-acetylcysteine; NHC_{im}, imidazol-2-ylidene; NHC_{tetr}, tetrazolylidene;

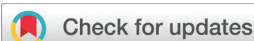
NHC_{tetr}, 1,2,3-triazol-5-ylidene; NHCs, N-heterocyclic carbene; PGP, P-glycoprotein; PI, propidium iodide; ROS, reactive oxygen species; Triton, Triton-X-100; TrxR, thio-redoxin reductase; tht, tetrahydrothiophene; VCR, vincristine

REFERENCES

- (1) Muggia, F. M.; Bonetti, A.; Hoeschele, J. D.; Rozenzweig, M.; Howell, S. B. Platinum Antitumor Complexes: 50 Years since Barnett Rosenberg's Discovery. *J. Clin. Oncol.* **2015**, *33* (35), 4219–4226.
- (2) Rosenberg, B.; Van Camp, L.; Krigas, T. Inhibition of Cell Division in Escherichia Coli by Electrolysis Products from a Platinum Electrode. *Nature* **1965**, *205* (4972), 698–699.
- (3) Turel, I. Special Issue: Practical Applications of Metal Complexes. *Molecules* **2015**, *20* (5), 7951–7956.
- (4) Hour, T.-C.; Lai, Y.-L.; Kuan, C.-I.; Chou, C.-K.; Wang, J.-M.; Tu, H.-Y.; Hu, H.-T.; Lin, C.-S.; Wu, W.-J.; Pu, Y.-S.; Sterneck, E.; Huang, A.-M. Transcriptional Up-Regulation of SOD1 by CEBPD: A Potential Target for Cisplatin Resistant Human Urothelial Carcinoma Cells. *Biochem. Pharmacol.* **2010**, *80* (3), 325–334.
- (5) Hsin, I.-L.; Wang, S.-C.; Li, J.-R.; Ciou, T.-C.; Wu, C.-H.; Wu, H.-M.; Ko, J.-L. Immunomodulatory Proteins FIP-GTs and Chloroquine Induce Caspase-Independent Cell Death via Autophagy for Resensitizing Cisplatin-Resistant Urothelial Cancer Cells. *Phytomedicine* **2016**, *23* (13), 1566–1573.
- (6) Hunger, S. P.; Raetz, E. A. How I Treat Relapsed Acute Lymphoblastic Leukemia in the Pediatric Population. *Blood, J. Am. Soc. Hematol.* **2020**, *136* (16), 1803–1812.
- (7) Longley, D. B.; Johnston, P. G. Molecular Mechanisms of Drug Resistance. *J. Pathol.* **2005**, *205* (2), 275–292.
- (8) Holohan, C.; Van Schaeybroeck, S.; Longley, D. B.; Johnston, P. G. Cancer Drug Resistance: An Evolving Paradigm. *Nat. Rev. Cancer* **2013**, *13* (10), 714–726.
- (9) Alves, R.; Gonçalves, A. C.; Jorge, J.; Almeida, A. M.; Sarmiento-ribeiro, A. B. Combination of Elacridar with Imatinib Modulates Resistance Associated with Drug Efflux Transporters in Chronic Myeloid Leukemia. *Biomedicines* **2022**, *10* (5), 1158.
- (10) Kostka, L.; Sivák, L.; Šubr, V.; Kovářová, J.; Šírová, M.; Říhová, B.; Sedláček, R.; Etrych, T.; Kovář, M. Simultaneous Delivery of Doxorubicin and Protease Inhibitor Derivative to Solid Tumors via Star-Shaped Polymer Nanomedicines Overcomes P-Gp- and STAT3-Mediated Chemoresistance. *Biomacromolecules* **2022**, *23* (6), 2522–2535.
- (11) Chen, H.; Shien, K.; Suzawa, K.; Tsukuda, K.; Tomida, S.; Sato, H.; Torigoe, H.; Watanabe, M.; Namba, K.; Yamamoto, H.; Soh, J.; Asano, H.; Miyoshi, S.; Toyooka, S. Elacridar, a Third-Generation ABCB1 Inhibitor, Overcomes Resistance to Docetaxel in Non-Small Cell Lung Cancer. *Oncol. Lett.* **2017**, *14* (4), 4349–4354.
- (12) Oun, R.; Moussa, Y. E.; Wheate, N. J. The Side Effects of Platinum-Based Chemotherapy Drugs: A Review for Chemists. *Dalt. Trans.* **2018**, *47* (19), 6645–6653.
- (13) Olelewe, C.; Awuah, S. G. Mitochondria as a Target of Third Row Transition Metal-Based Anticancer Complexes. *Curr. Opin. Chem. Biol.* **2023**, *72*, 102235.
- (14) Tialiou, A.; Chin, J.; Keppler, B. K.; Reithofer, M. R. Current Developments of N-Heterocyclic Carbene Au(I)/Au(III) Complexes toward Cancer Treatment. *Biomedicines* **2022**, *10* (6), 1417.
- (15) Borutzki, Y.; Skos, L.; Gerner, C.; Meier-Menches, S. M. Exploring the Potential of Metal-Based Candidate Drugs as Modulators of the Cytoskeleton. *ChemBioChem* **2023**.
- (16) Van Der Westhuizen, D.; Bezuidenhout, D. I.; Munro, O. Q. Cancer Molecular Biology and Strategies for the Design of Cytotoxic Gold(i) and Gold(iii) Complexes: A Tutorial Review. *Dalt. Trans.* **2021**, *50* (47), 17413–17437.
- (17) Yeo, C. I.; Ooi, K. K.; Tiekink, E. R. T. Gold-Based Medicine: A Paradigm Shift in Anti-Cancer Therapy? *Molecules* **2018**, *23*, 1410.
- (18) Porchia, M.; Pellei, M.; Marinelli, M.; Tisato, F.; Del Bello, F.; Santini, C. New Insights in Au-NHCs Complexes as Anticancer Agents. *Eur. J. Med. Chem.* **2018**, *146*, 709–746.

- (19) Liu, X.; Li, H.; Yin, X. NaOH-Promoted One-Pot Aryl Isothiocyanate Synthesis under Mild Benchtop Conditions. *Phosphorus, Sulfur Silicon Relat. Elem.* **2021**, *196* (9), 839–844.
- (20) Krabbendam, I. E.; Honrath, B.; Bothof, L.; Silva-Pavez, E.; Huerta, H.; Peñaranda Fajardo, N. M.; Dekker, F.; Schmidt, M.; Culmsee, C.; César Cárdenas, J.; Kruyt, F.; Dolga, A. M. SK Channel Activation Potentiates Auranofin-Induced Cell Death in Glio- and Neuroblastoma Cells. *Biochem. Pharmacol.* **2020**, *171*, 113714.
- (21) Freire Boulosa, L.; Van Loenhout, J.; Flieswasser, T.; De Waele, J.; Hermans, C.; Lambrechts, H.; Cuypers, B.; Laukens, K.; Bartholomeus, E.; Siozopoulou, V.; De Vos, W. H.; Peeters, M.; Smits, E. L. J.; Deben, C. Auranofin Reveals Therapeutic Anticancer Potential by Triggering Distinct Molecular Cell Death Mechanisms and Innate Immunity in Mutant P53 Non-Small Cell Lung Cancer. *Redox Biol.* **2021**, *42*, 101949.
- (22) Chen, L.; Ren, A.; Zhao, Y.; Chen, H.; Wu, Q.; Zheng, M.; Zhang, Z.; Zhang, T.; Zhong, W.; Lin, J.; Zhu, H. Direct Inhibition of Dioxygenases TET1 by the Rheumatoid Arthritis Drug Auranofin Selectively Induces Cancer Cell Death in T-ALL. *J. Hematol. Oncol.* **2023**, *16* (1), 4–9.
- (23) Mirabelli, C. K.; Johnson, R. K.; Sung, C. M.; Faucette, L.; Muirhead, K.; Croke, S. T. Evaluation of the in Vivo Antitumor Activity and in Vitro Cytotoxic Properties of Auranofin, a Coordinated Gold Compound, in Murine Tumor Models. *Cancer Res.* **1985**, *45*, 32–39.
- (24) Mirabelli, C. K.; Johnson, R. K.; Hill, D. T.; Faucette, L. F.; Girard, G. R.; Kuo, G. Y.; Sung, C. M.; Croke, S. T. Correlation of the in Vitro Cytotoxic and in Vivo Antitumor Activities of Gold(I) Coordination Complexes. *J. Med. Chem.* **1986**, *29*, 218–223.
- (25) Hopkinson, M. N.; Richter, C.; Schedler, M.; Glorius, F. An Overview of N-Heterocyclic Carbenes. *Nature* **2014**, *510* (7506), 485–496.
- (26) Ott, I. Metal N-Heterocyclic Carbene Complexes in Medicinal Chemistry. *Advances in Inorganic Chemistry* **2020**, *75*, 121–148.
- (27) Hickey, J. L.; Ruhayel, R. A.; Barnard, P. J.; Baker, M. V.; Berners-Price, S. J.; Filipovska, A. Mitochondria-Targeted Chemotherapeutics: The Rational Design of Gold(I) N-Heterocyclic Carbene Complexes That Are Selectively Toxic to Cancer Cells and Target Protein Selenols in Preference to Thiols. *J. Am. Chem. Soc.* **2008**, *130* (38), 12570–12571.
- (28) Berners-Price, S. J.; Filipovska, A. Gold Compounds as Therapeutic Agents for Human Diseases. *Metallomics* **2011**, *3* (9), 863–873.
- (29) Lazreg, F.; Cazin, C. S. J. Medical Applications of NHC-Gold and -Copper Complexes. *N-Heterocyclic Carbenes: Effective Tools for Organometallic Synthesis* **2014**, 173–198.
- (30) Baker, M. V.; Barnard, P. J.; Berners-Price, S. J.; Brayshaw, S. K.; Hickey, J. L.; Skelton, B. W.; White, A. H. Cationic, Linear Au (I) N-Heterocyclic Carbene Complexes: Synthesis, Structure and Anti-Mitochondrial Activity. *Dalt. Trans.* **2006**, No. 30, 3708–3715.
- (31) Modica-Napolitano, J. S.; Aprile, J. R. Delocalized Lipophilic Cations Selectively Target the Mitochondria of Carcinoma Cells. *Adv. Drug Delivery Rev.* **2001**, *49* (1–2), 63–70.
- (32) Stefan, L.; Bertrand, B.; Richard, P.; Le Gendre, P.; Denat, F.; Picquet, M.; Monchaud, D. Assessing the Differential Affinity of Small Molecules for Noncanonical DNA Structures. *ChemBioChem.* **2012**, *13* (13), 1905–1912.
- (33) Bertrand, B.; Stefan, L.; Pirrotta, M.; Monchaud, D.; Bodio, E.; Richard, P.; Le Gendre, P.; Warmerdam, E.; De Jager, M. H.; Groothuis, G. M. M.; Picquet, M.; Casini, A. Caffeine-Based Gold(I) N-Heterocyclic Carbenes as Possible Anticancer Agents: Synthesis and Biological Properties. *Inorg. Chem.* **2014**, *53* (4), 2296–2303.
- (34) Schlagintweit, J. F.; Jakob, C. H. G.; Wilke, N. L.; Ahrweiler, M.; Frias, C.; Frias, J.; König, M.; Esslinger, E. M. H. J.; Marques, F.; MacHado, J. F.; Reich, R. M.; Morais, T. S.; Correia, J. D. G.; Prokop, A.; Kühn, F. E. Gold(I) Bis(1,2,3-Triazol-5-Ylidene) Complexes as Promising Selective Anticancer Compounds. *J. Med. Chem.* **2021**, *64* (21), 15747–15757.
- (35) Richter, L. F.; Marques, F.; Correia, J. D. G.; Pöthig, A.; Kühn, F. E. Exploiting Click-Chemistry: Backbone Post-Functionalisation of Homoleptic Gold(i)-1,2,3-triazole-5-ylidene complexes. *Dalt. Trans.* **2023**, *52*, 17185.
- (36) Aucamp, D.; Kumar, S. V.; Liles, D. C.; Fernandes, M. A.; Harmse, L.; Bezuidenhout, D. I. Synthesis of Heterobimetallic Gold(i) Ferrocenyl-Substituted 1,2,3-Triazol-5-Ylidene Complexes as Potential Anticancer Agents. *Dalt. Trans.* **2018**, *47* (45), 16072–16081.
- (37) Hoyer, C.; Schwerk, P.; Suntrup, L.; Beerhues, J.; Nössler, M.; Albold, U.; Dervede, J.; Tedin, K.; Sarkar, B. Synthesis, Characterization, and Evaluation of Antibacterial Activity of Ferrocenyl-1,2,3-Triazoles, Triazolium Salts, and Triazolylidene Complexes of Gold(i) and Silver(I). *Eur. J. Inorg. Chem.* **2021**, *2021* (14), 1373–1382.
- (38) Schaper, L. A.; Wei, X.; Altmann, P. J.; Jelle, K.; Pöthig, A.; Drees, M.; Mink, J.; Herdtweck, E.; Bechlar, B.; Herrmann, W. A.; Kühn, F. E. Synthesis and Comparison of Transition Metal Complexes of Abnormal and Normal Tetrazolylidenes: A Neglected Ligand Species. *Inorg. Chem.* **2013**, *52* (12), 7031–7044.
- (39) Gabrielli, W. F.; Nogai, S. D.; McKenzie, J. M.; Cronje, S.; Raubenheimer, H. G. Tetrazolyl and Tetrazolylidene Complexes of Gold: A Synthetic and Structural Study. *New J. Chem.* **2009**, *33* (11), 2208–2218.
- (40) Gabrielli, W. F.; Nogai, S. D.; Nell, M.; Cronje, S.; Raubenheimer, H. G. Neutral Mononuclear and Dinuclear Complexes of Gold(I) Featuring Azole Ligands: Synthesis, Structure and Cytotoxicity. *Polyhedron* **2012**, *34* (1), 188–197.
- (41) Kinzhalov, M. A.; Legkodukh, A. S.; Anisimova, T. B.; Novikov, A. S.; Suslonov, V. V.; Luzyanin, K. V.; Kukushkin, V. Y. Tetrazol-5-Ylidene Gold(III) Complexes from Sequential [2 + 3] Cycloaddition of Azide to Metal-Bound Isocyanides and N4 Alkylation. *Organometallics* **2017**, *36* (20), 3974–3980.
- (42) Soto, K. M.; Luzardo-Ocampo, I.; López-Romero, J. M.; Mendoza, S.; Loarca-Piña, G.; Rivera-Muñoz, E. M.; Manzano-Ramírez, A. Gold Nanoparticles Synthesized with Common Mullein (*Verbascum Thapsus*) and Castor Bean (*Ricinus Communis*) Ethanolic Extracts Displayed Antiproliferative Effects and Induced Caspase 3 Activity in Human HT29 and SW480 Cancer Cells. *Pharmaceutics* **2022**, *14* (10), 2069.
- (43) Quero, J.; Royo, J. C.; Fodor, B.; Gimeno, M. C.; Osada, J.; Rodríguez-Yoldi, M. J.; Cerrada, E. Sulfonamide-Derived Dithiocarbamate Gold (I) Complexes Induce the Apoptosis of Colon Cancer Cells by the Activation of Caspase 3 and Redox Imbalance. *Biomedicines* **2022**, *10* (6), 1437.
- (44) Liu, B.; Li, J.; Zhou, P.; Pan, W.; Li, N.; Tang, B. Real-Time in Situ Sequential Fluorescence Activation Imaging of Cyt c and Caspase-9 with a Gold-Selenium-Bonded Nanoprobe. *Anal. Chem.* **2021**, *93* (50), 16880–16886.
- (45) Rouco, L.; Sanchez-Gonzalez, A.; Alvarino, R.; Alfonso, A.; Vazquez-Lopez, E. M.; Garcia-Martínez, E.; Maneiro, M. Combined Effect of Caspase-Dependent and Caspase-Independent Apoptosis in the Anticancer Activity of Gold Complexes with Phosphine and Benzimidazole Derivatives. *Pharmaceutics* **2021**, *14* (1), 10.
- (46) Foucquier, J.; Guedj, M. Analysis of Drug Combinations: Current Methodological Landscape. *Pharmacol. Res. Perspect.* **2015**, *3* (3), e00149.
- (47) Choroba, K.; Machura, B.; Szlapa-Kula, A.; Malecki, J. G.; Raposo, L.; Roma-Rodrigues, C.; Cordeiro, S.; Baptista, P. V.; Fernandes, A. R. Square Planar Au (III), Pt (II) and Cu (II) Complexes with Quinoline-Substituted 2, 2': 6', 2''-Terpyridine Ligands: From in Vitro to in Vivo Biological Properties. *Eur. J. Med. Chem.* **2021**, *218*, 113404.
- (48) Nandy, A.; Dey, S. K.; Das, S.; Munda, R. N.; Dinda, J.; Saha, K. D. Gold (I) N-Heterocyclic Carbene Complex Inhibits Mouse Melanoma Growth by P53 Upregulation. *Mol. Cancer* **2014**, *13*, 57.
- (49) Zhai, J.; Jia, Y.; Zhao, L.; Yuan, Q.; Gao, F.; Zhang, X.; Cai, P.; Gao, L.; Guo, J.; Yi, S.; Chai, Z.; Zhao, Y.; Gao, X. Turning On/Off the Anti-Tumor Effect of the Au Cluster via Atomically Controlling Its Molecular Size. *ACS Nano* **2018**, *12* (5), 4378–4386.

- (50) Rauscher, S.; Greil, R.; Geisberger, R. Re-Sensitizing Tumor Cells to Cancer Drugs with Epigenetic Regulators. *Curr. Cancer Drug Targets* **2021**, *21* (4), 353–359.
- (51) Li, Z.; Chen, C.; Chen, L.; Hu, D.; Yang, X.; Zhuo, W.; Chen, Y.; Yang, J.; Zhou, Y.; Mao, M.; Zhang, X.; Xu, L.; Ju, S.; Shen, J.; Wang, Q.; Dong, M.; Xie, S.; Wei, Q.; Jia, Y.; Zhou, J.; Wang, L. STAT5a Confers Doxorubicin Resistance to Breast Cancer by Regulating ABCB1. *Front. Oncol.* **2021**, *11*, 697950.
- (52) Huang, W.; Yang, S.; Cheng, Y.-S.; Sima, N.; Sun, W.; Shen, M.; Braisted, J. C.; Lu, W.; Zheng, W. Terfenadine Resensitizes Doxorubicin Activity in Drug-Resistant Ovarian Cancer Cells via an Inhibition of CaMKII/CREB1-Mediated ABCB1 Expression. *Front. Oncol.* **2022**, *12*, 1068443.
- (53) Schmidt, C.; Albrecht, L.; Balasupramaniam, S.; Misgeld, R.; Karge, B.; Brönstrup, M.; Prokop, A.; Baumann, K.; Reichl, S.; Ott, I. A Gold (I) Biscarbene Complex with Improved Activity as a TrxR Inhibitor and Cytotoxic Drug: Comparative Studies with Different Gold Metallo-drugs. *Metallomics* **2019**, *11* (3), 533–545.
- (54) Ott, I.; Qian, X.; Xu, Y.; Vlecken, D. H. W.; Marques, I. J.; Kubutat, D.; Will, J.; Sheldrick, W. S.; Jesse, P.; Prokop, A.; Bagowski, C. P. A Gold (I) Phosphine Complex Containing a Naphthalimide Ligand Functions as a TrxR Inhibiting Antiproliferative Agent and Angiogenesis Inhibitor. *J. Med. Chem.* **2009**, *52*, 763–770.
- (55) Rubbiani, R.; Kitanovic, I.; Alborzina, H.; Can, S.; Kitanovic, A.; Onambele, L. A.; Stefanopoulou, M.; Geldmacher, Y.; Sheldrick, W. S.; Wolber, G.; Prokop, A.; Wolf, S.; Ott, I. Benzimidazol-2-Ylidene Gold (I) Complexes Are Thioredoxin Reductase Inhibitors with Multiple Antitumor Properties. *J. Med. Chem.* **2010**, *53* (24), 8608–8618.
- (56) Serebryanskaya, T. V.; Lyakhov, A. S.; Ivashkevich, L. S.; Schur, J.; Frias, C.; Prokop, A.; Ott, I. Gold (I) Thiotetrazolates as Thioredoxin Reductase Inhibitors and Antiproliferative Agents. *Dalt. Trans.* **2015**, *44* (3), 1161–1169.
- (57) Schmidt, C.; Karge, B.; Misgeld, R.; Prokop, A.; Franke, R.; Brönstrup, M.; Ott, I. Gold (I) NHC Complexes: Antiproliferative Activity, Cellular Uptake, Inhibition of Mammalian and Bacterial Thioredoxin Reductases, and Gram-Positive Directed Antibacterial Effects. *Chem.—Eur. J.* **2017**, *23* (8), 1869–1880.
- (58) Schmidt, C.; Karge, B.; Misgeld, R.; Prokop, A.; Brönstrup, M.; Ott, I. Biscarbene Gold (I) Complexes: Structure-Activity-Relationships Regarding Antibacterial Effects, Cytotoxicity, TrxR Inhibition and Cellular Bioavailability. *Medchemcomm* **2017**, *8* (8), 1681–1689.
- (59) Ahrweiler-Sawaryn, M.-C.; Biswas, A.; Frias, C.; Frias, J.; Wilke, N. L.; Wilke, N.; Berkessel, A.; Prokop, A. Novel Gold (I) Complexes Induce Apoptosis in Leukemia Cells via the ROS-Induced Mitochondrial Pathway with an Upregulation of Harakiri and Overcome Multi Drug Resistances in Leukemia and Lymphoma Cells and Sensitize Drug Resistant Tumor Cells to Apoptosis. *Biomed. Pharmacother.* **2023**, *161*, 114507.
- (60) Abdalbari, F. H.; Telleria, C. M. The Gold Complex Auranofin: New Perspectives for Cancer Therapy. *Discovery Oncol.* **2021**, *12*, 42.
- (61) Xiao, Q.; Liu, Y.; Jiang, G.; Liu, Y.; Huang, Y.; Liu, W.; Zhang, Z. Heteroleptic Gold (I)-BisNHC Complex with Excellent Activity In Vitro, Ex Vivo and In Vivo against Endometrial Cancer. *Eur. J. Med. Chem.* **2022**, *236*, 114302.
- (62) Gurba, A.; Taciak, P.; Sacharczuk, M.; Młynarczuk-Biały, I.; Bujalska-Zadrożny, M.; Fichna, J. Gold (III) Derivatives in Colon Cancer Treatment. *Int. J. Mol. Sci.* **2022**, *23* (2), 724.
- (63) Koren, A. O.; Gaponik, P. N. Regioselective of Tetrazole and 5-Substituted Tetrazoles N2 Alkylation by Alcohols. *Chem. Heterocycl. Compd.* **1990**, *26*, 1366–1370.
- (64) Henry, R. A.; Finnegan, W. G. An Improved Procedure for the Deamination of 5-Aminotetrazole. *J. Am. Chem. Soc.* **1954**, *76* (1), 290–291.
- (65) Voitekhovich, S. V.; Gaponik, P. N.; Lyakhov, A. S.; Ivashkevich, O. A. Synthesis and Structure of 1-Tert-Butyl-3-R-Tetrazolium Salts. *Chem. Heterocycl. Compd.* **2001**, *37* (8), 949–959.

Cite this: *Dalton Trans.*, 2023, **52**, 17185

Exploiting click-chemistry: backbone post-functionalisation of homoleptic gold(i) 1,2,3-triazole-5-ylidene complexes†

Leon F. Richter, ^a Fernanda Marques, ^b João D. G. Correia, ^b Alexander Pöthig ^c and Fritz E. Kühn ^{*,a}

The synthesis of a homoleptic azide-functionalised Au(I) bis-1,2,3-triazole-5-ylidene complex is reported, starting from a backbone-modified 1,2,3-triazolium salt ligand precursor. The incorporated azide handle allows for a straightforward modification of the complex according to click-chemistry protocols without impacting the steric shielding around the metal center, demonstrating the superiority of the presented triazole ligand framework over imidazole based systems. Employing the SPAAC and the CuAAC reactions, post-modification of the complex is facilitated with two model substrates, while retaining very high anti-proliferative activity (nanomolar range IC₅₀ values) in A2780 and MCF-7 human cancer cells.

Received 18th September 2023,
Accepted 11th October 2023

DOI: 10.1039/d3dt03052k

rsc.li/dalton

Introduction

The ability to treat diseases on a cause-and-effect logic (“magic bullet”) as initially proposed by Paul Ehrlich early in the 20th century is one of the most significant achievements of modern medicine.^{1,2} The selective treatment of cancer, however, is still a big challenge. Unfortunately, commonly applied chemotherapeutic agents such as cisplatin often cause severe side-effects and are prone to invoke drug resistance.^{3,4} The experiences with platinum based drugs have motivated researchers to investigate other transition metals such as ruthenium or gold for their therapeutic applicabilities.^{5,6} To enhance the selectivity of antiproliferative drugs and thus enable targeted therapy, supramolecular encapsulation and chemical tethering are among the concepts currently under examination.⁷ In the first case a cytotoxic agent is encapsulated into a transporting framework (e.g. molecular cages) or fixed on carrier materials (e.g. nanoparticles) to be delivered to its target,⁸ whereas in the latter the covalent conjugation of the active compound (“warhead”) to a targeting vector leads to small molecule drug

conjugates (SMDCs) or antibody drug conjugates (ADCs).^{9,10} It has to be noted, however, that the cage encapsulation or nanoparticle fixation requires in many cases also a targeting system. In this case the “payload”, *i.e.* the anti-cancer agent is (usually) not covalently attached to the vector, but the cage or carrier is.¹¹ Accordingly, a vector-cage or a vector-nanoparticle system with an appropriately stable bond has to be constructed,¹² not a ligand vector connection as in the case presented here. The ligand-vector connection, however, must not (negatively) influence (*i.e.* reduce) the “payload” activity.

Organometallic compounds incorporating N-heterocyclic carbene (NHC) ligands are, for example, promising candidates for chemical tethering strategies, due to their facile synthesis and easy functionalisation, particularly *via* wingtip modification.

Berners-Price and co-workers originally described the high antiproliferative activity of a series of cationic mono- and binuclear Au(I) bis-NHC_{im} complexes.^{13,14} Further studies have shown that the mechanism of action of Au(I)-NHCs differ from that of cisplatin, inducing apoptosis through concurrent selective targeting of mitochondria and inhibition of the enzyme thioredoxin reductase.^{15,16} To further enhance the selectivity towards cancer cells, several examples of Au(I) NHC_{im} complexes suitable for post-modification have been reported. They bear *inter alia* hydroxyl,^{17–19} activated ester,^{10,20} azide²¹ and carboxylic acid^{22,23} functional groups, which are available for further bioconjugation. The azide-alkyne cycloaddition (AAC) reaction has proven successful on both pre- and post-functionalisation of Au(I) NHC_{im}-complexes.^{21,24} Whereas Au(I) imidazolylidene complexes have been extensively investigated with respect to their potential medicinal application,²⁵ their triazolylidene analogues are scarcely represented in literature.^{26,27}

^aTechnical University of Munich, TUM School of Natural Sciences, Department of Chemistry and Catalysis Research Centre, Molecular Catalysis, Lichtenbergstr. 4, 85748 Garching bei München, Germany. E-mail: fritz.kuehn@ch.tum.de

^bCentro de Ciências e Tecnologias Nucleares and Departamento de Engenharia e Ciências Nucleares, Instituto Superior Técnico, Universidade de Lisboa, CTN, Estrada Nacional 10 (km 139, 7), 2695-066 Bobadela LRS, Portugal

^cTechnical University of Munich, TUM School of Natural Sciences, Department of Chemistry, Catalysis Research Center, Lichtenbergstr. 4, 85748 Garching bei München, Germany

† Electronic supplementary information (ESI) available. CCDC 2268759. For ESI and crystallographic data in CIF or other electronic format see DOI: <https://doi.org/10.1039/d3dt03052k>

For mesoionic 1,2,3-triazole-based NHCs, the synthesis of tris-substituted triazolium salts – which give the NHC_{trz} ligand upon deprotonation – is achieved *via* the CuAAC click reaction of an organic azide and an alkyne,^{28,29} followed by alkylation with an alkyl halide (usually MeI).³⁰ A significant advantage of the NHC_{trz} ligand type over NHC_{im} is the easy functionalisation of the backbone by straightforward *N*-alkylation, which is, of course, not possible with the backbone of the imidazole system. While modification of the wingtip substituents is a common strategy to fine-tune the electronic and steric properties of the complexes,^{31,32} interestingly, no examples for backbone functionalised NHC_{trz} complexes have been reported in the literature so far (Chart 1). Recent research has shown that the Au(I) bis- NHC_{trz} complexes bearing mesityl (Mes) wingtips show high antiproliferative activity in several cancer cell types, which prompted the use of 1,4-dimesityl-1*H*-1,2,3-triazole as the basic framework in this work.²⁶ Post-functionalisation strategies typically include biologically native functional groups.^{22,23,33} While these have been reported for attaching small molecules,^{17,19,22,23,33,34} we only found one example where the post-conjugation to an antibody was facilitated, however here efficacy of the resulting ADCs was hampered due to their low cytotoxicity.¹⁰ The strain promoted azide alkyne cycloaddition (SPAAC) was established by Bertozzi *et al.* as a reliable, selective and versatile technique for the conjugation of biomolecules and was awarded with the Nobel prize in chemistry in 2022.³⁵ Copper-free click chemistry is widely employed for preparing agents for molecular imaging and drug delivery systems *in vivo*.^{36–39} Based on such applications,

the azide moiety is chosen in this work as the terminal functionality due to its bioorthogonality, its versatile reactivity by means of click chemistry (CuAAC, Staudinger ligation, SPAAC) and its excellent stability during complexation reactions. A highly flexible C_6 hydrocarbon spacer is incorporated to reduce steric stress with the metal periphery when using large targeting moieties such as peptides or antibodies, minimising non-specific interactions with biological targets.

Results and discussion

Synthesis of the ligand precursors

The rather straightforward synthesis pathway to the azide functionalised triazolium salt **3** is shown in Scheme 1. Initial sublimation (140 °C, 10^{-3} mbar) of the literature-known 1,4-dimesityl triazole prior to further reactions is important, since only oily products are obtained when using the crude product of the copper catalysed click reaction. Alkylation of 1,4-dimesityl triazole (**1**) is achieved with excess 1,6-diiodohexane in dry MeCN. Analytically pure iodine-substituted compound **2** is obtained after repeated precipitation of the concentrated reaction mixture with MeCN/Et₂O as indicated by the expected downfield shifting of the H_{trz} signal to 9.45 ppm (found at 8.33 ppm for **1**) and the triplet at 4.45 ppm, corresponding to the $\text{N}_{\text{trz}}\text{-CH}_2\text{-}$ group. Moreover, elemental analysis and a single peak at 516.33 *m/z* in electrospray ionisation mass spectrometry (ESI-MS) spectrum further confirm the high purity of **2**. Upon dissolving **2** in acetone, NaN_3 (2.00 eq.) in water is added and the solution is stirred for 4 days. The

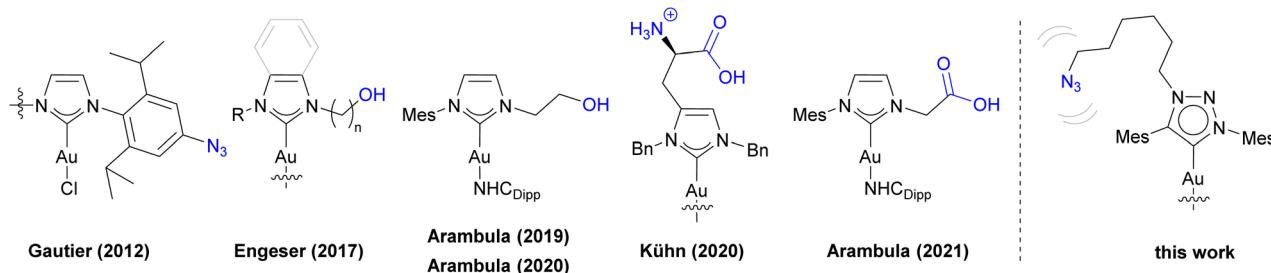
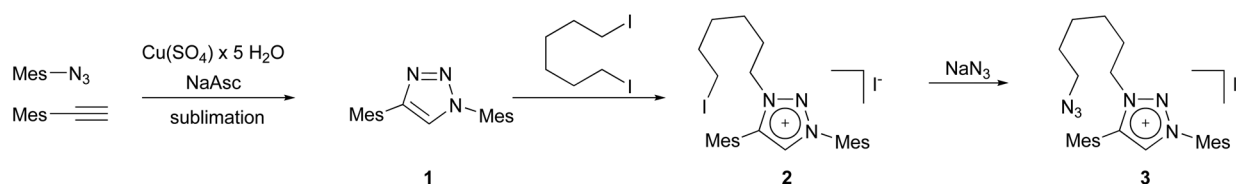


Chart 1 A selection of Au(I)- NHC_{im} complexes for post-conjugation in literature. In general, the imidazole system only allows for functionalisation of the wingtip substituents, resulting in a different steric shielding of the gold atom upon conjugation. The histidine-based bis-NHC complex, investigated in our group poses a nice exception, although post-functionalisation *via* esterification has been proven to lack stability in biological systems. The highly flexible azide-functionalised complex presented in this work overcomes those challenges, yielding biologically stable conjugates with no variance in steric shielding of the gold centre. The wavy line indicates an omitted identical substituent. Anions are omitted for clarity. The grey brackets on the right structure emphasise the high flexibility of the C_6 -spacer.



Scheme 1 3-Step synthesis of the ligand precursor **3** (see the ESI† for details).

progress of the nucleophilic substitution is monitored *via* ESI-MS, upon completion showing a single peak at 431.27 *m/z* corresponding to the cationic fragment of **3**. Upon precipitation with water, followed by filtration- and washing steps, the azide functionalised triazolium salt **3** is obtained in high purity as characterised by ^1H , ^{13}C -NMR, ESI-MS, elemental analysis and FT-IR. When compared to **2**, a slight downfield shift of the $-\text{CH}_2-\text{N}_3$ to 3.27 ppm ($-\text{CH}_2-\text{I}$ at 3.21 ppm) is noted. FT-IR of **3** shows the characteristic stretching vibration of the azide group at 2086 cm^{-1} .

Synthesis of the Au(I) complexes

The preparation of the homoleptic azide-functionalised Au(I) bis-NHC_{trz} complex **4** is achieved by two different synthetic pathways (Scheme 2). The weak base approach is used for the synthesis of **4-I**. Au(tht)Cl is mixed with **3** (2.00 eq.) and K_2CO_3 (3.00 eq.) in acetone. After stirring for 3 days at 60 °C, the product is isolated in 92% yield after simple precipitation from acetone/ Et_2O . In addition, **4-PF** is accessible *via* the convenient silver oxide route using Au(tht)Cl in a one-pot transmetallation reaction, followed by anion exchange with NH_4PF_6 . In each case, the successful synthesis of complex **4** is indicated by the disappearance of the H_{trz} in the ^1H -NMR spectrum, as well as the characteristic carbene resonance at 176.2 ppm in the ^{13}C -NMR spectrum, also reported for other Au(I) bis-NHC_{trz} complexes.²⁶ The chemical shifts are identical for the two complexes, since they only differ by their respective anion. Additionally, ESI-MS, elemental analysis, analytical HPLC and FT-IR indicate a high purity. Single crystal X-ray diffraction (SC-XRD) analysis of **4-I** depicts the expected nearly linear geometry around the Au(I) centre ($\text{C}_1-\text{Au}-\text{C}_{27} = 176.55^\circ$). The respective bond length of 2.013(3) Å (Au-C₁) and 2.012(3) Å (Au-C₂₇) is in accordance with other Au(I) bis-NHC_{trz} complexes (Fig. 1).^{26,40}

Post-functionalisation studies

For the post-functionalisation of **4**, common conjugation protocols for azide functionalities such as the copper catalysed (CuAAC) and strain promoted (SPAAC) azide/alkyne cyclo-

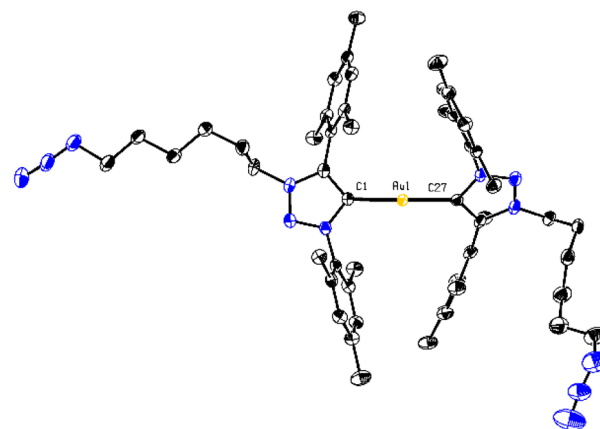
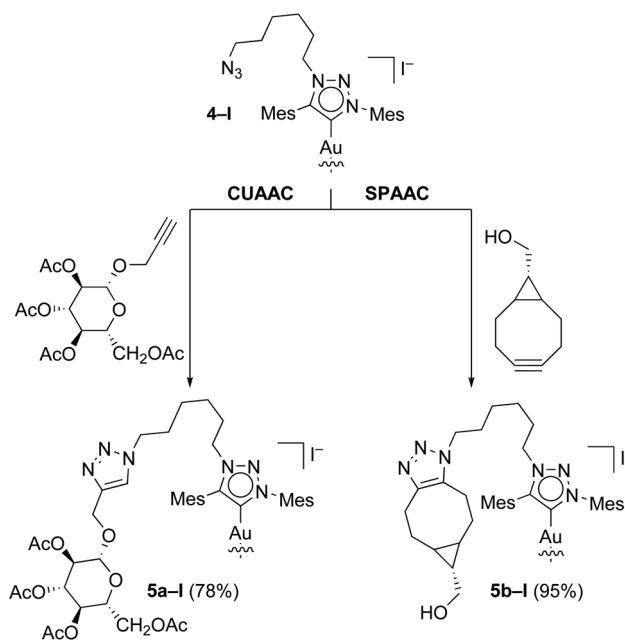
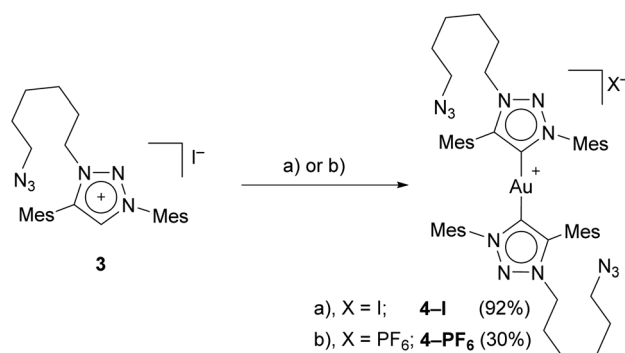


Fig. 1 ORTEP-style representation (50% probability levels) of the cationic fragment of compound **4-I**. Hydrogen atoms and anions are omitted for clarity. Color code: blue (N), black (C), yellow (Au). Selected bond lengths and angles: 2.013(3) Å (Au-C₁); 2.012(3) Å (Au-C₂₇); 176.55° (C₁-Au-C₂₇) CCDC 2268759.†



Scheme 3 Post-functionalisation of **4-I** to **5a-I** *via* the CuAAC reaction with 2-propynyl-tetra-*O*-acetyl- β -*D*-glucopyranoside and **4-I** to **5b-I** *via* the SPAAC reaction with bicyclononyne (BCN) (see ESI† for details).



Scheme 2 Synthesis of the symmetrical Au(I) bis-NHC_{trz} complexes from the functionalised ligand precursor **3**; (a) synthesis of **4-I** *via* the weak-base (K_2CO_3) approach; (b) synthesis of **4-PF₆** *via* transmetallation by Ag_2O and anion exchange (see the ESI† for details).

addition reaction are applied (Scheme 3). Therefore, a sugar derivative is reacted with **4-I** in a modified CuAAC procedure, giving the post-modified complex **5a-I** in 78% yield. To avoid partial decomposition of **4-I**, the reaction is conducted at room temperature with excess copper turnings in a water/DCM mixture. To the best of our knowledge, this is the first example of a conjugation *via* CuAAC reaction with an Au(I) bis-NHC complex. Exploiting the SPAAC reaction, **4-I** is also conjugated to a cyclooctyne derivative bearing a terminal hydroxyl group in 95% yield, giving analytically pure **5b-I** without further puri-

Table 1 IC₅₀ values ± SD (nM) for the tested compounds at 48 h incubation in ovarian cancer (A2780) and breast cancer (MCF-7) cell lines. The values are given in nanomolar concentrations (see ESI† for dose–response curves)

	A2780	MCF-7
Cisplatin ²⁶	3600 ± 1300	21 000 ± 6300
Auranofin ²⁶	430 ± 230	280 ± 140
Au(i) bis NHC _{trz} ²⁶	360 ± 90	84 ± 16
4-I	26.6 ± 1.3	261 ± 75
5a-I	100 ± 0.8	335 ± 138
5b-I	17.8 ± 0.4	35 ± 8.9

fication. The reaction proceeds smoothly in acetone, after 16 h, all starting material has been consumed as observed by ESI-MS spectrometry. Both conjugates are characterised by NMR spectroscopy, ESI-MS spectrometry, analytical HPLC and elemental analysis.

Medicinal evaluation

The antiproliferative activity of the cationic Au(i)-NHC_{trz} complexes **4-I**, **5a-I** and **5b-I** is assessed by monitoring their ability to inhibit cell growth using the MTT assay in human ovarian cancer (A2780) and breast cancer (MCF-7) cell lines (Table 1). The metallodrugs cisplatin and auranofin are included for reference. All presented compounds outrival cisplatin and auranofin in the tested cell lines. When comparing the cytotoxic activity of the presented complexes to that of the previously reported non-functionalised Au(i) bis-NHC_{trz} complex, it can be concluded that the antiproliferative activity of **4-I** is higher for A2780 cells, while being less active in the MCF-7 cell line. Conjugation of **4-I** to the model substrates slightly alters the antiproliferative activity in both cell lines, increasing it for **5b-I** (up to 17.8 nM in A2780 cells) and decreasing it for **5a-I**, while remaining in the nanomolar range. Therefore, the high cytotoxic activity is retained for the backbone modification, being a prerequisite for further conjugation reactions.

As previously demonstrated, besides selective induction of apoptosis and overcoming of important resistances (including cisplatin), Au(i) bis-NHC_{trz} complexes with mesityl wingtips show remarkable stability against cysteine and glutathione, therefore eliminating further stability testing of the presented compounds.²⁶

Conclusions

In summary, the backbone modification of the 1,2,3-triazolium ligand precursor with the terminal azide moiety represents a novel framework, that proves useful for the post-modification of Au(i) bis-NHC complexes. All prepared complexes show remarkable antiproliferative activity in human cancer cell lines, surpassing the drug cisplatin by several orders of magnitudes in the tested cell lines. The post-functionalisation of the presented framework with a targeting vector (peptide, modified antibody) and a clickable radiochelator

(*e.g.* NODA-GA or DOTA derivatives) thus paves the way for highly selective theranostic Au(i) complexes. Further work will be conducted on the introduction of other terminal functional groups (*e.g.* maleimide or amine) into the ligand precursor and the synthesis of heteroleptic Au(i) compounds. Also, the mechanism of action of those compounds is currently under investigation. Besides the medicinal applications described in this work, other fields such as catalysis and functional materials will also benefit from the versatile NHC_{trz} ligand system presented here.

Experimental

Materials and methods

All reagents were purchased from commercial suppliers and used without further purification. NMR spectra were recorded on a Bruker AVANCE DPX 400 and AV500C. Chemical shifts are reported in parts per million and referenced to the residual signal of the deuterated solvent (acetonitrile-*d*₃; 1.94 ppm, dimethylsulfoxide-*d*₆; 2.50 ppm). Elemental analyses (C/H/N) were performed by the microanalytical laboratory at Technische Universität München using a HEKAtech Euro EA-CHNS combustion analyser. ESI-MS data were acquired on a Thermo Fisher UltiMate 3000. FT-IR measurements were conducted on a PerkinElmer Frontier FT-IR spectrometer (ATR).

HPLC analyses were performed on a PerkinElmer LC pump 200 coupled to a Shimadzu SPD 10AV UV/Vis-spectrometer. Analytical reversed-phase HPLC-HESI-MS (heated ESI-MS) was performed on an UltiMate 3000 UHPLC focused chromatographic system (Dionex) connected to an LCQ Fleet mass spectrometer (Thermo Scientific) equipped with a C18 column (Hypersil GOLD aQ, 150 × 2.1 mm, 3 μm). Linear gradients of eluent A (0.1% [v/v] TFA in water) and eluent B (0.1% [v/v] TFA in acetonitrile) were applied according to methods: 0–25 min, 85–100% B; 25–30 min, 100% B and 0–25 min, 50–100% B; 25–30 min, 100% B.

Single-crystal X-ray diffraction

SC-XRD data were collected on a Bruker D8 Venture single crystal-X-ray diffractometer equipped with a CMOS detector (Bruker Photon-100), an IMS microfocus source with MoK_α radiation (λ = 0.71073 Å) and a Helios optic using the APEX4 software package.⁴¹ Measurements were performed on single crystals coated with perfluorinated ether. The crystals were fixed on top of a Kapton micro sampler and frozen under a stream of cold nitrogen. A matrix scan was used to determine the initial lattice parameters. Reflections were corrected for Lorentz and polarisation effects, scan speed, and background using SAINT.⁴¹ Absorption corrections including odd and even ordered spherical harmonics were performed using SADABS.⁴¹ Space group assignments were based upon systematic absences, E statistics, and successful refinement of the structures. The structures were solved using SHELXT with the aid of successive difference Fourier maps, and were refined against all data using SHELXL in conjunction with SHELXLE.^{42,43}

Hydrogen atoms were placed in calculated positions and refined using a riding model, with methylene, aromatic, and other C–H distances of 0.99 Å, 0.95 Å and 1.00 Å, respectively, and $U_{\text{iso}}(\text{H}) = 1.2U_{\text{eq}}(\text{C})$. Non-hydrogen atoms were refined with anisotropic displacement parameters. Full-matrix least-squares refinements were performed by minimizing $\sum w(F_o^2 - F_c^2)^2$ with the SHELXL weighting scheme. Neutral atom scattering factors for all atoms and anomalous dispersion corrections for the non-hydrogen atoms were taken from International Tables for Crystallography.⁴⁴ Images of the crystal structures were generated with Platon.⁴⁵

CCDC 2268759 contains the supplementary crystallographic data for this paper.†

General procedures for synthesis of the presented compounds

1,6-Diiodohexane, 2,4,6-trimethylaniline azide (=mesitylazide) and Au(tht)Cl were synthesized according to literature procedures.^{46–48} The identity and purity (>95%) of all biologically studied compounds were confirmed with elemental analysis and NMR spectroscopy.

1,4-Dimesityl-1H-1,2,3-triazole (1). 4.00 g of 2-ethynyl-1,3,5-trimethylbenzene (27.7 mmol, 1.0 eq.) and 5.37 g 2-azido-1,3,5-trimethylbenzene (33.3 mmol, 1.2 eq.) are suspended in 200 mL H₂O/*t*-BuOH (1 : 1) and stirred at 55 °C. To this suspension is then added 0.90 g CuSO₄(H₂O)₅ (3.61 mmol, 0.13 eq.) and 1.37 g NaAsc (6.93 mmol, 0.25 eq.). The mixture is stirred for 72 h at 55 °C. Then the mixture is cooled to 20 °C. EtOAc (200 mL) and EDTA/NH₃ solution (100 mL, 5 v/v respectively) are added, followed by separation of the orange organic layer. The green aqueous layer is then extracted with EtOAc (2 × 70 mL) and the combined organic layers are washed with H₂O (100 mL) and saturated NaCl_{aq} solution (100 mL), dried over NaSO₄, filtered and the solvent is removed *in vacuo*. The crude is washed with pentane (3 × 20 mL), dried and purified by sublimation (140 °C, 10^{–2} mbar) yielding 6.05 g **1** (19.8 mmol, 71%) as a pale-yellow powder.

¹H-NMR (400 MHz, DMSO-*d*₆, 298 K) δ (ppm): 8.33 (s, 1H, H_{trz}), 7.12 (s, 2H, H_{Ar}), 6.98 (s, 2H, H_{Ar}), 2.34 (s, 3H), 2.29 (s, 3H), 2.09 (s, 6H), 1.96 (s, 6H). **Anal. calcd for C₂₀H₂₃N₃** (%): C 78.65; H 7.59; N 13.76. Found: C 78.77; H 7.71; N 13.89. **MS-ESI, positive (*m/z*):** [trzH]⁺ calcd, 306.20; found, 306.33.

3-(6-Iodoheptyl)-1,4-dimesityl-1H-1,2,3-triazolium iodide (2). To a solution of 1.00 g **1** (3.27 mmol, 1.00 eq.) in 30 mL dry MeCN is added 2.34 mL g 1,6-diiodohexane (4.80 g, 14.2 mmol, 4.34 eq.). The solution is then refluxed for 2 d at 90 °C. The solvent is removed *in vacuo*, the remains is dissolved in 2 mL MeCN, precipitated by the addition of excess Et₂O and the solvent is decanted. The remaining solvent is removed *in vacuo* and the remains is washed with Et₂O (3 × 5 mL) and pentane (2 × 5 mL), followed by removing of volatiles. 1.56 g of **2** is obtained as a yellow solid (2.42 mmol, 74%).

¹H-NMR (400 MHz, DMSO-*d*₆, 298 K) δ (ppm): 9.45 (s, 1H, H_{trz}), 7.28 (s, 2H, H_{Ar}), 7.20 (s, 2H, H_{Ar}), 4.44 (m, 2H, NCH₂CH₂C), 3.21 (t, *J* = 6.8 Hz, 2H, CH₂CH₂I), 2.38 (d, 5.6 Hz, 6H, *p*-Me), 2.21–2.02 (m, 12H, *o*-Me), 1.87 (m, 2H, NCH₂CH₂C),

1.68 (p, *J* = 6.8 Hz, 2H, CH₂CH₂I), 1.39–1.19 (m, 4H, H_{al}). **¹³C-NMR** (101 MHz, DMSO-*d*₆, 298 K) δ (ppm): 142.18 (*p*-C_{Ar}), 141.81 (*p*-C_{Ar}), 140.85 (C_{trz}C_{Ar}), 138.18 (*o*-C_{Ar}), 134.21 (*o*-C_{Ar}), 132.98 (C_{trz}), 131.30 (C_{trz}C_{Ar}), 129.61 (*m*-C_{Ar}), 129.03 (*m*-C_{Ar}), 117.87 (NC_{Ar}), 51.32 (NCH₂C), 32.36 (C_{al}), 28.83 (C_{al}), 27.42 (C_{al}), 24.35 (C_{al}), 20.89 (*p*-Me), 20.75 (*p*-Me), 19.67 (*o*-Me), 16.68 (*o*-Me), 8.60 (CH₂I). **Anal. calcd for C₂₆H₃₅I₂N₃** (%): C 48.54; H 5.48; N 6.53. Found: C 48.78; H 5.40; N 6.58. **MS-ESI, positive (*m/z*):** MS-ESI, positive (*m/z*): [HL^d]⁺ calcd, 516.19, found 516.17.

3-(6-Azidoheptyl)-1,4-dimesityl-1H-1,2,3-triazolium iodide (3). 300 mg **2** (0.46 mmol, 1.00 eq.) is dissolved in 5 mL acetone. To this solution is slowly added a solution of 66 mg NaN₃ (1.01 mmol, 2.20 eq.) in 2 mL H₂O. The orange mixture is stirred for 3 d at 20 °C, changing from orange to slightly yellow. The mixed solution is then diluted with 50 mL H₂O, the white precipitate is filtered, washed with H₂O (2 × 5 mL) and pentane (2 × 5 mL). Drying under reduced pressure yields 136 mg of **3** (0.24 mmol, 52%) as a white powder.

¹H-NMR (400 MHz, DMSO-*d*₆, 298 K) δ (ppm): 9.40 (s, 1H, H_{trz}), 7.27 (s, 2H, H_{Ar}), 7.20 (s, 2H, H_{Ar}), 4.43 (t, *J* = 7.0 Hz, 2H, NCH₂CH₂C), 3.27 (t, *J* = 6.8 Hz, 2H, CCH₂CH₂N₃), 2.37 (d, 6H, *p*-Me), 2.12 (s, 12H, *o*-Me), 1.87 (t, *J* = 7.0 Hz, 2H, NCH₂CH₂C), 1.45 (q, *J* = 6.8 Hz, 2H, CCH₂CH₂N₃), 1.34–1.18 (m, 4H, H_{al}). **¹³C-NMR** (101 MHz, DMSO-*d*₆, 298 K) δ (ppm): 142.20 (*p*-C_{Ar}), 141.83 (*p*-C_{Ar}), 140.87 (C_{trz}C_{Ar}), 138.20 (*o*-C_{Ar}), 134.22 (*o*-C_{Ar}), 132.99 (C_{trz}), 131.31 (C_{trz}C_{Ar}), 129.62 (*m*-C_{Ar}), 129.03 (*m*-C_{Ar}), 117.89 (NC_{Ar}), 51.30 (NCH₂C), 50.41 (CCH₂N₃), 27.82 (C_{al}), 27.50 (C_{al}), 25.30 (C_{al}), 25.02 (C_{al}), 20.87 (*p*-Me), 20.75 (*p*-Me), 19.63 (*o*-Me), 16.63 (*o*-Me). **Anal. calcd for C₂₆H₃₅I₂N₃** (%): C 55.91; H 6.32; N 15.05. Found: C 55.87; H 6.26; N 14.81. **MS-ESI, positive (*m/z*):** [HLⁱ]⁺ calcd, 431.29; found 431.3. **FT-IR** (ATR): $\tilde{\nu}$ [cm^{–1}] = 2921, 2861 (m, C–H_{aliphatic}), 2086 (vs, azide).

[Au(L)₂]PF₆ (4-PF₆). 200 mg of the ligand precursor **3** (0.36 mmol, 2.00 eq.) and Ag₂O (0.19 mmol, 1.05 eq.) are dissolved in 4 mL DCM and stirred for 1 h at 20 °C. Then Au(tht)Cl (0.18 mmol, 1.00 eq.) is added and the mixture is stirred for additional 16 h at 20 °C. The mixture is filtered over Celite and the solvent is removed *in vacuo*. The remains are then dissolved in 6 mL acetone/H₂O (2 : 1) and slowly added to a solution of 44 mg NH₄PF₆ (0.27 mmol, 1.50 eq.) in acetone/H₂O (2 : 1). Acetone is removed *in vacuo* and the white solid is extracted with DCM (3 × 3 mL), washed with H₂O (2 mL) and saturated NaCl_{aq} solution (2 mL), dried over NaSO₄, filtered and the solvent is partly removed *in vacuo*. The product is then precipitated with pentane, yielding 65.2 mg (30%, 0.05 mmol) of the product as a white powder.

¹H-NMR (400 MHz, acetonitrile-*d*₃, 298 K) δ (ppm): 7.00 (s, 4H, H_{Ar}), 6.97 (s, 4H, H_{Ar}), 4.11 (t, *J* = 7.0 Hz, 4H, NCH₂CH₂), 3.18 (t, *J* = 6.8 Hz, 4H, CH₂CH₂N₃), 2.42 (d, 12H, *p*-Me), 1.82 (s, 12H, *o*-Me), 1.75 (s, 12H, *o*-Me), 1.73–1.68 (m, 4H, NCH₂CH₂), 1.43 (p, *J* = 6.9 Hz, 4H, CH₂CH₂N₃), 1.28–1.12 (m, 8H, H_{al}). **¹³C-NMR** (126 MHz, acetonitrile-*d*₃, 298 K) δ (ppm): 176.20 (C_{carbene}), 146.81 (C_{trz}C_{Ar}), 141.66 (*p*-C_{Ar}), 141.48 (*p*-C_{Ar}), 138.88 (*o*-C_{Ar}), 136.33 (*o*-C_{Ar}), 134.96 (C_{trz}C_{Ar}), 129.97 (*m*-C_{Ar}), 129.62 (*m*-C_{Ar}), 123.13 (NC_{Ar}), 51.80 (CCH₂N₃), 51.24 (NCH₂C), 29.15

(C_{al}), 28.95 (C_{al}), 26.38 (C_{al}), 26.25 (C_{al}), 21.39 (*p*-Me), 21.35 (*p*-Me), 20.25 (*o*-Me), 17.24 (*o*-Me). ³¹P-NMR (162 MHz, acetonitrile-d₃, 298 K) δ (ppm): -146.80 (m, PF₆⁻). **Anal. calcd for C₅₂H₆₈AuF₆N₁₂P (%)**: C 51.91; H 5.70; N 13.97. Found: C 52.18; H 5.99; N 13.44. **MS-ESI, positive (*m/z*):** [Au(L)₂]⁺ calcd, 1057.54; found, 1057.7.

[Au(L)₂]^aI (4-I). 100 mg of ligand precursor 3 (0.18 mmol, 2.04 eq.), 28.1 mg Au(tht)Cl (0.09 mmol, 1.00 eq.) and 36.4 mg K₂CO₃ (0.26 mmol, 3.00 eq.) are suspended in 4 mL acetone and stirred for 72 h at 60 °C. The progress of the reaction is monitored by ESI-MS. The mixture is then filtered over Celite and the solvent is removed *in vacuo*. The remains are then dissolved in 1 mL Acetone and precipitated by addition of 20 mL Et₂O. The solvent is decanted and the white powder is washed with pentane (2 × 3 mL), followed by drying *in vacuo*, yielding 95.6 mg 4-I (0.08 mmol, 92%).

¹H-NMR (400 MHz, acetonitrile-d₃, 298 K) δ (ppm): 7.00 (s, 4H, H_{Ar}), 6.97 (s, 4H, H_{Ar}), 4.11 (t, *J* = 7.0 Hz, 4H, NCH₂CH₂), 3.18 (t, *J* = 6.8 Hz, 4H, CH₂CH₂N₃), 2.42 (d, 12H, *p*-Me), 1.82 (s, 12H, *o*-Me), 1.75 (s, 12H, *o*-Me), 1.73–1.68 (m, 4H, NCH₂CH₂), 1.43 (p, *J* = 6.9 Hz, 4H, CH₂CH₂N₃), 1.28–1.12 (m, 8H, H_{al}). ¹³C-NMR (126 MHz, acetonitrile-d₃, 298 K) δ (ppm): 176.20 (C_{carbene}), 146.81 (C_{trzc}C_{Ar}), 141.66 (*p*-C_{Ar}), 141.48 (*p*-C_{Ar}), 138.88 (*o*-C_{Ar}), 136.33 (*o*-C_{Ar}), 134.96 (C_{trzc}C_{Ar}), 129.97 (*m*-C_{Ar}), 129.62 (*m*-C_{Ar}), 123.13 (NC_{Ar}), 51.80 (CCH₂N₃), 51.24 (NCH₂C), 29.15 (C_{al}), 28.95 (C_{al}), 26.38 (C_{al}), 26.25 (C_{al}), 21.39 (*p*-Me), 21.35 (*p*-Me), 20.25 (*o*-Me), 17.24 (*o*-Me). **Anal. calcd for C₅₂H₆₈AuIN₁₂ (%)**: C 52.70; H 5.78; N 14.18. Found: C 52.70; H 5.62; N 13.96. **MS-ESI, positive (*m/z*):** [Au(L)₂]⁺ calcd, 1057.54; found, 1057.7.

[Au(L)^a]₂I (5a-I). 30.0 mg of complex 4-I (25 μmol, 1.00 eq.) and 19.6 mg of 2-propinyl-tetra-*O*-acetyl-β-*D*-glucopyranoside (51 μmol, 2.00 eq.) are dissolved in 3 mL DCM. Subsequently, 2 mL of deionised water and 500 mg copper turnings are added. The mixture is stirred for 48 h and the formation of small copper particles is observed under strong stirring. The progress of the reaction is monitored by ESI-MS. After filtering over Celite, 1 mL of an aqueous solution of NH₃ (10%) and EDTA (5%) is added. The organic phase is separated and the aqueous phase is extracted with DCM (2 × 3 mL). After combining the organic phase, washing with water (2 mL) and brine (2 mL), drying over NaSO₄ and filtering, the solvent is removed *in vacuo*. The remains are then dissolved in 0.1 mL of Acetone and precipitated by addition of 5 mL Et₂O. The solvent is decanted and the white powder is washed with pentane (2 × 3 mL), followed by drying *in vacuo*, yielding 39 mg 5a-I (19.7 μmol, 78%) as a yellow powder.

¹H-NMR (400 MHz, acetonitrile-d₃, 298 K) δ (ppm): 7.65 (s, 2H, H_{trzc}), 6.99 (s, 4H, H_{Ar}), 6.97 (s, 4H, H_{Ar}), 5.20 (t, *J* = 9.6 Hz, 2H, CHOAc), 5.02 (t, *J* = 9.7 Hz, 2H, CHOAc), 4.92–4.77 (m, 4H, CHOAc + OCH₂C'_{trzc}), 4.72 (d, *J* = 8.1 Hz, 2H, OCHO), 4.67 (d, *J* = 12.5 Hz, 2H, OCH₂C'_{trzc}), 4.28–4.19 (m, 6H, N'CH₂C + CH₂OAc), 4.15–4.04 (m, 6H, NCH₂C + CH₂OAc), 3.82 (ddd, *J* = 10.0, 4.9, 2.5 Hz, 2H, CHOAc), 2.42 (d, *J* = 7.1 Hz, 12H, *p*-Me), 2.02 (s, 6H, OAc), 1.97 (s, 6H, OAc), 1.93 (s, 6H, OAc), 1.89 (s, 6H, OAc), 1.81 (s, 12H, *o*-Me), 1.74 (s, 12H, *o*-Me), 1.69 (m, 8H,

NCH₂CH₂ + N'CH₂CH₂), 1.17 (m, 8H, H_{al}). ¹³C-NMR (126 MHz, acetonitrile-d₃, 298 K) δ (ppm): 176.07 (C_{carbene}), 171.26 (OAc), 170.77 (OAc), 170.45 (OAc), 170.17 (OAc), 146.69 (C_{trzc}C_{Ar}), 144.21 (C'_{trzc}CO), 141.58 (*p*-C_{Ar}), 141.39 (*p*-C_{Ar}), 138.80 (*o*-C_{Ar}), 136.22 (*o*-C_{Ar}), 134.88 (C_{trzc}C_{Ar}), 129.89 (*m*-C_{Ar}), 129.54 (*m*-C_{Ar}), 124.46 (C'_{trzc}H), 123.03 (NC_{Ar}), 100.20 (OCHO), 73.12 (COAc), 72.37 (COAc), 71.85 (COAc), 69.15 (COAc), 63.17 (OCH₂C'_{trzc}), 62.60 (CCH₂OAc), 51.13 (NCH₂C), 50.43 (N'CH₂C), 30.35 (NCH₂C), 29.01 (N'CH₂C), 26.06 (C_{al}), 26.03 (C_{al}), 21.34 (*p*-Me), 21.30 (*p*-Me), 20.81 (OAc), 20.75 (OAc), 20.19 (*o*-Me), 17.19 (*o*-Me). **Anal. calcd for C₈₆H₁₁₂AuIN₁₂ (%)**: C 52.76; H 5.77; N 8.59. Found: C 53.12; H 6.00; N 8.59. **MS-ESI, positive (*m/z*):** [Au(L^a)₂]⁺ calcd, 1829.78; found, 1829.05, [Au(L^a)₂ + H]²⁺ calcd, 915.39; found, 915.83.

[Au(L^b)₂]^aI (5b-I). 30.0 mg of complex 4-I (25 μmol, 1.00 eq.) is dissolved in 2 mL acetone. Subsequently, a solution of 9.51 mg BCN-OH (63 μmol, 2.50 eq.) in 1 mL acetone is slowly added at 25 °C and the solution is stirred for 16 h at 25 °C. The progress of the reaction is monitored by ESI-MS. The solution is then filtered over Celite and the solvent is removed *in vacuo*. The remains are then dissolved in 0.1 mL of Acetone and precipitated by addition of 5 mL Et₂O. The solvent is decanted and the white powder is washed with pentane (2 × 3 mL), followed by drying *in vacuo*, yielding 35.8 mg 5b-I (24 μmol, 95%) as a white powder.

¹H-NMR (400 MHz, acetonitrile-d₃, 298 K) δ (ppm): 6.99 (s, 4H, H_{Ar}), 6.97 (s, 4H, H_{Ar}), 4.09 (q, *J* = 7.2 Hz, 8H, NCH₂CH₂), 3.56 (m, 4H, CH₂OH), 2.97 (m, 2H, H_{al}), 2.85 (m, 2H, H_{al}), 2.75 (m, 2H, H_{al}), 2.60 (m, 2H, H_{al}), 2.42 (d, *J* = 6.8 Hz, 12H, *p*-Me), 2.09 (m, 4H, H_{al}), 1.80 (s, 12H, *o*-Me), 1.74 (s, 12H, *o*-Me), 1.65 (m, 8H), 1.51 (m, 4H), 1.20–1.12 (m, 8H), 1.04 (p, *J* = 8.2 Hz, 2H), 0.95–0.81 (m, 4H). ¹³C-NMR (101 MHz, acetonitrile-d₃, 298 K) δ (ppm): 176.20 (C_{carbene}), 146.80 (C_{trzc}C_{Ar}), 145.22 (C_{Ar}), 141.64 (*p*-C_{Ar}), 141.46 (*p*-C_{Ar}), 138.87 (*o*-C_{Ar}), 136.32 (*o*-C_{Ar}), 134.95 (C_{trzc}C_{Ar}), 134.06 (C_{Ar}), 129.98 (*m*-C_{Ar}), 129.63 (*m*-C_{Ar}), 123.12 (NC_{Ar}), 59.26 (C_{al}), 51.24 (NCH₂C), 48.16 (C_{al}), 30.27 (C_{al}), 29.09 (C_{al}), 26.60 (C_{al}), 26.18 (C_{al}), 26.13 (C_{al}), 23.43 (C_{al}), 23.26 (C_{al}), 22.64 (C_{al}), 21.91 (C_{al}), 21.45 (*p*-Me), 21.40 (*p*-Me), 20.29 (*o*-Me), 20.24 (*o*-Me), 19.79 (C_{al}), 17.29 (*o*-Me). **Anal. calcd for C₇₂H₉₆AuIN₁₂O₂·H₂O (%)**: C 57.42; H 6.57; N 11.18. Found: C 57.43; H 6.52; N 10.81. **MS-ESI, positive (*m/z*):** [Au(L^b)₂]⁺ calcd, 1357.74; found, 1357.40, [Au(L^b)₂ + H]²⁺ calcd, 679.37; found, 679.72, [Au(L^b)₂ + 2H]³⁺ calcd, 453.25; found, 453.63.

MTT assays

For the adherent cell lines (A2780 and MCF7 – 20,000 cells per well), cell viability was determined using the tetrazolium dye MTT that is reduced to its insoluble formazan by metabolic active cells. Cells were seeded at a density of 2 × 10⁴ cells in 200 μL of appropriate medium and were treated with different concentrations of the compounds; untreated cells and cells treated with the solvent DMSO (0.5%) served as controls. After 48 h of incubation, the medium was discarded, and the cells were incubated with 200 μL of a MTT solution in PBS (0.5 mg mL⁻¹). After 3 h at 37 °C, the solution was removed, and

200 μL of DMSO was applied to each well to solubilize the purple formazan crystals formed. The absorbance at 570 nm was measured using a plate spectrophotometer (PowerWave XS, BioTek). The IC_{50} values were calculated using the GraphPad Prism software (v. 5.0).

Conflicts of interest

There are no conflicts to declare.

Acknowledgements

João D. G. Correia and Fernanda Marques acknowledge Fundação para a Ciência e a Tecnologia (FCT) for funding through project UIDP/04349/2020. The authors thank Miriam Feckl for experimental support.

References

- 1 F. Heynick, *Br. J. Psychiatry*, 2009, **195**, 456.
- 2 K. Strebhardt and A. Ullrich, *Nat. Rev. Cancer*, 2008, **8**, 473.
- 3 L. Galluzzi, I. Vitale, J. Michels, C. Brenner, G. Szabadkai, A. Harel-Bellan, M. Castedo and G. Kroemer, *Cell Death Dis.*, 2014, **5**, 1–18.
- 4 L. Galluzzi, L. Senovilla, I. Vitale, J. Michels, I. Martins, O. Kepp, M. Castedo and G. Kroemer, *Oncogene*, 2012, **31**, 1869–1883.
- 5 S. A. Patil, A. P. Hoagland, S. A. Patil and A. Bugarin, *Future Med. Chem.*, 2020, **12**, 2239–2275.
- 6 J. F. Machado, J. D. G. Correia and T. S. Morais, *Molecules*, 2021, **26**, 3153.
- 7 G. Moreno-Alcántar, P. Picchetti and A. Casini, *Angew. Chem., Int. Ed.*, 2023, **62**, e202218000.
- 8 A. Pöthig and A. Casini, *Theranostics*, 2019, **9**, 3150–3169.
- 9 M. J. Matos, C. Labão-Almeida, C. Sayers, O. Dada, M. Tacke and G. J. L. Bernardes, *Chem. – Eur. J.*, 2018, **24**, 12250–12253.
- 10 N. Curado, G. Dewaele-Le Roi, S. Poty, J. S. Lewis and M. Contel, *Chem. Commun.*, 2019, **55**, 1394–1397.
- 11 B. Woods, R. D. M. Silva, C. Schmidt, D. Wragg, M. Cavaco, V. Neves, V. F. C. Ferreira, L. Gano, T. S. Morais, F. Mendes, J. D. G. Correia and A. Casini, *Bioconjugate Chem.*, 2021, **32**, 1399–1408.
- 12 J. Han, A. F. B. Räder, F. Reichart, B. Aikman, M. N. Wenzel, B. Woods, M. Weinmüller, B. S. Ludwig, S. Stürup, G. M. M. Groothuis, H. P. Permentier, R. Bischoff, H. Kessler, P. Horvatovich and A. Casini, *Bioconjugate Chem.*, 2018, **29**, 3856–3865.
- 13 P. J. Barnard, M. V. Baker, S. J. Berners-Price and D. A. Day, *J. Inorg. Biochem.*, 2004, **98**, 1642–1647.
- 14 M. V. Baker, P. J. Barnard, S. J. Berners-Price, S. K. Brayshaw, J. L. Hickey, B. W. Skelton and A. H. White, *Dalton Trans.*, 2006, 3708–3715.
- 15 J. L. Hickey, R. A. Ruhayel, P. J. Barnard, M. V. Baker, S. J. Berners-Price and A. Filipovska, *J. Am. Chem. Soc.*, 2008, **130**, 12570–12571.
- 16 P. J. Barnard and S. J. Berners-Price, *Coord. Chem. Rev.*, 2007, **251**, 1889–1902.
- 17 S. Sen, Y. Li, V. Lynch, K. Arumugam, J. L. Sessler and J. F. Arambula, *Chem. Commun.*, 2019, **55**, 10627–10630.
- 18 T. Diehl, M. T. S. Krause, S. Ueberlein, S. Becker, A. Trommer, G. Schnakenburg and M. Engeser, *Dalton Trans.*, 2017, **46**, 2988–2997.
- 19 C. H. G. Jakob, B. Dominelli, J. F. Schlagintweit, P. J. Fischer, F. Schuderer, R. M. Reich, F. Marques, J. D. G. Correia and F. E. Kühn, *Chem. – Asian J.*, 2020, **15**, 4275–4279.
- 20 W. Niu, X. Chen, W. Tan and A. S. Veige, *Angew. Chem., Int. Ed.*, 2016, **55**, 8889–8893.
- 21 A. Hospital, C. Gibard, C. Gaulier, L. Nauton, V. Théry, M. El-Ghozzi, D. Avignant, F. Cisnetti and A. Gautier, *Dalton Trans.*, 2012, **41**, 6803–6812.
- 22 S. Sen, M. W. Perrin, A. C. Sedgwick, V. M. Lynch, J. L. Sessler and J. F. Arambula, *Chem. Sci.*, 2021, **12**, 7547–7553.
- 23 C. H. G. Jakob, B. Dominelli, E. M. Hahn, T. O. Berghausen, T. Pinheiro, F. Marques, R. M. Reich, J. D. G. Correia and F. E. Kühn, *Chem. – Asian J.*, 2020, **15**, 2754–2762.
- 24 S. D. Köster, H. Alborzinia, S. Can, I. Kitanovic, S. Wölfl, R. Rubbiani, I. Ott, P. Riesterer, A. Prokop, K. Merz and N. Metzler-Nolte, *Chem. Sci.*, 2012, **3**, 2062–2072.
- 25 F. Guarra, A. Pratesi, C. Gabbiani and T. Biver, *J. Inorg. Biochem.*, 2021, **217**, 111355.
- 26 J. F. Schlagintweit, C. H. G. Jakob, N. L. Wilke, M. Ahrweiler, C. Frias, J. Frias, M. König, E. M. H. J. Esslinger, F. Marques, J. F. MacHado, R. M. Reich, T. S. Morais, J. D. G. Correia, A. Prokop and F. E. Kühn, *J. Med. Chem.*, 2021, **64**, 15747–15757.
- 27 D. Aucamp, S. V. Kumar, D. C. Liles, M. A. Fernandes, L. Harmse and D. I. Bezuidenhout, *Dalton Trans.*, 2018, **47**, 16072–16081.
- 28 C. W. Tornøe, C. Christensen and M. Meldal, *J. Org. Chem.*, 2002, **67**, 3057–3064.
- 29 V. V. Rostovtsev, L. G. Green, V. V. Fokin and K. B. Sharpless, *Angew. Chem., Int. Ed.*, 2002, **41**, 2596–2599.
- 30 P. Mathew, A. Neels and M. Albrecht, *J. Am. Chem. Soc.*, 2008, **130**, 13534–13535.
- 31 D. Canseco-Gonzalez and M. Albrecht, *J. Chem. Soc., Dalton Trans.*, 2013, **42**, 7424–7432.
- 32 J. M. Aizpurua, R. M. Fratila, Z. Monasterio, N. Pérez-Esnaola, E. Andreieff, A. Irastorza and M. Sagartzazu-Aizpurua, *New J. Chem.*, 2014, **38**, 474–480.
- 33 S. Sen, M. W. Perrin, A. C. Sedgwick, E. Y. Dunskey, V. M. Lynch, X. P. He, J. L. Sessler and J. F. Arambula, *Chem. Commun.*, 2020, **56**, 7877–7880.
- 34 S. Sen, S. Hufnagel, E. Y. Maier, I. Aguilar, J. Selvakumar, J. E. Devore, V. M. Lynch, K. Arumugam, Z. Cui, J. L. Sessler

- and J. F. Arambula, *J. Am. Chem. Soc.*, 2020, **142**, 20536–20541.
- 35 N. J. Agard, J. A. Prescher and C. R. Bertozzi, *J. Am. Chem. Soc.*, 2004, **126**, 15046–15047.
- 36 H. C. Kolb, M. G. Finn and K. B. Sharpless, *Angew. Chem., Int. Ed.*, 2001, **40**, 2004–2021.
- 37 S. Lee, H. Koo, J. H. Na, S. J. Han, H. S. Min, S. J. Lee, S. H. Kim, S. H. Yun, S. Y. Jeong, I. C. Kwon, K. Choi and K. Kim, *ACS Nano*, 2014, **8**, 2048–2063.
- 38 A. A. Neves, Y. A. Wainman, A. Wright, M. I. Kettunen, T. B. Rodrigues, S. McGuire, D. E. Hu, F. Bulat, S. Geninatti Crich, H. Stöckmann, F. J. Leeper and K. M. Brindle, *Angew. Chem., Int. Ed.*, 2016, **55**, 1286–1290.
- 39 H. Wang, R. Wang, K. Cai, H. He, Y. Liu, J. Yen, Z. Wang, M. Xu, Y. Sun, X. Zhou, Q. Yin, L. Tang, I. T. Dobrucki, L. W. Dobrucki, E. J. Chaney, S. A. Boppart, T. M. Fan, S. Lezmi, X. Chen, L. Yin and J. Cheng, *Nat. Chem. Biol.*, 2017, **13**, 415–424.
- 40 D. Canseco-Gonzalez, A. Petronilho, H. Mueller-Bunz, K. Ohmatsu, T. Ooi and M. Albrecht, *J. Am. Chem. Soc.*, 2013, **135**, 13193–13203.
- 41 *APEX Suite of crystallographic software*, APEX 4, Bruker AXS Inc.: Madison, Wisconsin, USA, 2021.
- 42 C. B. Hübschle, G. M. Sheldrick and B. Dittrich, *J. Appl. Crystallogr.*, 2011, **44**, 1281–1284.
- 43 G. M. Sheldrick, *Acta Crystallogr., Sect. C: Struct. Chem.*, 2015, **71**, 3–8.
- 44 A. J. Wilson, *International Tables for Crystallography*, Kluwer Academic Publishers, Dordrecht, 1992.
- 45 A. L. Spek, *Acta Crystallogr., Sect. D: Biol. Crystallogr.*, 2009, **65**, 148–155.
- 46 F. L. Breusch and F. Baykut, *Chem. Ber.*, 1953, **86**, 684–688.
- 47 R. Uson, A. Laguna, M. Laguna, D. A. Briggs, H. H. Murray and J. P. Fackler Jr., *Inorg. Synth.*, 1989, **26**, 85–91.
- 48 K. Barral, A. D. Moorhouse and J. E. Moses, *Org. Lett.*, 2007, **9**, 1809–1811.